EFFECT OF MILLING ON SINTERING BEHAVIOR AND MICROSTRUCTURAL EVOLUTION IN W-Ni-Fe HEAVY ALLOYS

A Thesis Submitted

In Partial Fulfillment of the Requirements

For the Degree of

Master of Technology

by

Amit Shrivastava

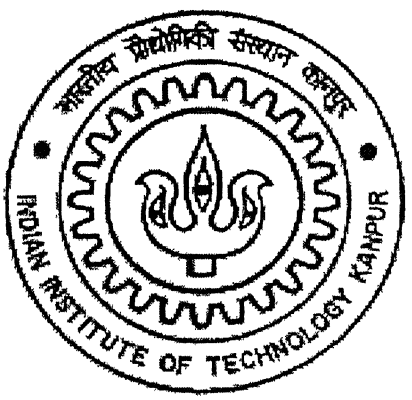

DEPARTMENT OF MATERIALS AND METALLURGICAL ENGINEERING

INDIAN INSTITUTE OF TECHNOLOGY, KANPUR

FEBRUARY 2003

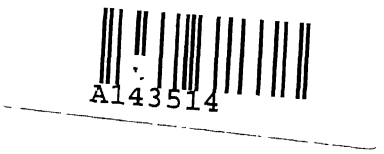

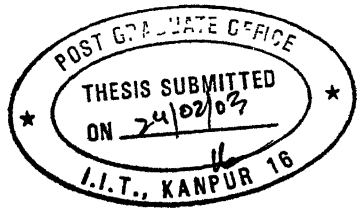

CERTIFICATE

It is certified that the work contained in the thesis entitled **"Effect of Milling on Sintering Behavior and Microstructural Evolution in W-Ni-Fe Heavy Alloys"** by **Amit Shrivastava (Roll No. Y110601)** has been carried out under my supervision and to the best of my knowledge this work has not been submitted elsewhere for a degree.

Anish Upadhyaya
Assistant Professor
Department of Materials and Metallurgical Engineering
Indian Institute of Technology, Kanpur.

ABSTRACT

The present work investigates the effect of powder size, chemistry and milling on the microstructural evolution and sintering behavior of W-N-Fe heavy alloys. To study the effect of powder size 4 μm and 10μm average size tungsten powders were selected. Two different compositions having 92wt% and 95wt% tungsten were prepared, to observe the effect of chemical composition. Two different powder preparation routes were selected. In first case selected compositions were prepared by just mixing the elemental powders. Second method of powder preparation was milling of mixed powder of selected composition in two different types of mill, namely ball mill and attritor mill. The compacts were sintered at 1400°C and 1500°C corresponding to solid-state and liquid phase sintering, respectively. Compacts prepared by attritor milled powder achieved near theoretical density even in solid-state sintering condition. It was observed that the microstructure of sintered compacts depends on milling. the binder distribution was more uniform in attritor milled and ball milled W-Ni-Fe alloys, as compared to the same composition prepared by mixing. The microstructural contiguity, connectivity, dihedral angle, and grain size of milled W-Ni-Fe alloys were lower than the as milled alloys, which leads to improved mechanical properties.

Table of Contents

List of Figures

List of Tables

Acknowledgements

I would like to express my sincere gratitude to Dr. Anish Upadhyaya for his able guidance and support throughout my post-graduate study at Indian Institute of Technology, Kanpur. His leadership was immeasurable help to my early identification of an industrially significant area of research.

I would like to thank Mr. S. C. Soni of the MME Department for his technical assistance during the present research work.

I would also like to thank Mr. D. Sarathy of WIDIA (India) Ltd. for providing all the powders used, in this work. I am also thankful to Mr. V Singh and P. Singh of Heavy alloy Penetrator Plant (HAPP) for helpful suggestions

My time in IIT Kanpur was enriched by my laboratory mates Sukanta, Shankar, Rout, Maya, Kausik, Chiru, Pampa, Anirban, Jayant, shashank and Ravikiran. I would also like to thank my friends Ashish, Santosh, Sanjay, Balram, Rahul, Pramod, Siddharth, Amitesh, D. Satish Kumar and Animesh all of whom made my stay at IIT Kanpur a pleasant one.

At this time I would like to express my deep sense of gratitude to my beloved grandparents and parents for their immense patience, moral support, courage and inspiration during this research programme.

Amit Shrivastava
25th February 2003
IIT, Kanpur

Chapter 1
INTRODUCTION

Tungsten heavy alloys were first discovered in 1930's [1]. Tungsten is a refractory metal with a fusion point of 3420°C [2]. A typical composition of tungsten heavy alloy ranges from 80-98% tungsten (by weight). The balance is generally a mixture of relatively low melting transition element, such as nickel, iron, copper, and cobalt [3]. A typical microstructure of these alloys contains dispersed tungsten spheroids (b.c.c.) in an alloy matrix phase (f.c.c.). Generally the density of these alloys ranges between 16 to 18g/cm^3, which is considerably higher than the density of lead. Sintered heavy alloys offer a unique combination of properties such as high strength (1000-1700 MPa), high ductility (10-30%), good corrosion resistance, and easy machinability [4]. These alloys are used for radiation absorption, kinetic energy penetrators, and counter balance weights. Recently they have been projected as a viable replacement of depleted uranium (DU: U-0.75Ti) alloys for kinetic energy penetrators.

Since tungsten has very high melting point, these alloys are consolidated through P/M route. Liquid phase sintering is the most commonly used mechanism for consolidation of these high density alloys. In the past the work has been focused on modifying the matrix composition and post sintering heat treatment to achieve full densification and optimal mechanical properties. Being a strategic material very little has been reported in the open literature on the effect of powder modifications by milling on the sintering response Milling of powders is an effective method for microstructural property improvement of sintered products. It is a technique from which composite powders are obtained using a high-energy attritor mill or a ball mill. Milling reduces the powder size. Churn and German [5] have reported that mechanical properties generally improve when tungsten spheroid size becomes finer and the W/W interface reduces. Due to refinement in tungsten spheroid size, contiguity reduces the crack path through matrix is preferred, which results in ductile mode of fracture Milling effects the sintering behavior and causes microstructural changes, which have key role in governing properties of these alloys.

Chapter 2 provides a comprehensive review of various processing aspects of tungsten heavy alloys (WHAs). In chapter 3 scope of the present work is discussed.

This includes reasons for milling and microstructural evolution in tungsten nickel iron heavy alloys. Chapter 4 describes in detail the experimental procedures applied in present work. In Chapter 5, the results of all the experimental works are given in detail. In Chapter 6 results of experiments are discussed Finally chapter 7 summarizes the findings of this work.

Chapter 2
BACKGROUND

2.1. W-Ni-Fe Heavy Alloys

Although tungsten based sintered heavy alloys with Cu-Ni binder were initially developed, attention was eventually diverted to Fe-Ni binder because of better-attained mechanical properties. These alloys have the best combination of optimal mechanical properties and cost effectiveness among all tungsten based heavy alloys. Other tungsten based heavy alloys are W-Cu-Ni, W-Co-Ni, and W-Cr-Ni. W-Co-Ni alloys are costly due to higher cost of cobalt. Moreover the presence of W_6Co_7 intermetallic phase in this system deteriorates the mechanical properties. In addition a relatively higher amount of cobalt is required (about 20%) to achieve 20 % elongation. Upadhyaya [6] has reported that straight nickel binder proved to be better as compared to the binary Co-Ni binders as far as the mechanical properties were concerned. The W-Cr-Ni alloy exhibit higher ultimate tensile strength but possesses poor ductility. In addition presence of brittle σ phase makes W-Cr-Ni alloys suitable for only high hardness applications.

W-Ni-Fe alloy exhibit excellent combination of ductility and strength and can be cold worked to a reduction of 70% without intermediate annealing [7]. Typically the ordnance grade W-Ni-Fe alloys contain 90-93% tungsten, 1-7 wt% nickel, and 0.8-3 wt% iron. These are ferromagnetic in nature. Higher addition of iron causes a significant matrix strengthening effect and improves high temperature strength. Figure 2.1 [8] shows the binary phase diagram of Ni-Fe. It shows that nickel-iron in 7:3 have melting point about1445°C. Figure 2.2 [9] shows the ternary phase diagram of W-Ni-Fe alloys. Chances of intermetallic phase formation shown in Figure 2.2 can be avoided by fast cooling. In W-Ni-Fe heavy alloys matrix consists about 20% dissolved tungsten. The equilibrium phase diagram shows that in this composition matrix will exist in γ (f.c.c.) form. For W-Ni-Fe system, it has been seen that at 1435°C a eutectic melt forms. But in practice, due to inhomogeneous mixing of powders the melt formation occurs at 1465°C. In W-Ni-Fe system tungsten grains are embedded in Ni-Fe matrix. The solubility of W in the matrix is low But due to increase in nickel content in the system the solubility of tungsten increase, which is harmful in respect of mechanical property.

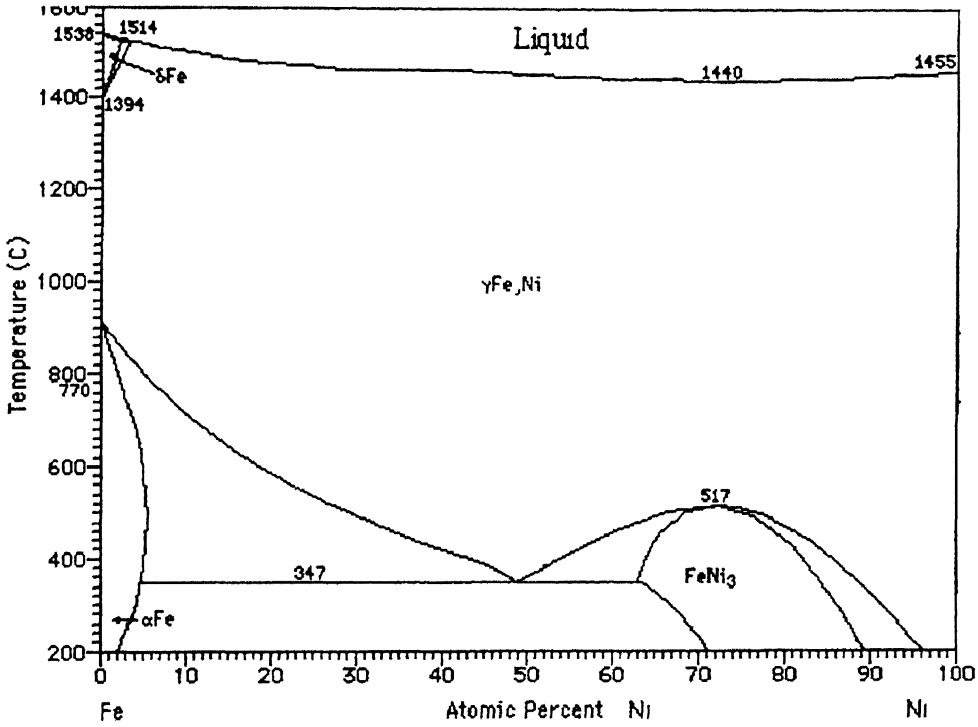

Figure 2.1. Fe-Ni Equilibrium diagram [8].

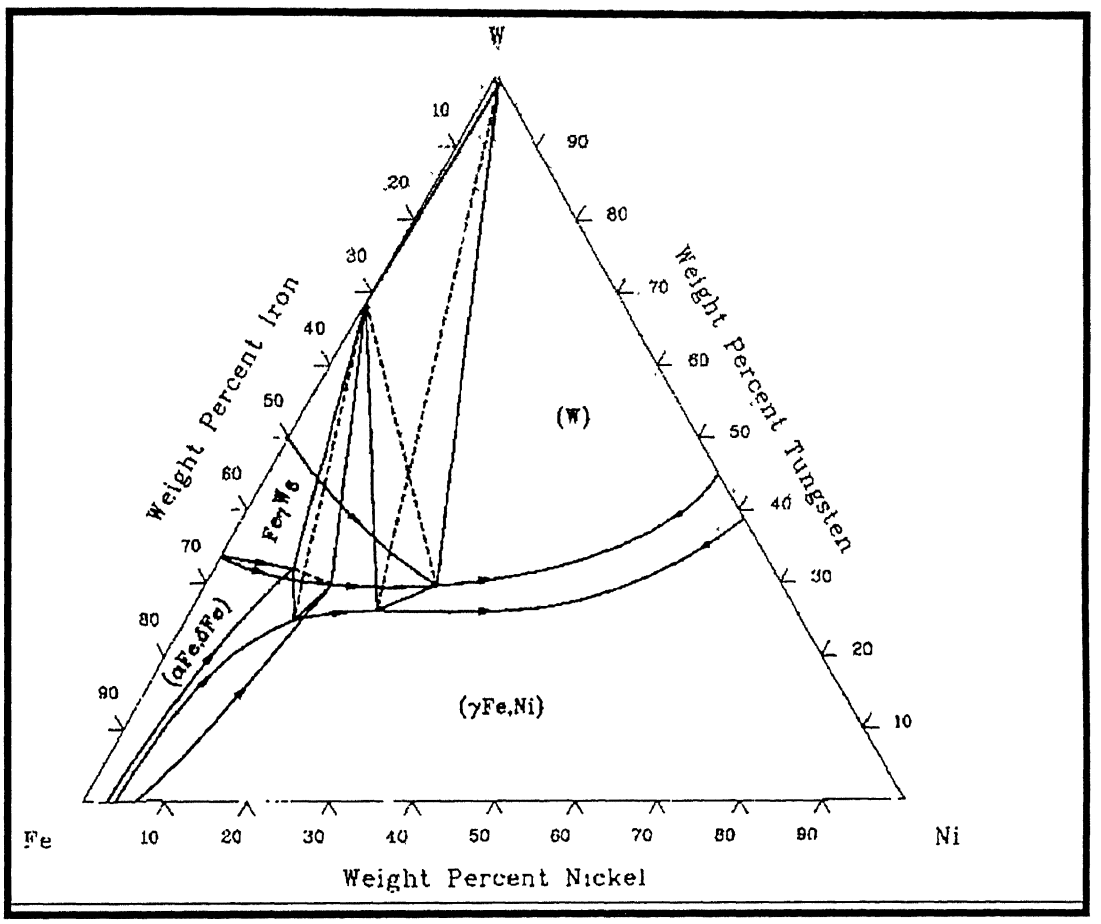

Figure 2.2. Ternary phase diagram of W-Ni-Fe alloys [9].

The formation of different intermetallics depends upon Ni to Fe ratio in the system. The possibility of formation of intermetallics is minimum when the nickel to iron ratio is 7:3. Nickel to iron ratio plays an important role in the selection of W-Ni-Fe alloys for specific applications. Typically Ni to Fe ratio ranges between 1:1 and 4:1. Various research have been carried out in variation of nickel to iron ratio on the mechanical properties of W-Ni-Fe alloys. Mechanical properties of as sintered alloy depends upon the Ni:Fe ratio. The most important factor that should be considered for selecting is to avoid the formation of brittle intermetallic phases at the tungsten /matrix interface. Caldwell [10] has shown that an intermetallic phase of Fe_7W_6 forms at low Ni to Fe ratios, where as at ratios higher than 4:1, Ni_2W, NiW and Ni_4W intermetallic phases form. In another report Caldwell [11] has argued that it is possible to use higher or lower Ni to Fe ratio and to achieve high mechanical properties by using proper heat treatment. The Ni to Fe ratio higher than either 7.3 or 8:2 can significantly improve mechanical properties if proper heat treatment is performed to control the precipitation of brittle intermetallic phases.

2.2. Processing of W-Ni-Fe Heavy Alloys

Since tungsten has very high melting point, P/M processing is the only method for fabrication of these alloys. Figure 2.3 shows the schematic view of processing method of W-Ni-Fe heavy alloys. Figure 2.4 shows the typical microstructure of solid-state and liquid phase sintered W-Ni-Fe heavy alloys. It is clear from the Figure 2.4 that in solid-state sintered alloy, enough porosity (encircled) remains; however liquid phase sintered alloy has rounded tungsten spheroids in nickel/iron matrix without any porosity.

The required composition is prepared by mixing the constituent powders. Homogeneous mixing is must to avoid the chances of liquid pool formation and proper distribution of liquid phase formed during sintering. Generally, these alloys are compacted or injection molded to form green compacts at pressure ranging between 150-250 MPa. Sintering is performed in the range of 1465°C to 1525°C. Typically, the liquid phase sintering is done for 1 h. After sintering, samples are heat treated to further enhance mechanical properties.

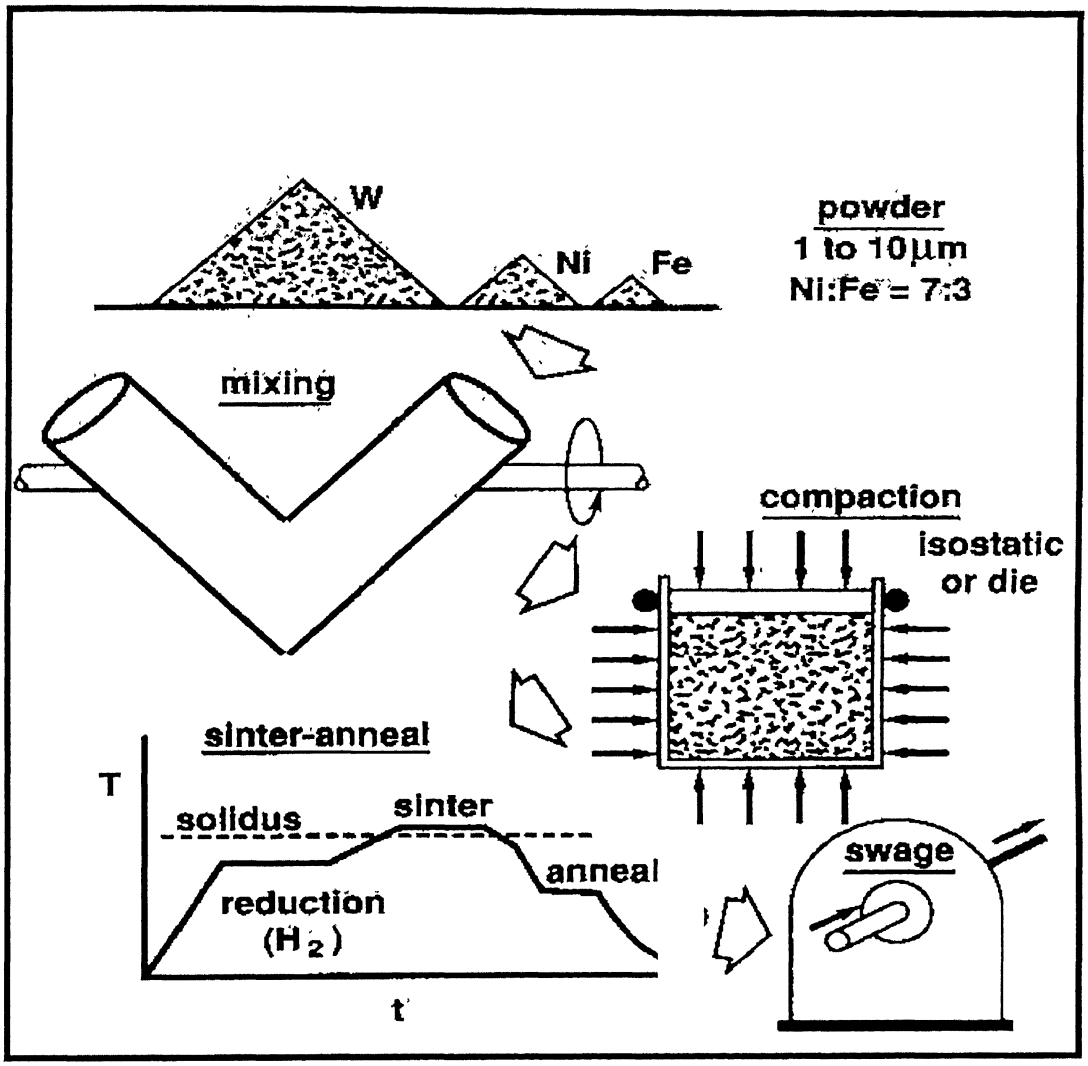

Figure 2.3: Schematic diagram for fabrication of tungsten heavy alloys by P/M processing.

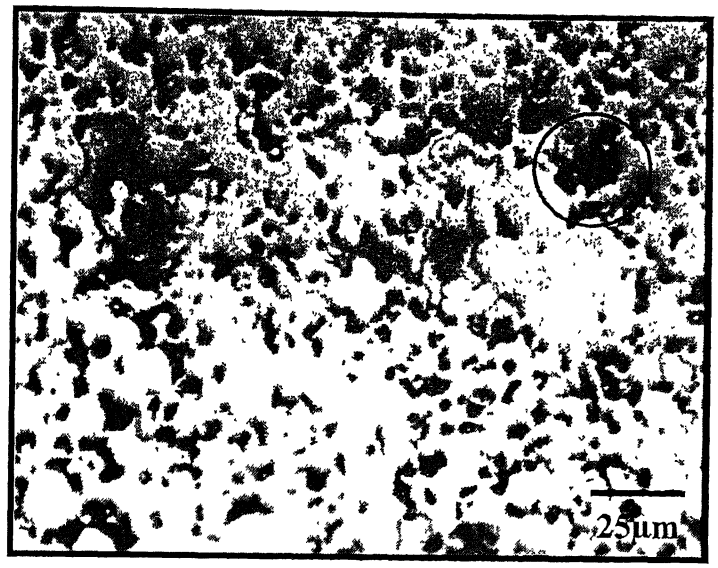

(a)

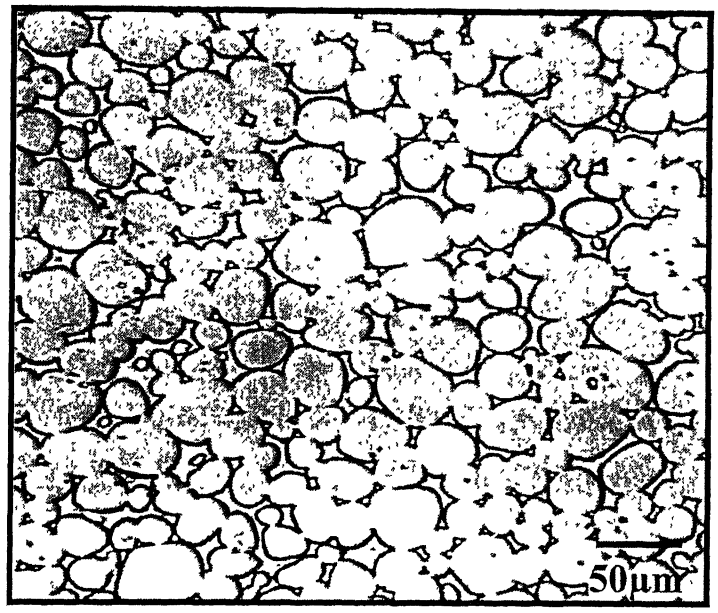

(b)

Figure 2.4: Typical microstructures of (a) solid-state and (b) liquid phase sintered 95.1W-3.45Ni-1.45Fe alloy

2.3. Earlier Research

2.3.1. Powders preparation

Properties of heavy alloys are known to vary with process parameter such as sintering temperature, time and atmosphere. Properties of these alloys also depends on powder preparation techniques. Eroglu and Baykara [12] have reported that for finer grade tungsten powder alloys prepared by attritor milling gives higher strength and ductility as compared to those prepared simply by mixing the constituent powders However compared to finer grade coarser tungsten powder generally resulted in alloys with higher ductility when Turbula mixer was used. Asthana and Upadhyaya [13] have reported the effect of different type of ball millings on size distribution of powders. They found that planetary milling is more effective than centrifugal milling for reduction in tungsten particle size. Suryanarayana [14] has reported that narrower particle size distribution is achieved in attritor milled powders as compared to ball milled.

2.3.2 Sintering

Liquid phase sintering is commonly used for consolidating heavy alloys to achieve full density. It is possible to achieve full densification even by solid-state sintering provided the tungsten powder size smaller than 5μm. For this, either the starting tungsten size is smaller or else one can mill the powder to reduce the size. Higher densification can also be achieved by solid state sintering of mechanically alloyed or milled powders. Steps of solid state sintering are shown in Figure 2.5 [15]. Ryu and Hong [16] have reported 99% theoretical density in case of mechanically alloyed powder, through solid-state sintering at 1300°C. High yield strength (up to 1100 MPa) and hardness (about 300 HV_2) can be achieved with solid-state sintering but ductility and impact energy will be low, due to a large area fraction of brittle tungsten/tungsten interface.

Extensive work has been carried out by several researchers [17-22] on liquid phase sintering of heavy alloys. Basic steps involved in liquid phase sintering are shown in Figure 2.6 [23]. German has classified liquid phase sintering into nine stages including, distortion; these are (1) green compact; (2) liquid phase melting, (3) liquid phase pendular bond formation; (4) densification due to a funicular liquid phase distortion; (5) pore filling; (6) pore closure; (7) liquid egression on external surface

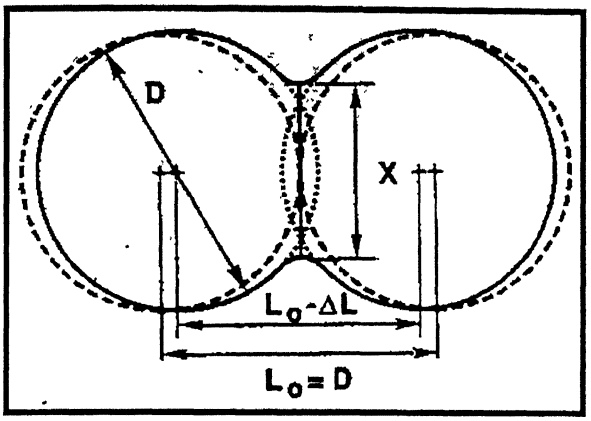

Initial Stage:Neck Growth

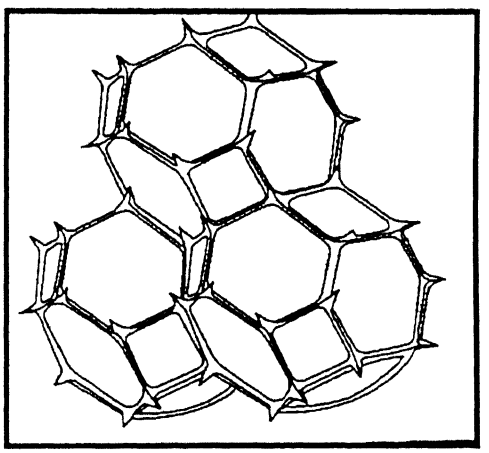

Intermediate Stage:
Tetrakaidecahedron grains

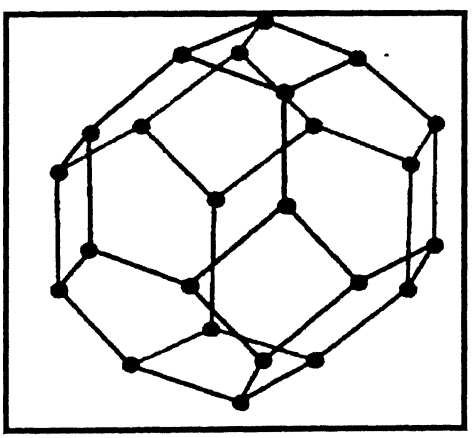

Final Stage: Spherical pores at grain corners

Figure 2.5: Stages of Solid State Sintering [15]

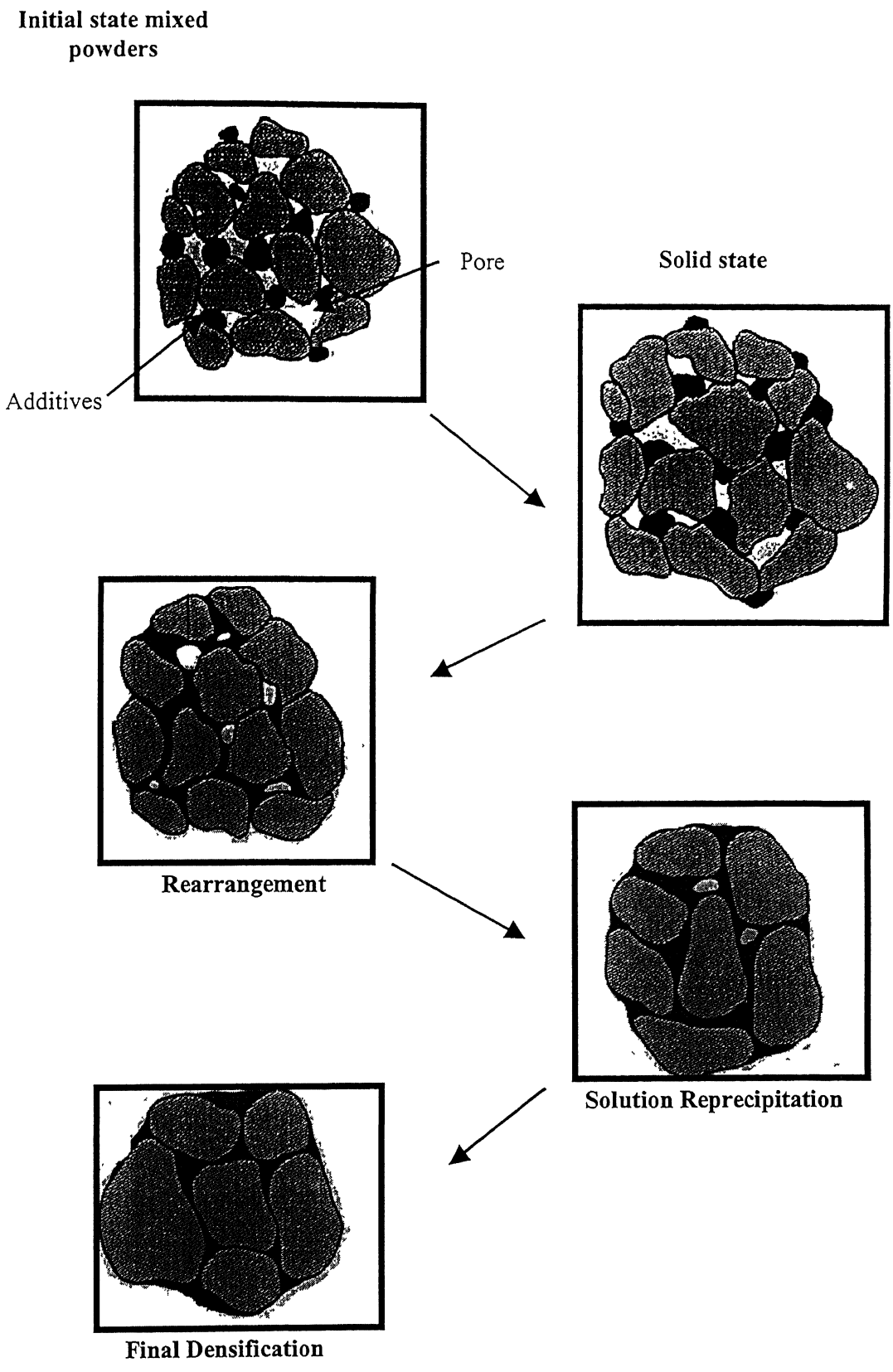

Figure 2.6: Schematic Diagram to show the stages in liquid phase sintering [23].

and pore entrapment in the contact; (8) loss of capillarity; (9) sinter bonding. It is not necessary of all these stages to occur during liquid phase sintering. It has also been reported that compact shape and changes in microstructure during liquid phase sintering are affected by the initial pore structure and alloy composition [17]. Pores affect distortion in liquid phase sintering. If pores are not saturated by liquid during rearrangement, residual capillary forces help to resist distortion. However once the pores are filled and the capillary forces are lost, only solid bonds can provide strength. If the solid bonds have not formed due to grain rearrangement, the component strength falls to a level that cannot resist distortion.

Upadhyaya and Srikanth [18] studied the effect of particle size and binder compostion on sintering properties of heavy alloys. They found that finer tungsten particle size gives better-sintered properties. They also studied the effect of binder composition and sintering temperature on sintered properties.

In liquid phase sintering larger tungsten grains grow at the expense of the smaller ones. Yoon and coworkers [19-22] have done work on grain coarsening of W-Ni-Fe heavy alloys. They have reported that with limited amount of liquid phase present, under the influence of the densification force arising from the pores, grain growth occurs preferentially away from the areas where the grains are in close contact. Thus grain shape accommodation occurs during growth and this enables complete densification.

2.3.3 Alloying Addition

Addition of any alloying constituent that has solubility in the Ni-Fe matrix material reduces the tungsten solubility. The change in chemical equilibrium due to alloying addition induces the morphological changes [24,25], which can ultimately affect the mechanical properties of these alloys. Addition of fourth element such as Mo or Re causes morphological change in tungsten matrix interface and resulted irregular shape of tungsten grains [26-28] Bose and German [28] studied the effect of Mo and Ta additions in W-Ni-Fe heavy alloys. For the tungsten heavy alloys containing molybdenum, the matrix has essentially a constant solubility of 8-11 at% for the tungsten. Since grain growth constant is directly proportional to the solubility limit of tungsten/combined body centered cubic materials (in case of alloying addition), it reduces due to reduction in solubility limit, which ultimately results in finer tungsten grains. This causes higher ultimate tensile strength with considerable

ductility. Addition of Mn results in the morphological change of tungsten grains from roundish to angular shape. Addition of cobalt also reduces the grain growth rate [29]. Addition of scavengers such as Ca and La reduces the embrittling effect of phosphorus by forming a stable compound with phosphorus of possibly the form $LaPO_4$ [30].

2.3.4 Heat Treatment

Sintering of heavy alloys is carried out in H_2 atmosphere to prevent oxidation, and reduce whatever oxides that exist on the powder surface. The elongation of as-sintered (liquid phase sintered) 96wt% tungsten (balance Ni and Fe) remains less than 10% [31]. Heat treatment of this alloy, in vacuum at 800°C or at 1150°C in Ar for few minutes increased the same to 20% [31,32]. Vacuum/Argon heat treatment reduces hydrogen embrittlement in W-Ni-Fe alloys. Dissolved hydrogen induces brittleness. Hydrogen weakens mainly the interface between tungsten grain and matrix. Due to low partial pressure of H_2 in Ar Atmosphere, solubility of H_2 reduces and it comes out.

When liquid phase sintered W-Ni-Fe alloys are cyclically heat treated at 1100°C and resintered at 1485°C, undulation of W/matrix interface resulted. Due to cyclic heat treatment residual thermal stresses resulted. Local yielding of tungsten grain is believed to occur during the cyclic heat treatment. Undulation appears therefore to result from preferential dissolution of material at regions with higher strain energy and precipitation of materials at regions with lower strain energy [26]. Matrix penetration of grain boundary also occurs due to cyclic heat treatment [33, 34]. It also improves ductility due to reduction in W/W brittle interface area. Ageing treatment of tungsten heavy alloys is also possible. Strengthening by ageing of heavy alloys caused by precipitation hardening of tungsten grains [35]. Thermo-mechanical treatment of tungsten heavy alloys improves the tensile strength, fracture elongation and impact energy [36].

Chapter 3

SCOPE OF THE PRESENT WORK

As it is evident from previous chapters sintered heavy alloys consists of nearly pure tungsten grains in the ductile matrix. The combination of density, strength, machinability and corrosion resistance makes tungsten heavy alloys unique in the field of materials. Due to these property combinations, these alloys are used in many areas including radiation shielding, counter weights, kinetic energy penetrators, vibration damping devices and heavy-duty electrical contacts. An important recent application of these alloys is for kinetic energy penetrators. Their penetration behavior is slightly inferior than the depleted uranium which was being used for this purpose, but due to health hazards problems related to use of uranium objects, tungsten heavy alloys have became the only other option for the purpose.

Sintering behavior and microstructural features have an important role in deciding mechanical properties of these alloys. Figure 2.7 and 2.8 show the trend of tensile strength and percentage elongation respectively with change in contiguity. In addition to Full densification, morphology of tungsten grains and other microstructural parameters, such as contiguity, connectivity, volume fraction of matrix and W/matrix interface area per unit volume are deciding factors of optimal mechanical properties. Present work emphasizes on sintering behavior and microstructural evolution of W-Ni-Fe heavy alloys This work mainly is related to processing of W-Ni-Fe heavy alloys through two different sintering mechanism; firstly, solid-state sintering and secondly liquid phase sintering. Effect of milling on sintering behavior was studied. Little work has been reported so far on solid-state sintering of W-Ni-Fe heavy alloys. It was one of the main object of the present work to achieve full densification and favorable microstructural features.

In the present work we achieved very high theoretical sintered density ranging between 88-100%, with high hardness (275-350 HV_2). The alloy consolidated through this mechanism can be use in such applications where high density is of prime importance e.g. counter balance weights. Full densification was also achieved in liquid phase sintered alloys.

Microstructural changes due to milling were also studied. We quantified the changes in pore volume fraction, average pore size, contiguity, connectivity, dihedral

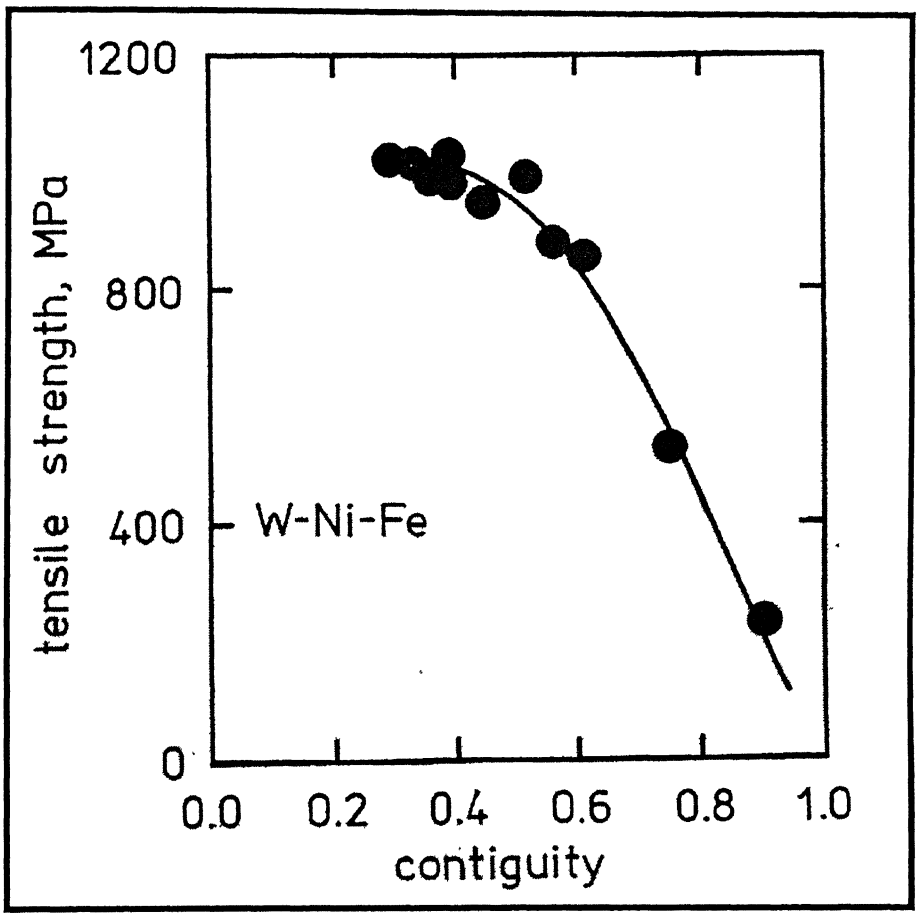

Figure 2.7: Maximum tensile strength for various tungsten heavy alloys with respect to contiguity [37].

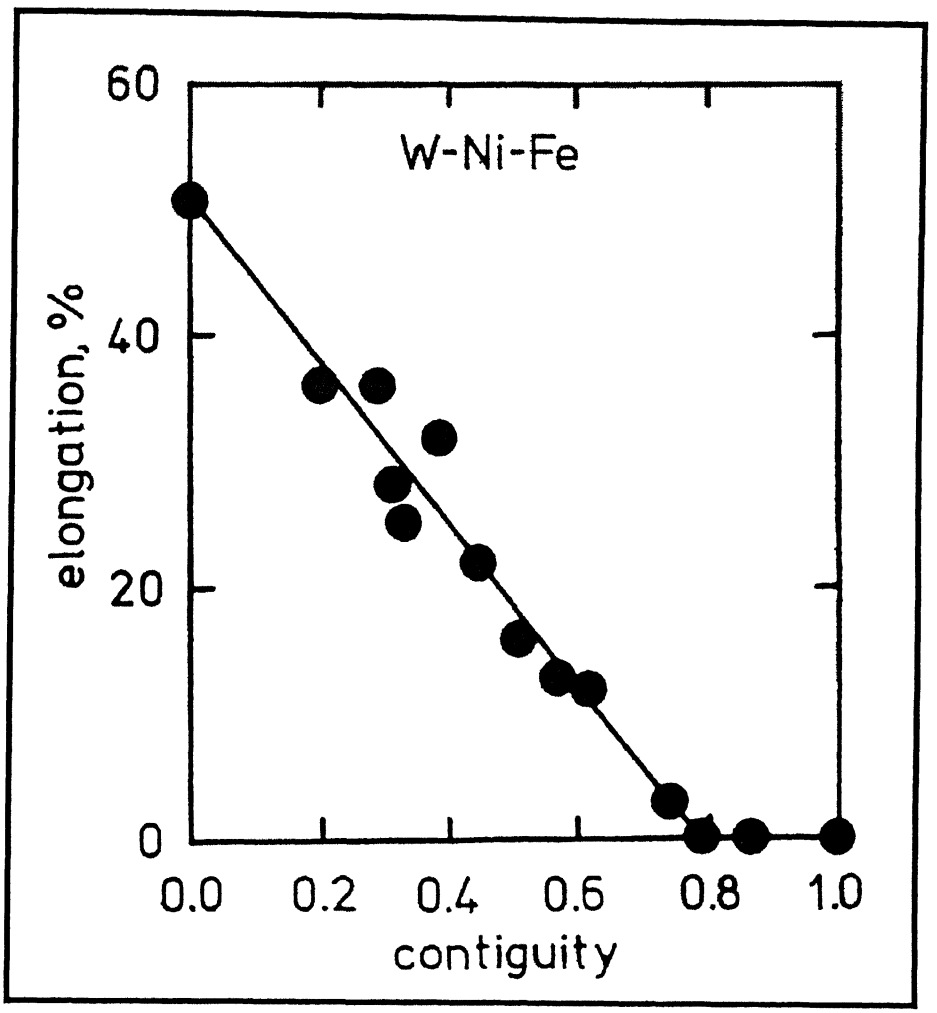

Figure: 2.8: Percentage elongation for various tungsten heavy alloys with respect to contiguity [37].

angle, volume fraction of matrix, and W/matrix interface area per unit volume due to milling. These microstructural properties have an important role in governing mechanical properties of these alloys. Effect of powder milling on hardness and micro hardness of these alloys were also quantified.

Till now there is only one plant at Tirchy in India which is producing W-Ni-Fe heavy alloys from imported powders only through liquid phase sintering for kinetic energy penetrators. For all other applications these alloys are being imported. In this present work, first time in India, we tried to fabricate W-Ni-Fe heavy alloys through solid-state sintering from powders produced in India itself and achieved almost full densification. The alloy produced can be used as counter balance weights and in other applications where ductility is not of prime importance

Chapter 4

EXPERIMENTAL PROCEDURE

For the present study elemental were mixed in two different compositions having 92 and 95 wt% tungsten. These compositions were prepared by two different size tungsten powders. After mixing the constituents for chosen compositions these mix were milled in ball and attritor mills. Cylindrical compacts were prepared by mixed, ball milled and attritor milled powders. Densification behavior was studied and quantification of microstructural parameters was done for these sintered alloys. Experimental details of the present study are summarized in Table 4.1.

4.1 Materials

The elemental powders used for this study were supplied by WIDIA India Ltd. The powder characteristics of as received powders are summarized in Table 4.2

4.2 Powder Characterization

The as received elemental powders were characterized for their size distribution and morphology.

4.2.1 Particle Size and Size Distribution

A Laser Scattering Analyzer (model: Economy, Laser Klasse 1; supplier Fritsch, Germany) was used for analyzing the particle size of the powders. Low angle Fraunhofer light scattering using monochromatic (laser) light and dispersed particles were used in this case. The particles were suspended in a suspension made using 2 to 4 g of powder dissolved in approximately 60 ml of distilled water with 10% sodium meta-phosphate The particles were passed through a laser beam in a circulating water stream. The light scattered after interaction with the particles were measured by detectors, which are placed strategically. The size of the particles affects both the intensity and angular extent of scattering. With the coherent light scattering angle varies inversely with the particle diameter. The scattering depends on the refractive index of the particle in the suspension

Table 4.1 Experimental Details

* Alloys	(i) 92.5W-6.15Ni-1.1Fe-0.25Co and (ii) 95.1W-3.45Ni-1.45Fe
* Average tungsten Particle size	(i) 4.2 μm and (ii) 9.7μm
* Preparation route:	
• Mixing	30 min.
• Milling, 3 h	(i) Ball milling (ii) Attritor milling
* Compaction pressure	200 MPa
* Debiding/Pre-sintering	(i) 450°C (for cylindrical samples) (ii) 1000°C (for tensile samples) } H_2 atmosphere
* Sintering temperature	(i) 1400°C and (ii) 1500°C
* Sintering atmosphere	Reducing (H_2)
* Post sintering treatment	1000°C, 15 min., Argon atmosphere (only for tensile samples)
* Lubricant (Acrawax)	2 wt% (only in milled powders)

Table 4.2 Powder characteristics of as received elemental powders

Characteristics		W		Ni	Fe	Co
		Fine	Coarse*			
Apparent Density, g/cm^3		5.22	5.54	2.71	3.84	1.38
Particle size, μm	D_{10}	2.0	3.8	3.8	1.4	4.44
	D_{50}	4.2	9.7	11.0	7.0	11.4
	D_{90}	6.2	42.5	31.8	19.0	27.6

* *Coarse tungsten powder having bimodal distribution.*

medium, wavelength of light and particle size and shape. Figure 4.1 to 4.4 show the size distribution plot of tungsten (fine and coarse), nickel, iron and cobalt powders. Figure 4.1(b) shows the bimodal distribution of coarse tungsten powders.

4.2.2 Particle Shape

The particle shapes of the powders were obtained using a JEOL, JSM-840A, scanning electron (SEM) in the secondary electron (SE) mode. The magnification of SEM was far greater than the optical microscope. Figurers 4.5 to 4.8 show the morphology of elemental powders used for the present work.

4.3 Powder Preparation

Two different compositions that were 92.5W-6.15Ni-1.1Fe-0.25Co and 95.1W-3.45Ni-1.45Fe (all wt%) prepared by using coarse and fine tungsten powders. Two different preparation routes, mixing and milling were chosen for preparing the alloy compositions.

4.3.1 Powder Mixing

Elemental powders taken in the desired weight fraction were mixed in Turbula mixer (Figure 4.9). Mixing was done for 30 min for both the compositions with different powder sizes.

4.3.2 Milling

Two types of milling technique were employed to the simply mixed powders of desired compositions. First type of mill used was planetary type of ball mill (Figure 4.10) and second one attritor mill (Figure 4.11). In both type of mill, balls taken were made of tungsten carbide. These were spherical in shape. In both type of milling ball to powder ratio (by weight) were taken 10:1. Acetone was used in both type of milling process for removal of heat generated and prevention of oxidation of powders during milling. Milling was done for three hours in all the cases. Milled powders were warmed at 60°C for complete evaporation of acetone in TEMPO oven (Figure 4.12).

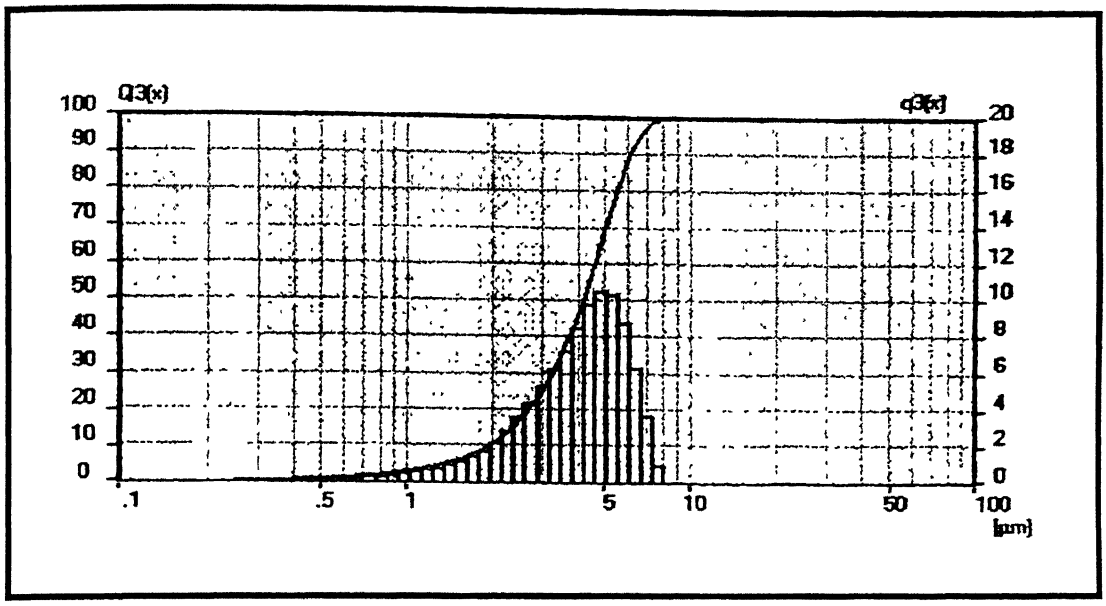

(a)

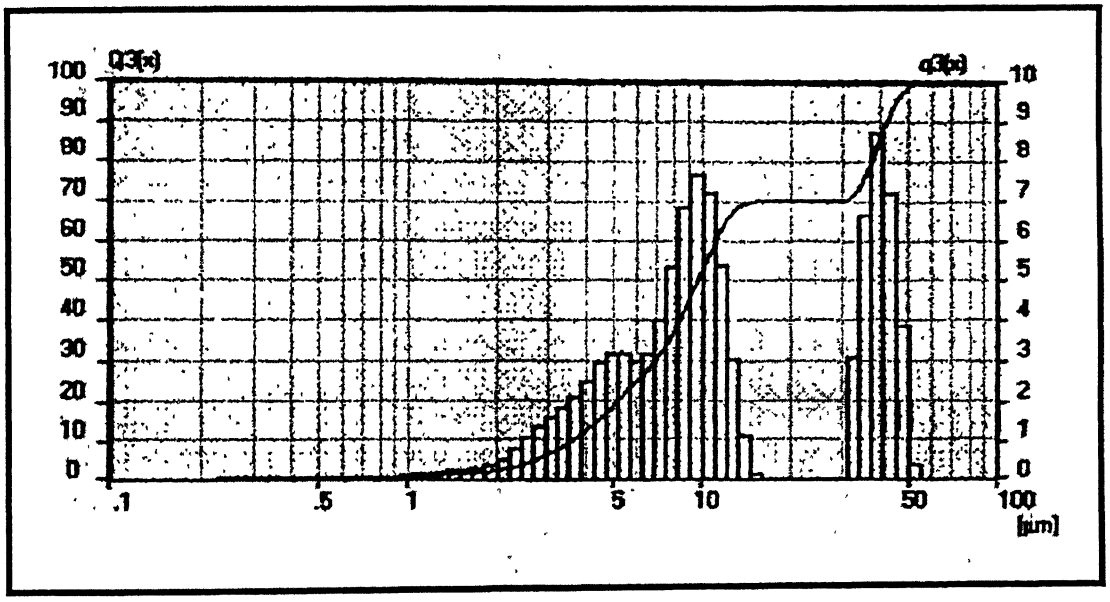

(b)

Figure 4.1: Particle size distribution of (a) fine and (b) coarse tungsten powders.

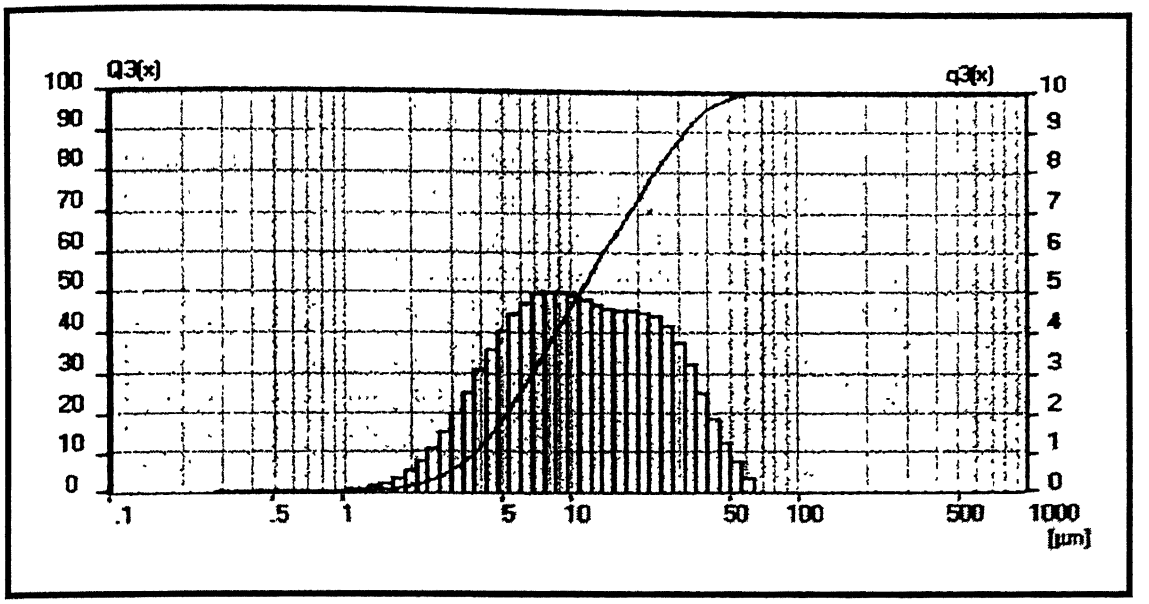

Figure 4.2: Particle size distribution plot of nickel powder

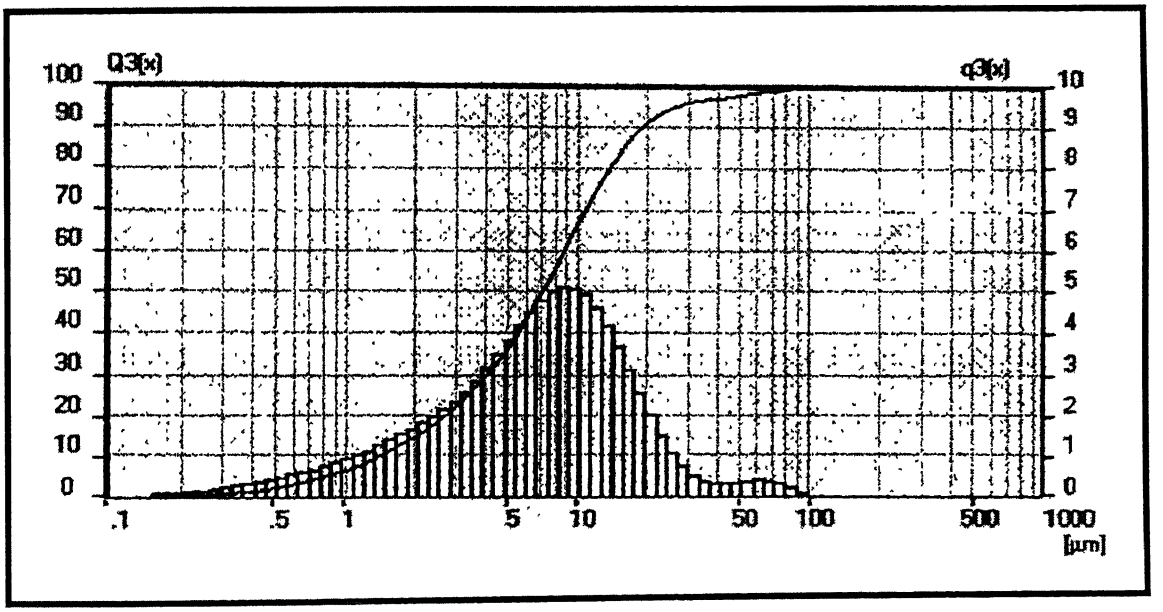

Figure 4.3: Particle size distribution plot of iron powder.

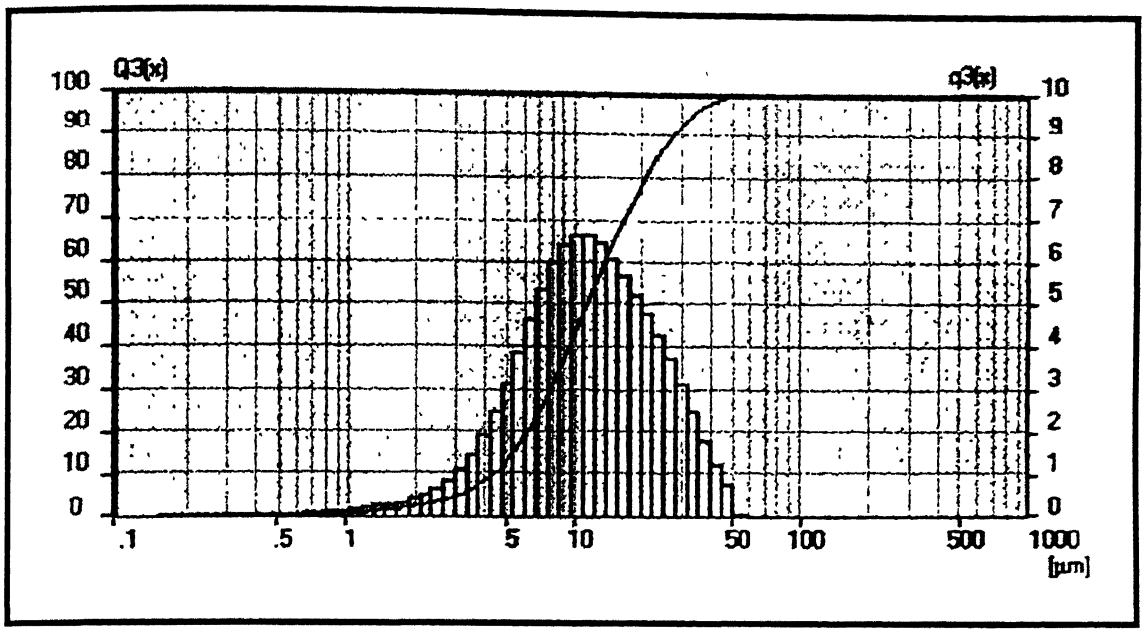

Figure 4.4: Particle size distribution plot of cobalt powder.

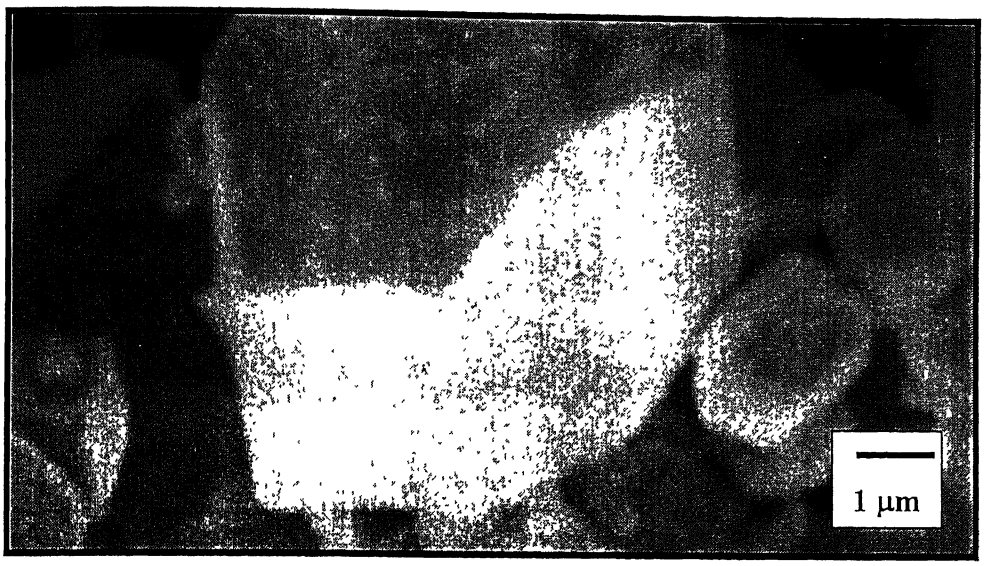

Figure 4.5: SEM micrograph of tungsten powder

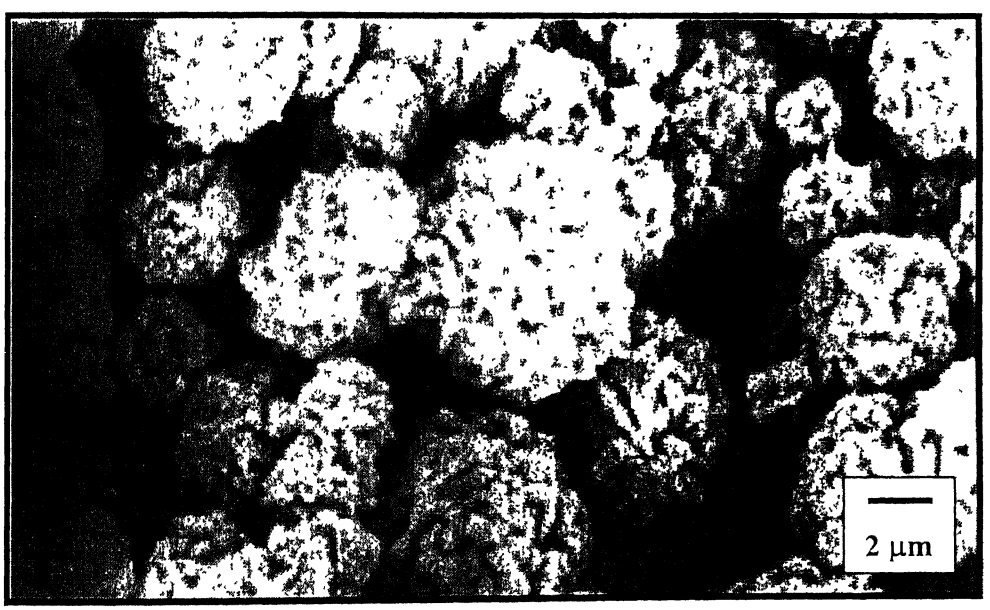

Figure 4.6: SEM micrograph of nickel powder

Figure 4.7: SEM micrograph of iron powder

Figure 4.8: SEM micrograph of cobalt powder.

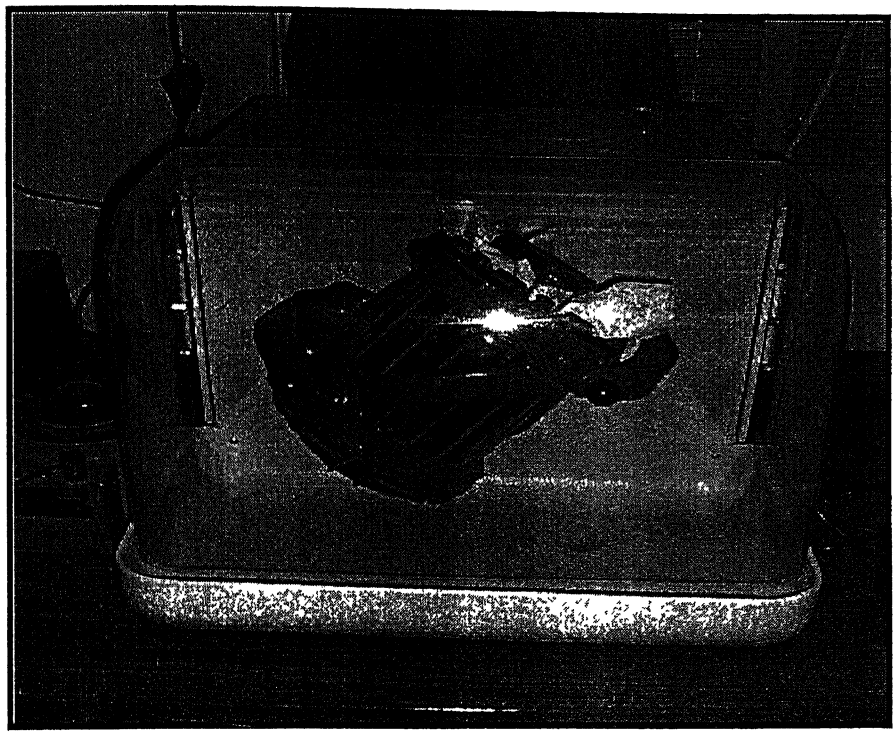

Figure 4.9: Turbula Mixer

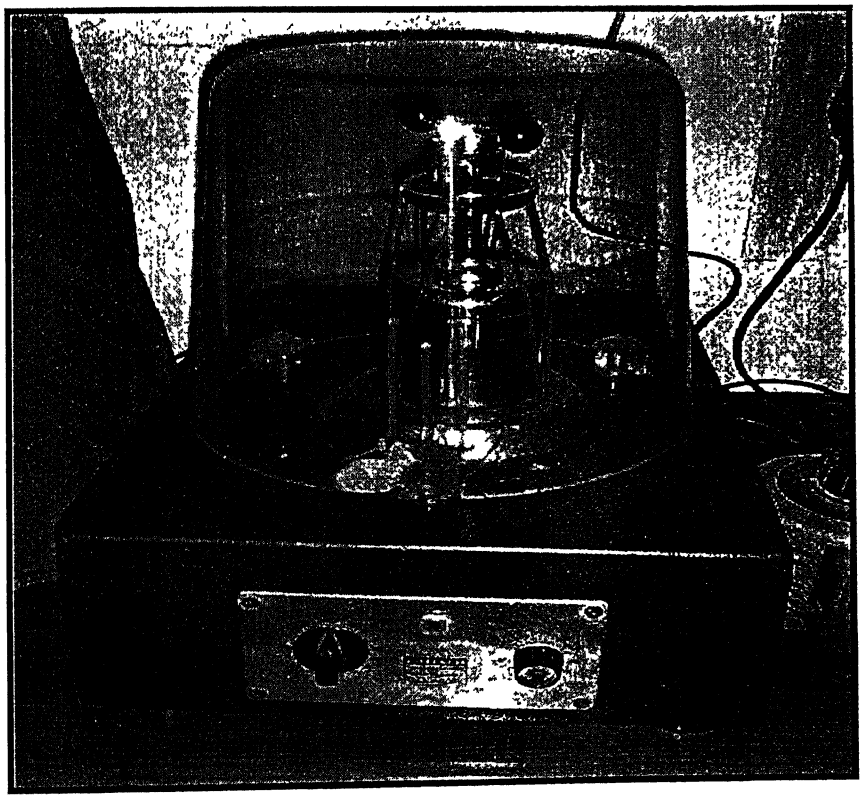

Figure 4.10: Ball mill.

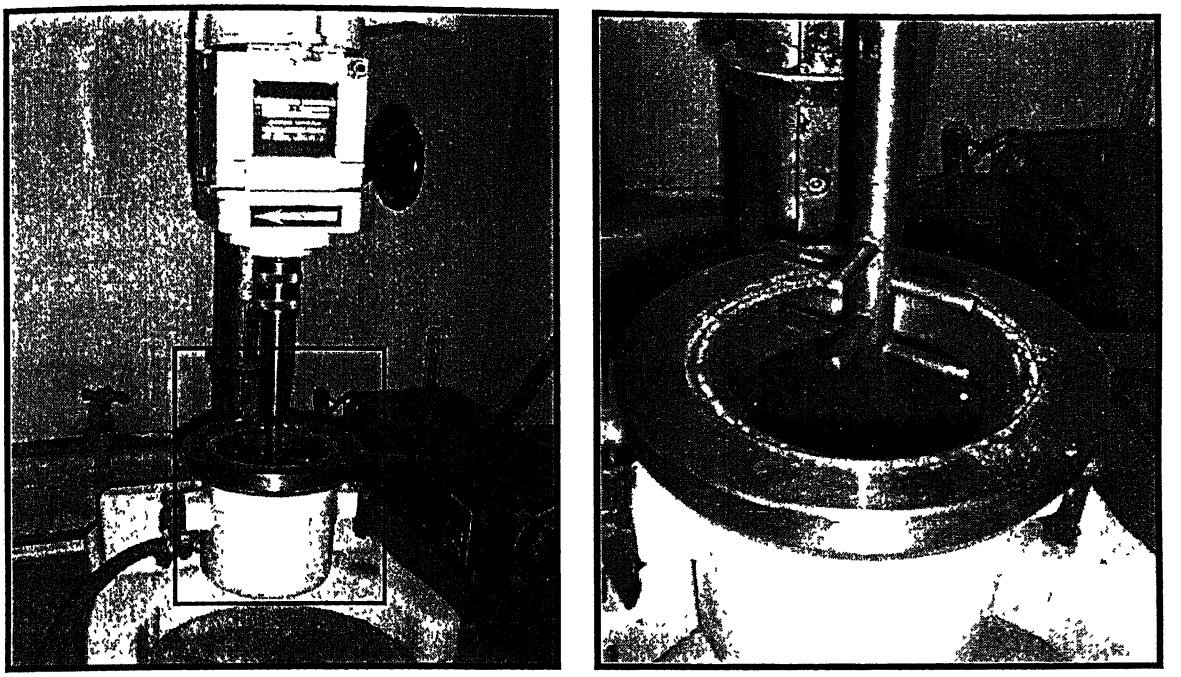

(a) (b)

Figure 4.11: Attritor mill (a) whole mill assembly and (b) Area in inset in first picture.

Figure 4.12: Tempo oven

4.4 Compaction

A die of 12.7 mm inner diameter was used for making green compacts of cylindrical shape. The pressure applied was uniaxially i.e. in one direction using a semi-automatic hydraulic press (Model: CTM 50) of 50 T capacity (Figure 4.13). The pressure applied was 200 MPa for making all the cylindrical compacts. A floating die was used for compacting tensile samples (Figure 4.14). Figure 4.15 shows the standard specifications of tensile samples by Metal Powder Industries Federation, USA. Samples according to specifications were prepared for this study. The dies were made of high chromium high carbon steel for making all the cylindrical compacts. The dies were cleaned with acetone during compaction. Zinc-stearate was used as die wall lubricant in powder and spray form during compaction, which facilitated compaction and subsequent removal of compacted samples. Die wall lubricants usually do not work satisfactorily and resulted in delamination of milled powders. Therefore solid lubricants are being admixed to the metal powder [37]. Added to the wall lubrication powder lubricant was used. For consolidation of milled powders 2wt% and 3.5wt% acrawax was used as lubricant for cylindrical and tensile samples respectively.

4.5 Debinding/Pre-sintering

Debinding/Pre-sintering of green compacts having acrawax was carried out in a tubular type, SiC-heated horizontal furnace (rating 1.5 kVA, Figure 4.16). The tube of the furnace was made up of doubly recrystallized alumina with an inner diameter of 38 mm and length of 980 mm. The furnace possessed a heating zone approximately 105 mm, with a capacity to attain 1400°C with an accuracy of ±3°C. The atmosphere used for debinding was reducing (H_2, Dew point –35°C), to prevent the samples from oxidation. For cylindrical samples debinding was carried out at 450°C for 1 h. Tensile sample were pre-sintered at 900°C for debinding and to provide enough strength for handling. The green samples were placed inside the furnace by means of alumina boat. The alumina boat was used because it possess higher melting point and doesn't contaminate samples. It also prevents sticking of samples after sintering. Both the ends of alumina tube was sealed using a SILASTC (RVT 700) adhesive/sealant to prevent leakage of hydrogen

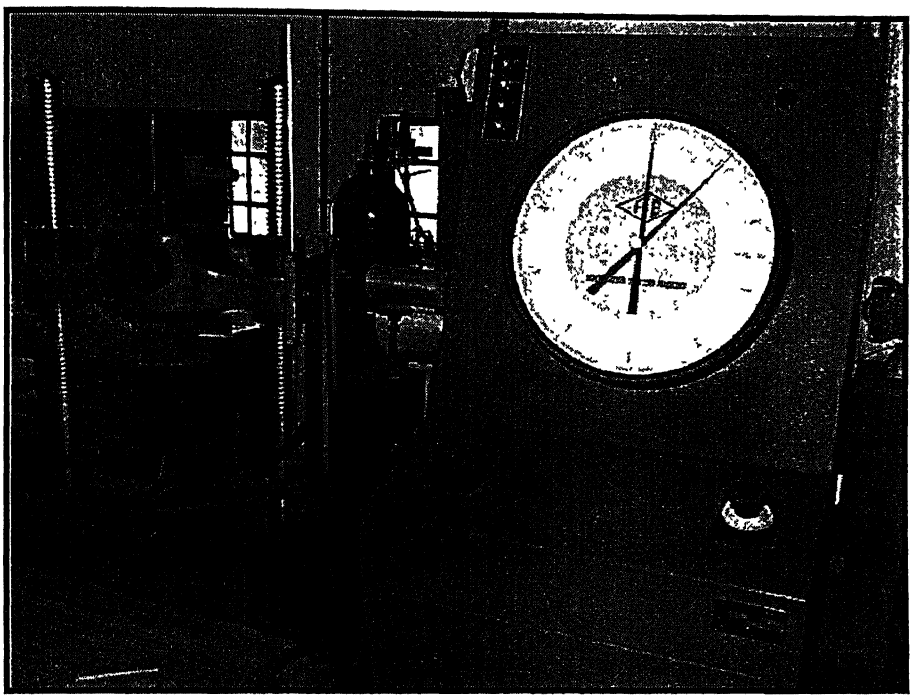

Figure 4.13: Hydraulic press.

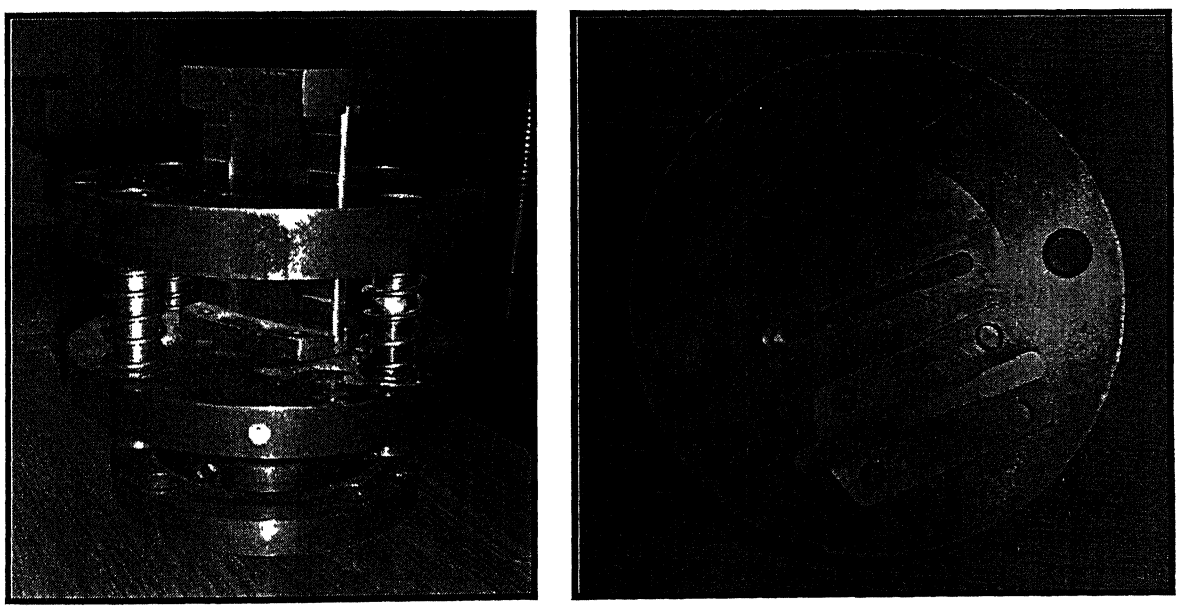

(a) (b)

Figure 4.14: Floating die (a) Front view and (b) Top view.

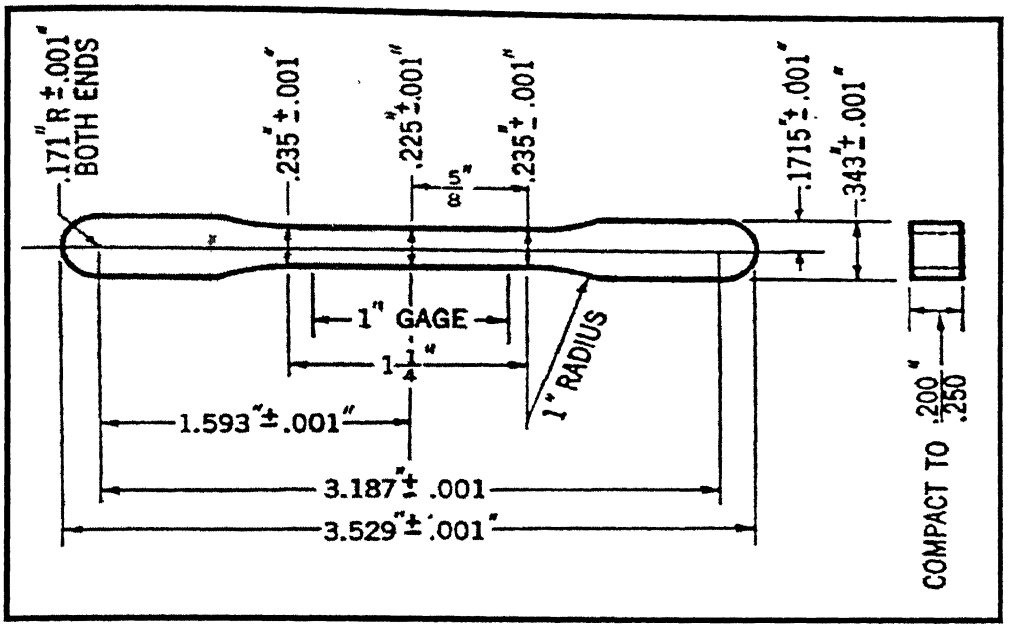

Figure 4.15: Flat unmachined tensile baar, pressure area 1 0 sq. in. (dimensions specified are those of the compacts when in the die).

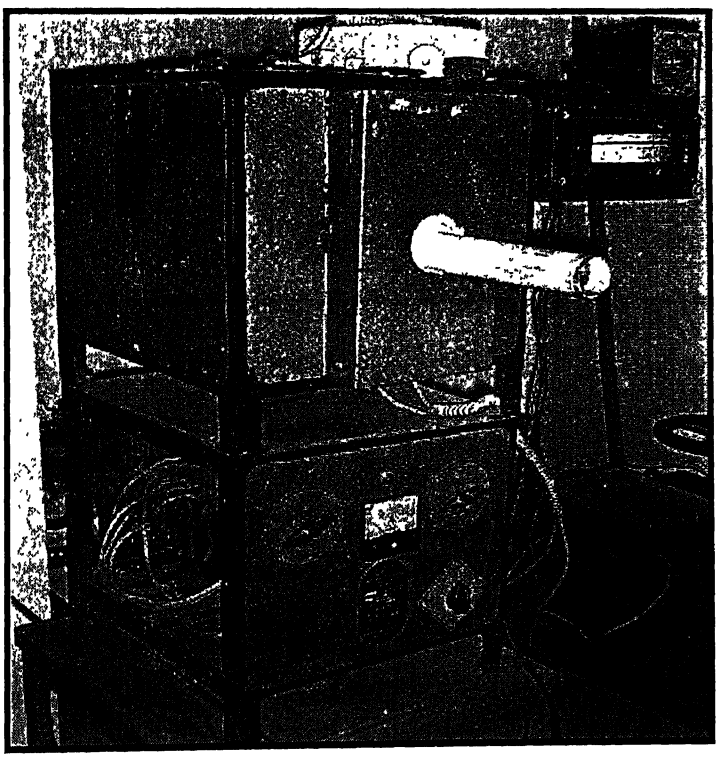

Figure 4.16: Debinding furnace.

during sintering. The heating rate was maintained at 5°C/min for all the samples. An automatic temperature controller was used to monitor the temperature. After soaking for 1 hour at desired temperatures, all the samples were furnace cooled. Hydrogen atmosphere was maintained up to 200°C during cooling to prevent oxidation.

4.6 Sintering

Sintering of green/debound samples was carried out in a $MoSi_2$ (superKanthal) heated, automatic programmable tubular furnace (OKAY, MODEL 70T4, Figure 4.17) The schematic diagram of the tubular furnace is shown in Figure 4.18. The tube of this furnace was also made up of doubly recrystallized alumina with inner diameter of 38 mm and length 980 mm. This furnace possessed a heating zone approximately 110 mm, with a capacity to attain 1700°C with an accuracy of ±3°C. Sintering was carried out at two different temperatures, which were 1400 and 1500°C for solid-state and liquid phase sintering respectively. Reducing atmosphere was maintained with the help of commercially pure dry hydrogen (Dew point, -35°C). Same alumina boat was used in this furnace also. Figure 4.19 shows the sintering cycle followed for solid-state and liquid phase sintering. Samples were heated to required temperature after holding at 1000°C for 1 h. This soaking was done to attain temperature homogenization in the sample and to provide enough time for reduction of oxide layer formed on the powder particles. The samples were allowed to cool in the furnace itself and the hydrogen atmosphere was maintained up to 200°C to prevent oxidation during cooling.

4.7 Post Sintering Heat-treatment

Post sintering heat-treatment of tensile samples were carried out at 1000°C for 15 min in the same $MoSi_2$ heated horizontal tubular furnace. Heating rate was maintained 10°C/min. Inert atmosphere was maintained with the help of commercially pure argon. This treatment was carried out for removal of hydrogen embrittlement. Argon atmosphere was maintained up to 150°C during cooling to avoid oxidation of samples.

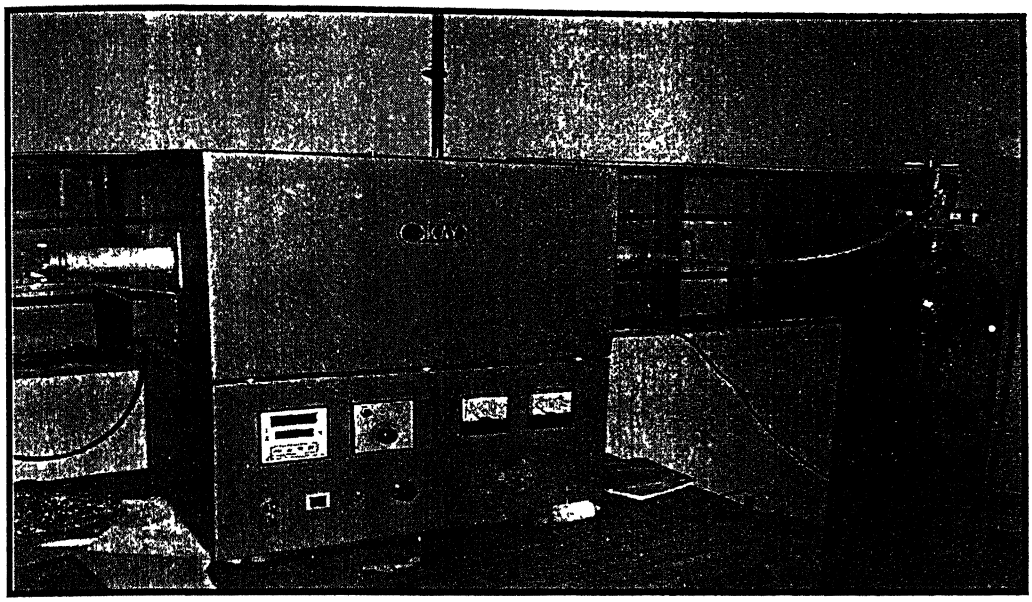

Figure 4.17: $MoSi_2$ (superKanthal)heated, automatic programmable tubular furnace

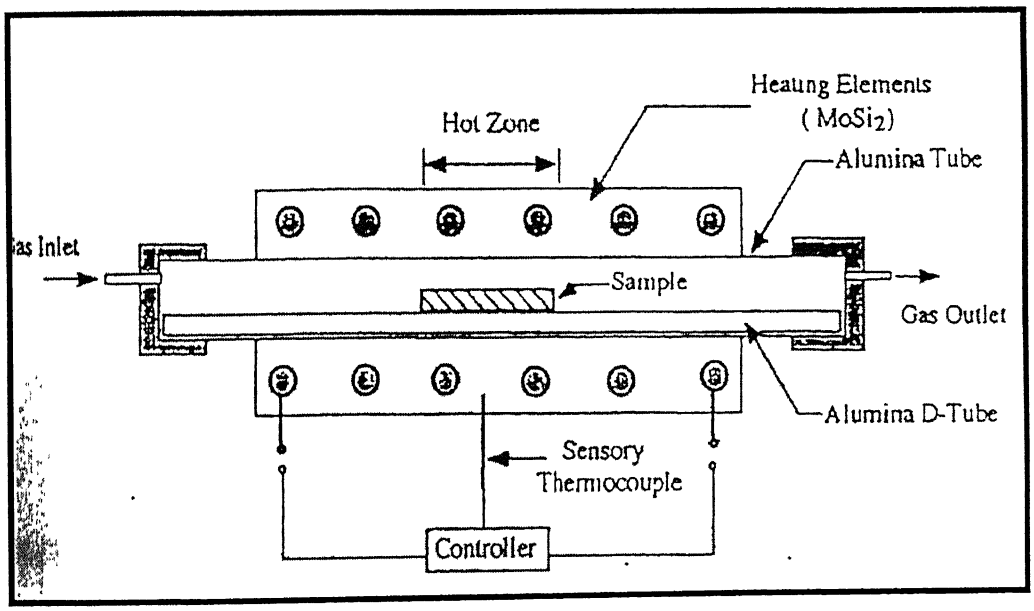

Figure 4.18: Schematic diagram of $MoSi_2$ heated horizontal tubular furnace.

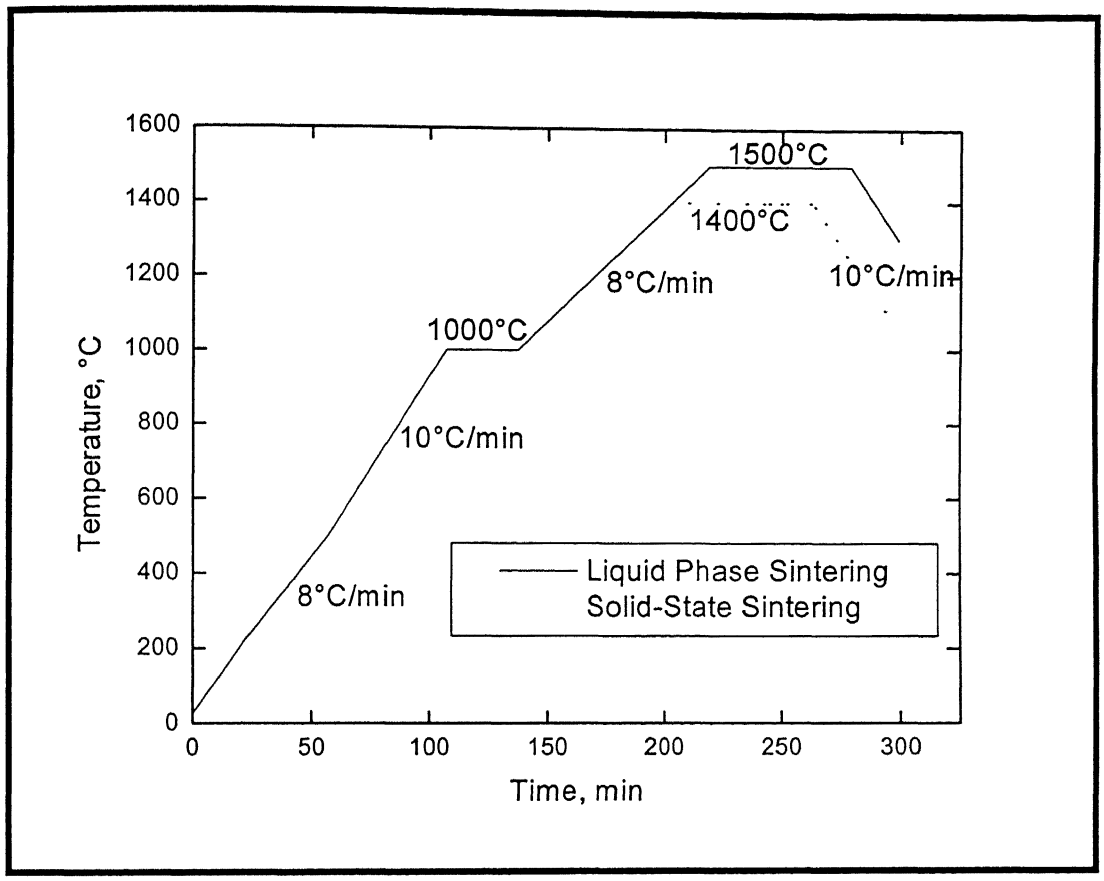

Figure 4.19: Sintering cycles followed for solid-state and liquid phase sintering.

4.8 Densification Behavior *(Sintered Theoretical Density and Densification Parameter)*

The densities of cylindrical green compacts and sintered compacts were determined through dimensional measurements. The Sintered densities were also measured by Archimedes method as well. An analytical balance (*Metller H31AR*) was used for all the measurements. Density was calculated using following formula:

$$\rho_S = \frac{W_{SA}}{W_{SA} - W_{SW}} \qquad \text{..... (4.1)}$$

where, ρ_S is the relative density of the sample, W_{SA} is the weight of the sample in air; W_{SW} is the weight of the sample in the water.

The theoretical density of the compositions was calculated using the inverse rule of mixing as per the formula given

$$\frac{1}{\rho_{th}} = \frac{w_1}{\rho_1} + \frac{w_2}{\rho_2} + \frac{w_3}{\rho_3} \qquad \text{..... (4.2)}$$

where w_1, w_2, and w_3 are the weight fractions and ρ_1, ρ_2, and ρ_3 are the theoretical densities of individual components. ρ_{th} is the theoretical density of the mixture. This simple formula however assumes that the individual components do not react and or not soluble in each other [18].

Densification parameter *(Ψ)* was also calculated by equation 4.3

$$\psi = \frac{\rho_s - \rho_g}{\rho_{th} - \rho_g} \qquad \text{..... (4.3)}$$

where ρ_g, ρ_s, and ρ_{th} are green density, sintered density and theoretical density, respectively.

4.9 Microstructural Studies

Since tungsten heavy alloys have enough contrast in micrographs without etching, so all the optical micrographs were taken in unetched condition. Scanning electron micrographs of elemental powders and milled powders were also taken.

The volume fraction of the matrix, dihedral angle, contiguity, connectivity, interfacial surface area of tungsten matrix per unit volume, and average tungsten spheroid size were characterized by microstructural analysis by LEICA@500IW image analyzer.

4.9.1 Pore Fraction and Average Pore Size

Pore fraction and average pore size calculation for solid-state sintered specimens were done automatically with the help of LEICA@500IW image analyzer.

4.9.2 Volume Fraction of Matrix

Volume fractions of matrix were calculated with the help of same image analyzer, semi-automatically. For this calculation grids shown as in Figure 4.20 was superimposed on the micrographs. By finding the ratio of intersections falling on a particular phase with total number of intersections, volume fraction of that particular phase can be calculated. Same procedure was applied in the present study. For accuracy same procedure was repeated in 30 fields of views of the same sample, and mean was considered as final result.

4.9.3 Dihedral Angle, (φ)

The angle formed by grain boundary with liquid during sintering is called dihedral angle [14]. A dihedral angle is shown in Figure 4.21. Dihedral calculation was done by measuring 200 angles on a micrograph. After measuring angles, a plot was drawn between percentage cumulative versus dihedral angle, and the angle corresponding to median value was determined of that particular alloy.

4.9.4 Contiguity and Connectivity

The contiguity factor which is a microstructural measure of the relative interface area of solid-solid bonds versus the total interface area during liquid phase sintering, was calculated using the well-known formula [38]

$$C_{ss} = \frac{2N_{SS}}{2N_{SS} + N_{SL}} \qquad \text{.....} \qquad (4.4)$$

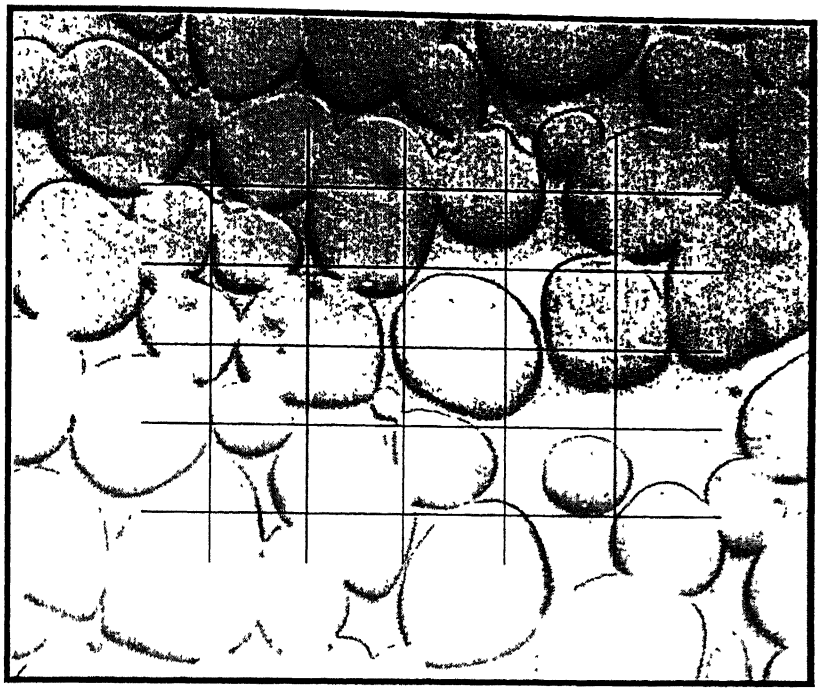

Figure 4.20: Superimposing grid on a micrograph for calculation of volume fraction of a particular phase of interest.

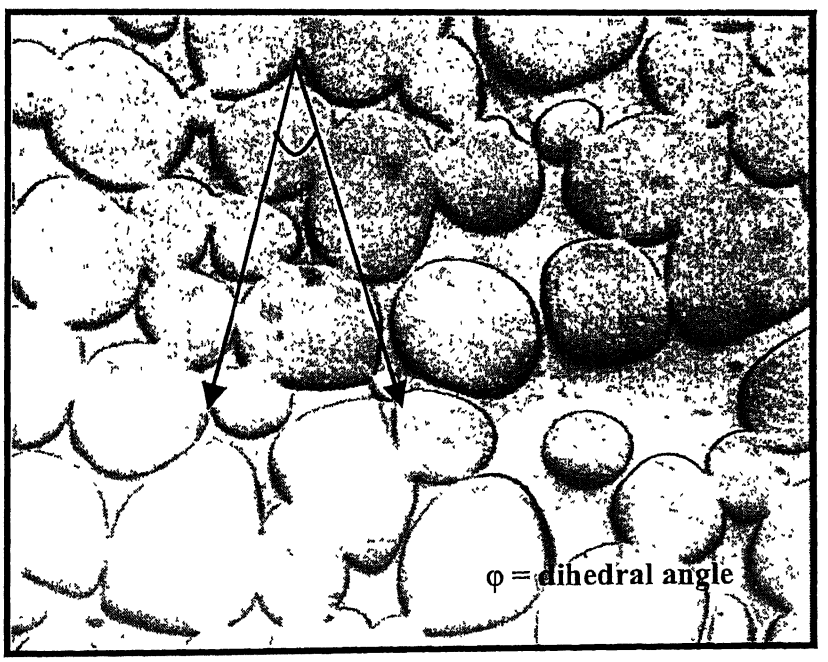

Figure 4.21 Dihedral angle Measurement.

where N_{SS} is the number of tungsten-tungsten contacts per unit length of any given intercept, N_{SL} is the number of tungsten-matrix contacts per unit length of given intercept. The same calculation was done on thirty fields of views of a particular alloy of interest, and mean was taken as contiguity factor of that particular alloy. Connectivity is number of touching nearest grains for a given grain. The connectivity calculation was done by counting the number of nearest touching grains for 200 chosen grains in a micrograph of a alloy of interest; and mean was taken as connectivity of that particular alloy.

4.9.5 Interface Area of Tungsten/Matrix Per Unit Volume, (S_{WM})

Interface area of tungsten/matrix per unit volume (S_{WM}) is calculated by equation 4.5

$$S_{WM} = \frac{2X}{NL} \qquad \ldots\ldots\ldots\ldots\ldots \quad (4.5)$$

where X is the number of tungsten matrix interface counted in given intercepts, N is the number of intercepts and L is the length of the intercept. Average value of 30 reading was taken to reduce the error.

4.9.6 Grain Size

Grain size calculation was done by equation 4.6

$$G = \frac{4V_W}{S_{WW} + S_{WM}} \qquad \ldots\ldots\ldots\ldots\ldots \quad (4.6)$$

where G is grain size, V_W is volume fraction of tungsten in observed microstructure, S_{WW} is interfacial area of tungsten/tungsten grains per unit volume, and S_{WM} is interfacial area of tungsten/matrix per unit volume.

4.10 Mechanical Properties

Bulk hardness, micro hardness, strength and ductility (%elongation) calculations were done in the present study.

4.10.1 Bulk Hardness

Bulk hardness values of sintered compacts were measured by LECO V-100-C1 Vickers hardness tester (Figure at 4.22) 30 kg load. A diamond pyramid indenter was used. The load was applied for 15 s. The indentation observed under attached microscope was square shaped. The length of diagonals of the square indentation was measured. The tester itself calibrated the Vickers Hardness (HV) by using the value taken of diagonals.

4.10.2 Micro-hardness

Leitz 8299 micro-hardness tester (Figure 4.23) was used to perform the micro-hardness tests. Test was performed on the tungsten grains and matrix phase. The load used for indentation was 5 g and 50 g for matrix and tungsten spheroid respectively. The load was applied for 15 s. the indentation was square shaped. Diagonal length of square was measured by scale attached on the microscope. Hardness was obtained, directly from the chart given in manual for corresponding load and diagonal length.

4.10.3 Strength and Ductility

Tensile samples were compacted according to specifications shown in Figure 4.15. These samples were liquid phase sintered at 1500°C. After sintering heat treatment was done at 1000°C for 15 min in Ar atmosphere. Tensile test was performed on Sintered flat samples in universal testing machine.

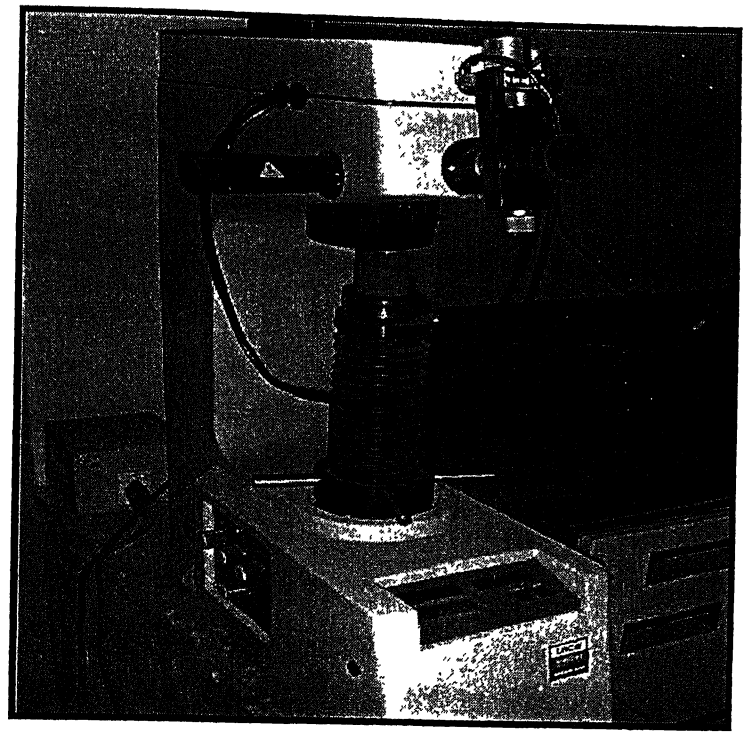

Figure 4.22: LECO V-100-C1 Vickers macrohardness tester.

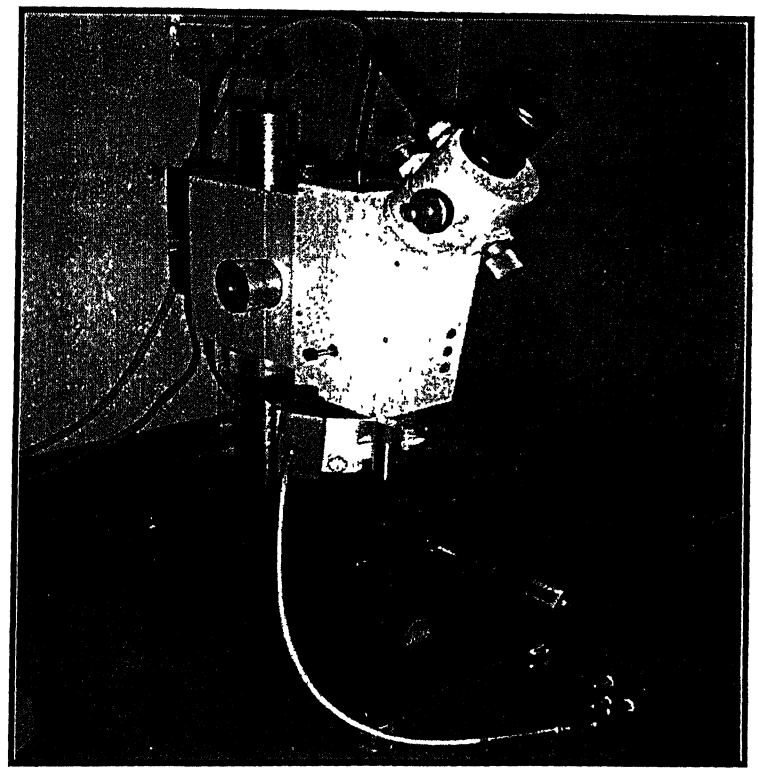

Figure 4.23: Leitz 8299 micro-hardness tester.

Chapter 5

EXPERIMENTAL RESULTS

5.1 Particle Size and Size Distribution

Particle size analysis of mixed, ball milled and attritor milled powders was done. Results of particle size analysis are summarized in Table 5.1.

Table 5.1: Results of particle size analysis

Compositions		Particle Size (μm)		
		Mixed	Ball Milled	Attritor Milled
92.5W (fine)-6.15Ni-1.1Fe-0.25Co	D_{10}	3.5	2 5	1.8
	D_{50}	8.2	5.9	5.0
	D_{90}	17.0	14.3	9.6
95.1W (fine)-3.45Ni-1.45Fe	D_{10}	2.4	2.4	2.3
	D_{50}	7.2	5.6	5.2
	D_{90}	19.9	10.4	8.8
92.5W (coarse)-6.15Ni-1.1Fe-0.25Co	D_{10}	6.58	4.4	3.3
	D_{50}	15.4	6.8	8.7
	D_{90}	31.6	10.43	17.6
95.1W (coarse)-3.45Ni-1.45Fe	D_{10}	4.4	5.1	4.5
	D_{50}	11 6	8.2	9.7
	D_{90}	29.3	10.3	20.2

It is clear from the Table 5.1 that average particle size reduced due to milling. In case of attritor milling average particle size was minimum.

Figures 5.1 to 5.12 show that average particle size of powders of chosen compositions for this study, reduced due to milling. Range of particle size also reduces. In case of mixed powder the range of particle size was very wide, but after milling range became narrower.

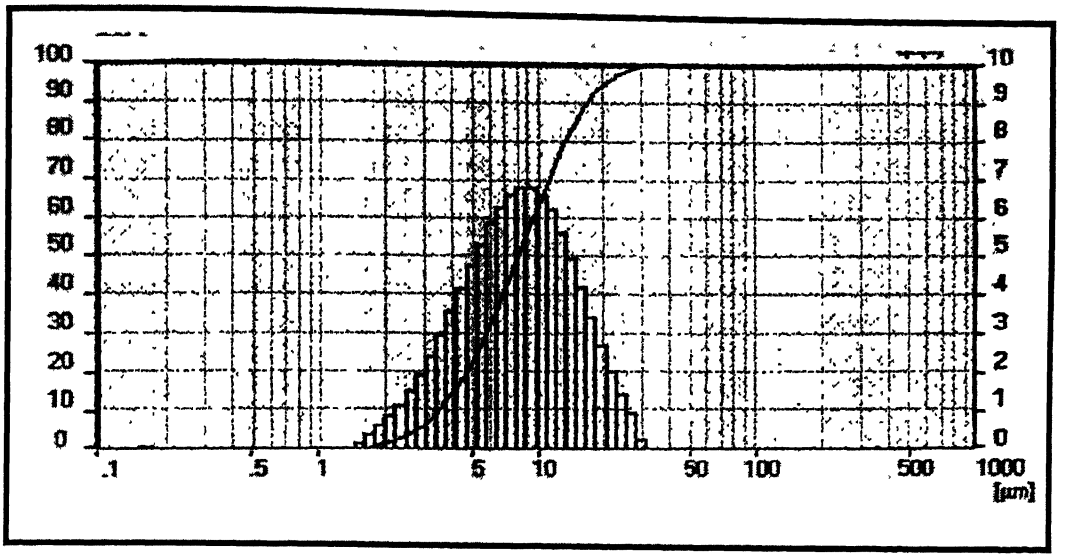

Figure 5.1: Particle size distribution curve of 92.5W (fine)-6.15Ni-1.1Fe-0.25Co (all wt%), mixed powders.

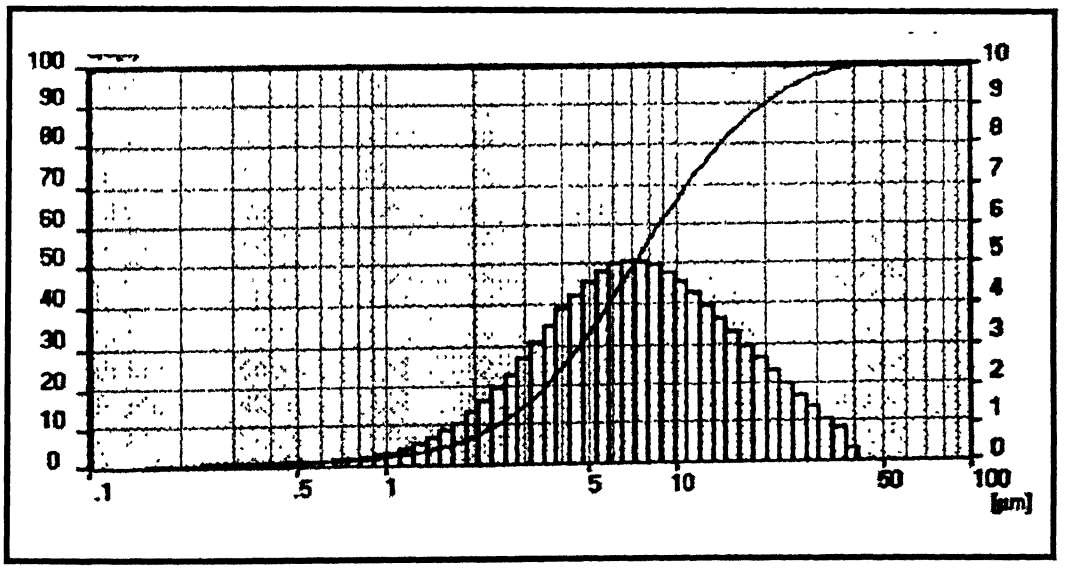

Figure 5.2: Particle size distribution curve of 95.1W (fine)-3.45Ni-1.45Fe (all wt%), mixed powders.

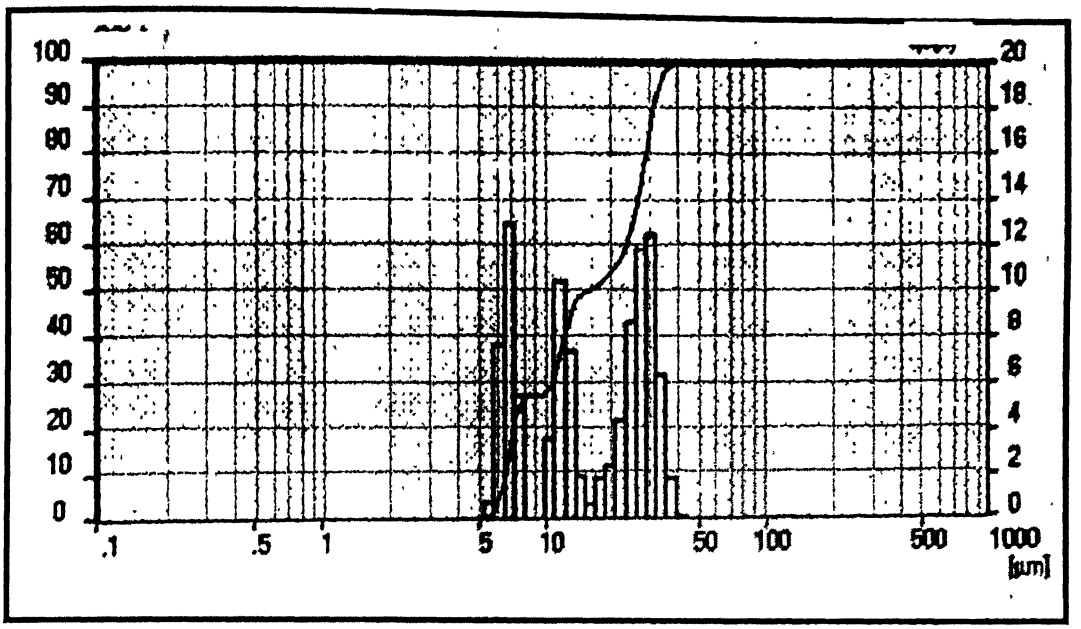

Figure 5.3: Particle size distribution curve of 92 5W (coarse)-6.15Ni-1.1Fe-0.25Co (all wt%), mixed powders

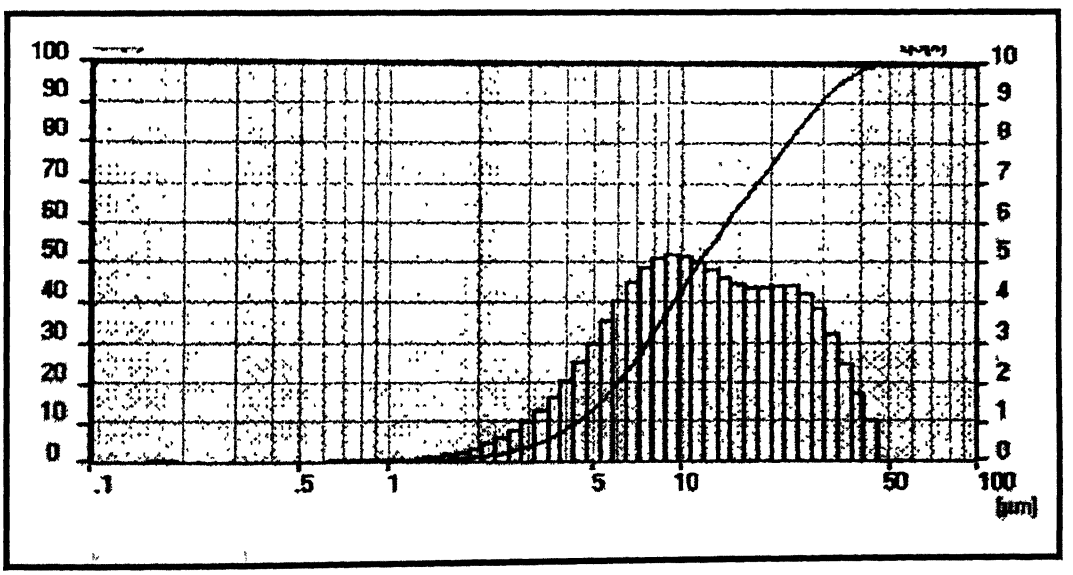

Figure 5.4: Particle size distribution curve of 95.1W (coarse)-3.45Ni-1.45Fe (all wt%), mixed powders.

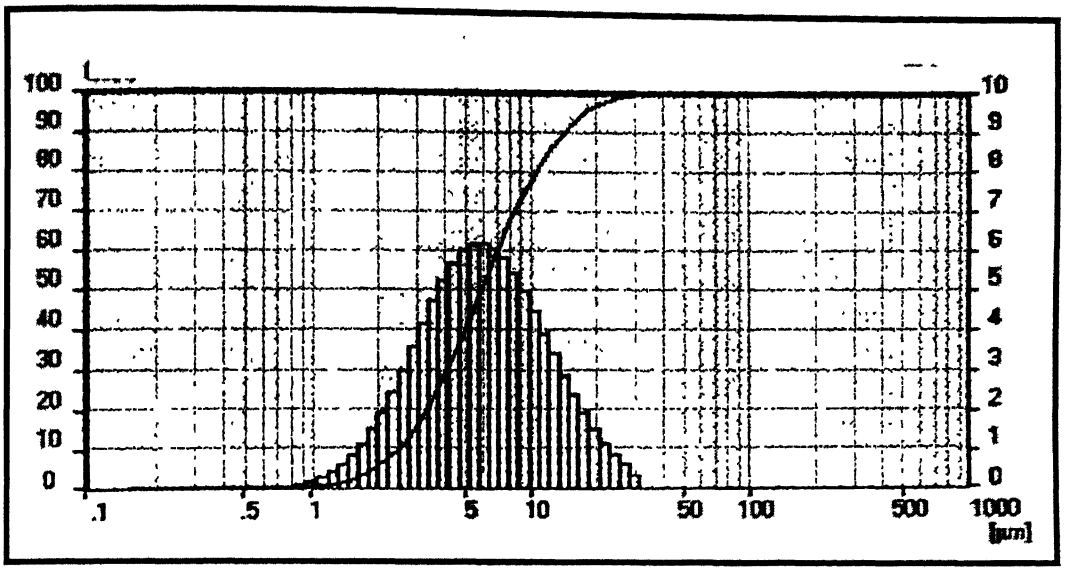

Figure 5.5: Particle size distribution curve of 92.5W (fine)-6.15Ni-1.1Fe-0 25Co (all wt%), ball milled powders.

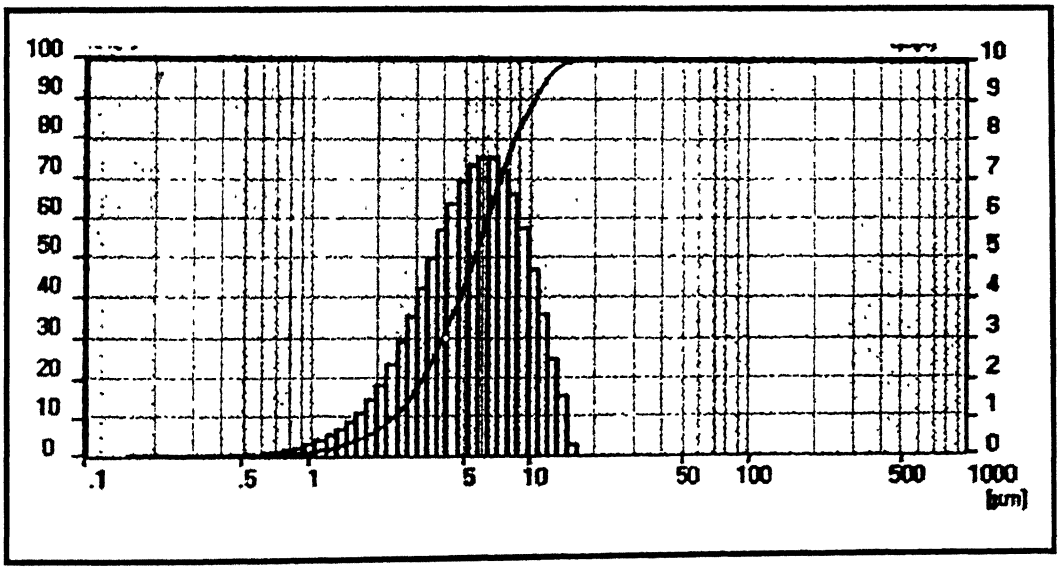

Figure 5.6: Particle size distribution curve of 95 1W (fine)-3 45Ni-1 45Fe (all wt%), ball milled powders.

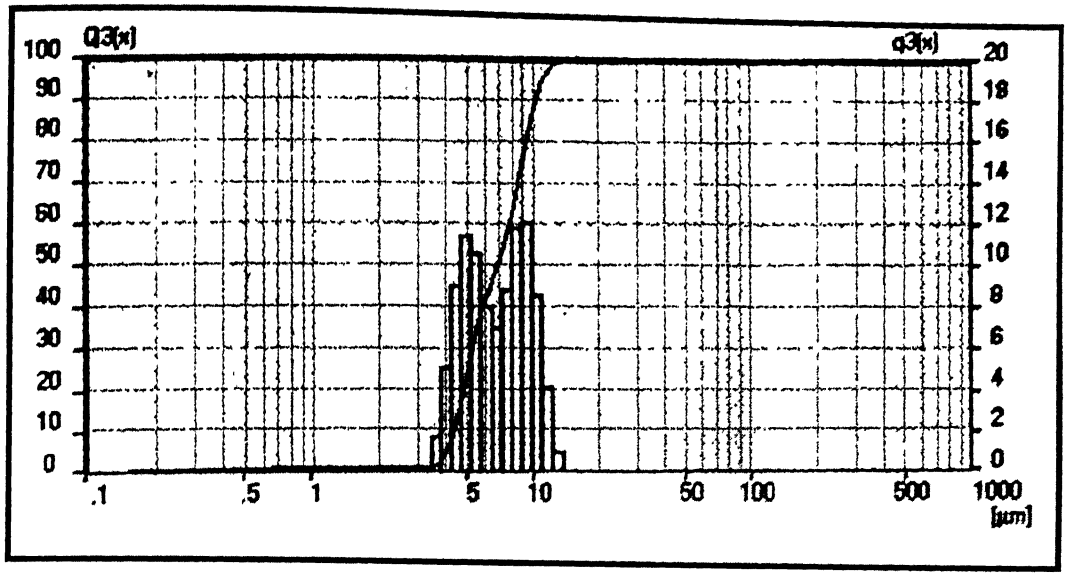

Figure 5.7: Particle size distribution curve of 92.5W (coarse)-6.15Ni-1.1Fe-0.25Co (all wt%), ball milled powders

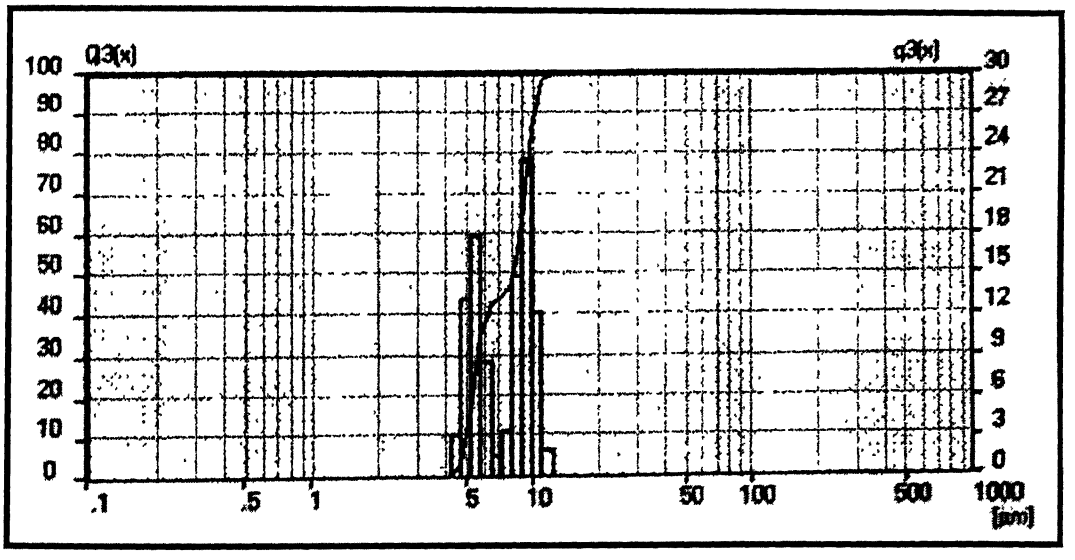

Figure 5.8: Particle size distribution curve of 95.1W (coarse)-3.45Ni-1.45Fe (all wt%), ball milled powders.

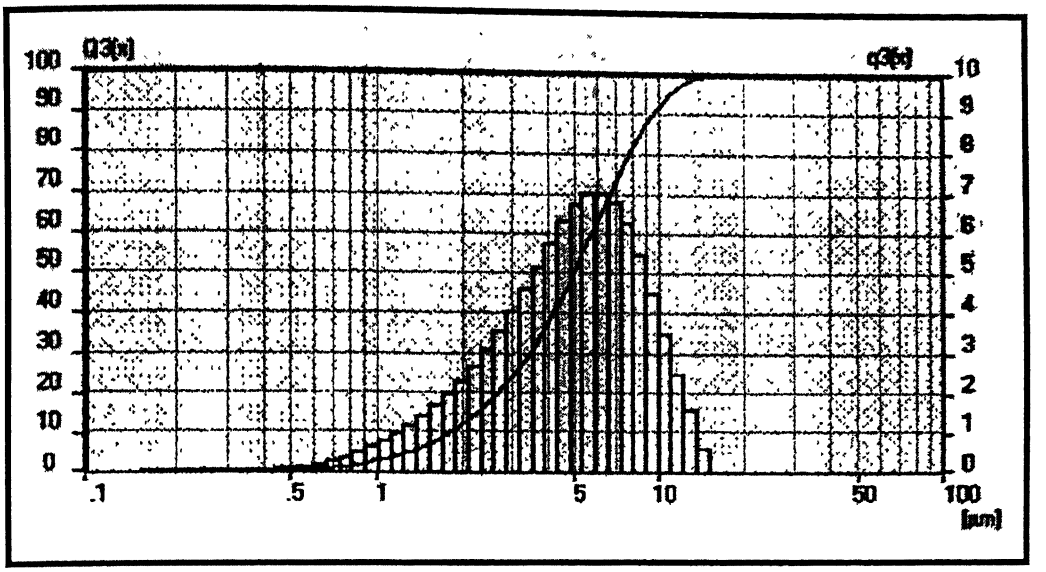

Figure 5.9: Particle size distribution curve of 92.5W (fine)-6.15Ni-1.1Fe-0.25Co (all wt%), attritor milled powders.

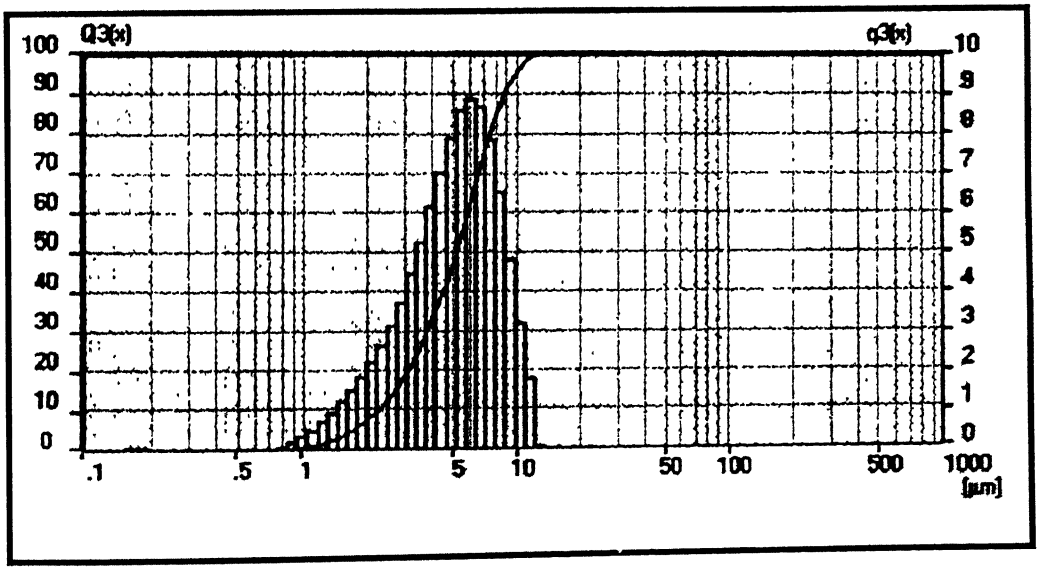

Figure 5.10: Particle size distribution curve of 95.1W (fine)-3.45Ni-1.45Fe (all wt%), attritor milled powders.

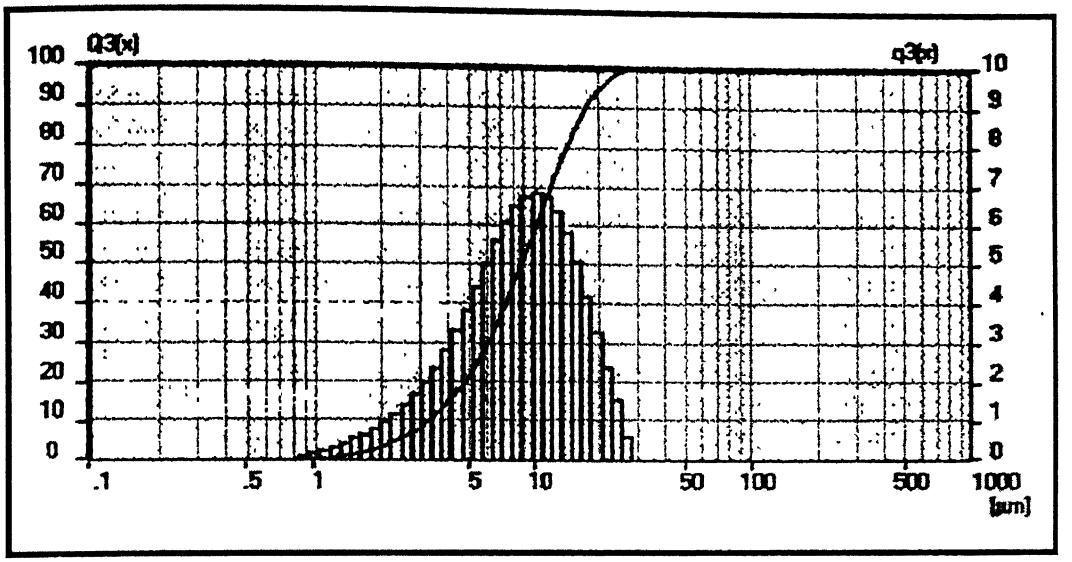

Figure 5.11: Particle size distribution curve of 92.5W (coarse)-6.15Ni-1.1Fe-0.25Co (all wt%), attritor milled powders.

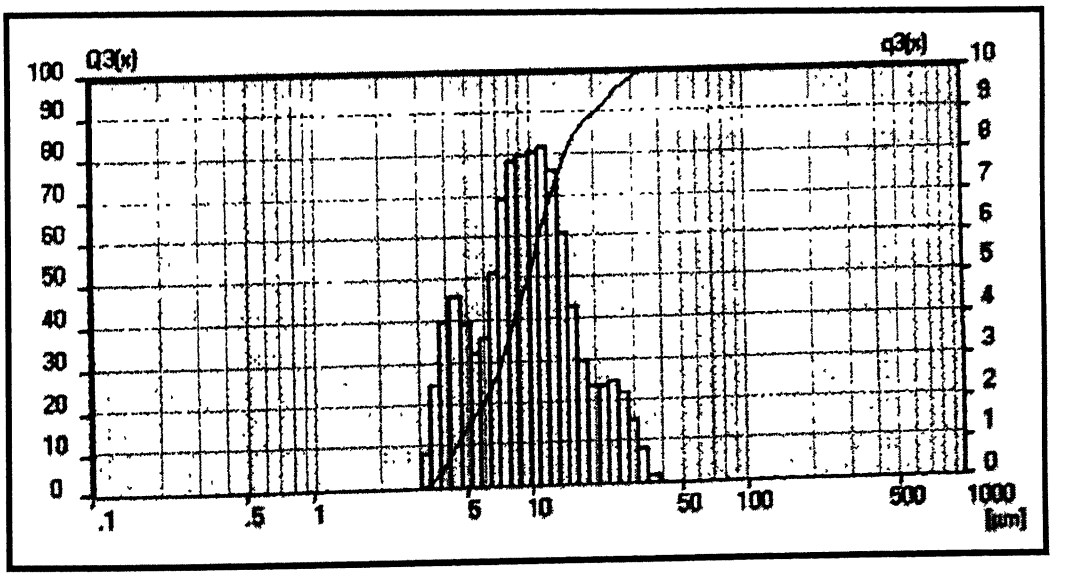

Figure 5.12: Particle size distribution curve of 95.1W (coarse)-3.45Ni-1.45Fe (all wt%), attritor milled powders.

5.2 Milling

As it is clear from Figure 4.5 to 4.8 that elemental powders used for present study have their distinct morphology. In the mixed form they retained their morphology as shown in Figure 5.13. It was observed that due to milling fragmentation and proper mixing of these powders occurred, and it was difficult to distinguish them on the basis of their distinct morphology. Figures 5.14 and 5.15 show the scanning electron micrographs of ball milled and attritor milled powders respectively.

It is clear from Figure 5.16 that powders became flaky due to attritor milling. It is also clear from Figure 5.17 that due to milling ductile powders (Ni and Fe) welded up with hard tungsten particles.

5.3 Effect of Milling on Green Density

Figure 5.18 shows the results of percentage theoretical density calculations of green cylindrical samples prepared by mixed, ball-milled and attritor-milled powders. It was observed that samples prepared by finer powders and higher tungsten content, posses lower percentage theoretical density. It was also observed that the samples prepared by milled powders posses lower green density in comparison to samples prepared by mixed powders. In case of attritor milled powder, green density was lowest.

5.4 Density and Densification Parameter

Figure 5.19 shows the comparison of sintered density achieved by solid-state sintering of mixed, ball milled and attritor milled powder compacts. Figure 5.20 shows the comparison of densification parameters of the same. It was observed that percentage theoretical density and densification parameter of solid-state sintered compacts was higher in case of milled powders. It was observed that Percentage theoretical density and densification parameter were highest in case of compacts prepared by attritor milled powders. Full densification was achieved in case of attritor milled powder with finer tungsten powder by solid-state sintering.

Figure 5.21 and Figure 5.22 show the comparison of sintered density and densification parameters respectively, of liquid phase sintered compacts, prepared by mixed, ball milled and attritor milled powders. The result pattern was same, as it was

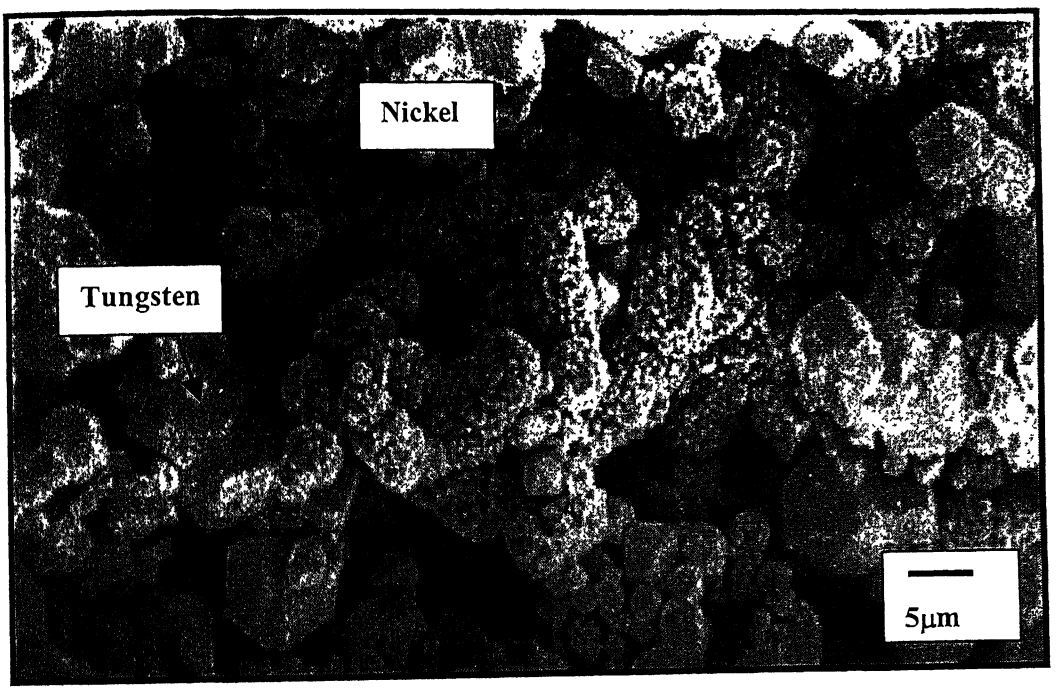

Figure 5.13: Scanning electron micrograph of mixed powders.

Figure 5.14: Scanning electron micrograph of 95.1W (coarse)-3.45Ni-1.45Fe ball milled powders.

Figure 5.15: Scanning electron micrograph of 95.1W (coarse)-3.45Ni-1.45Fe attritor milled powder.

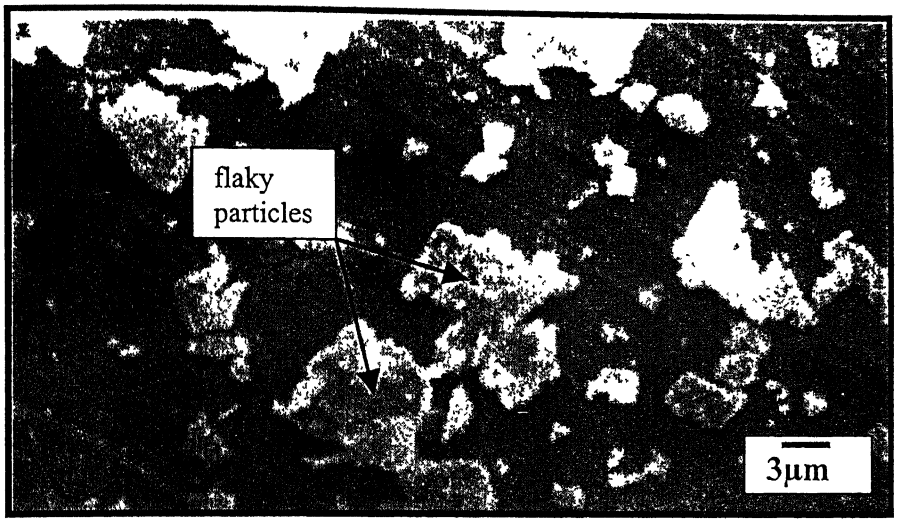

Figure 5.16: Effect of attritor milling on morphology of mixed powder of 95.1W(fine)-3.45Ni-1.45Fe composition

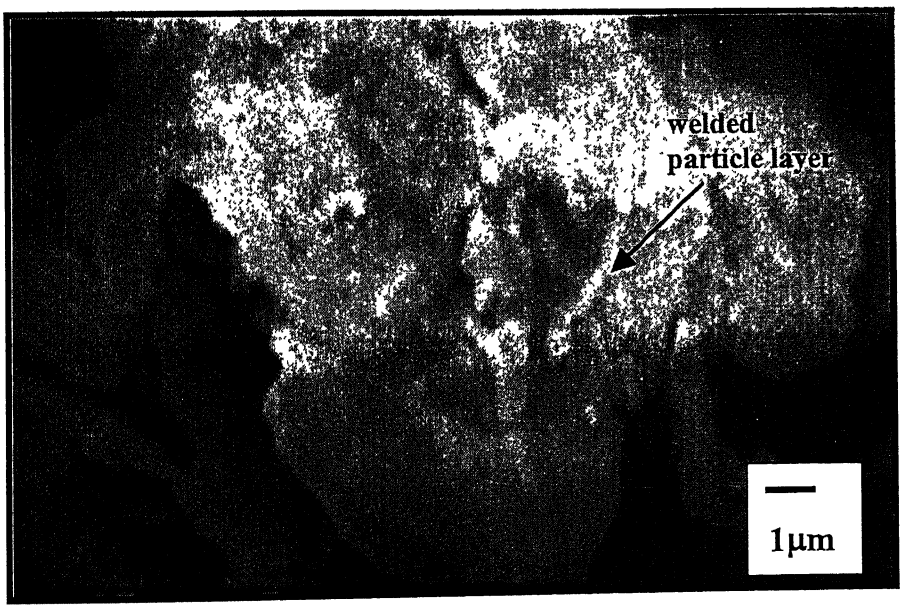

Figure 5.17: Welded layer formation on tungsten powders.

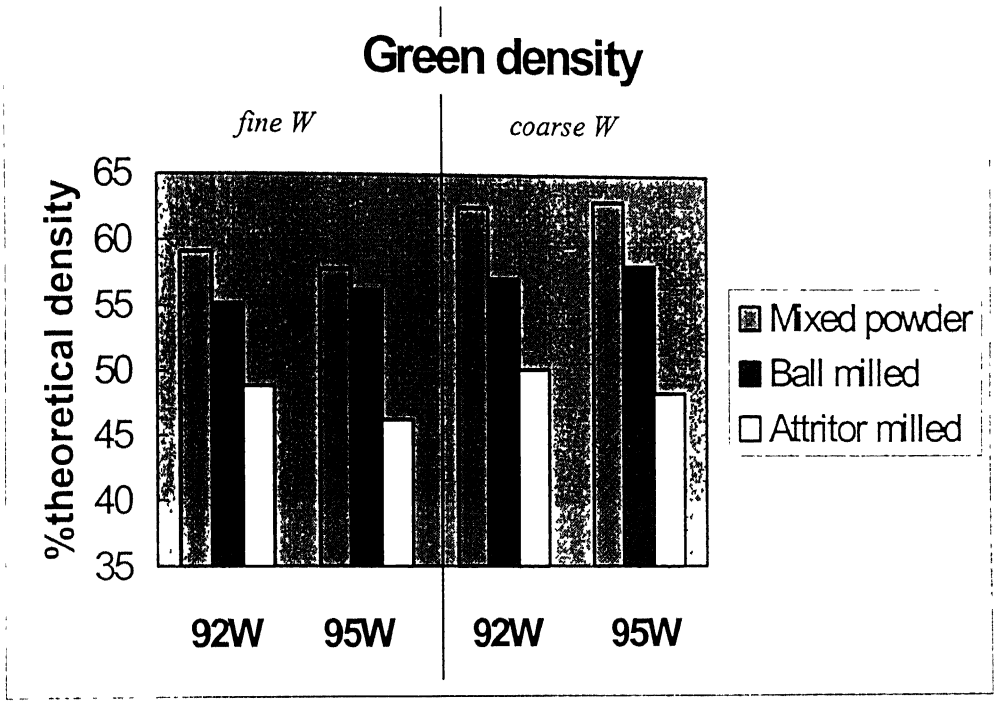

Figure 5.18: Comparison of percentage theoretical density of green samples prepared by mixed, ball milled and attritor milled powders.

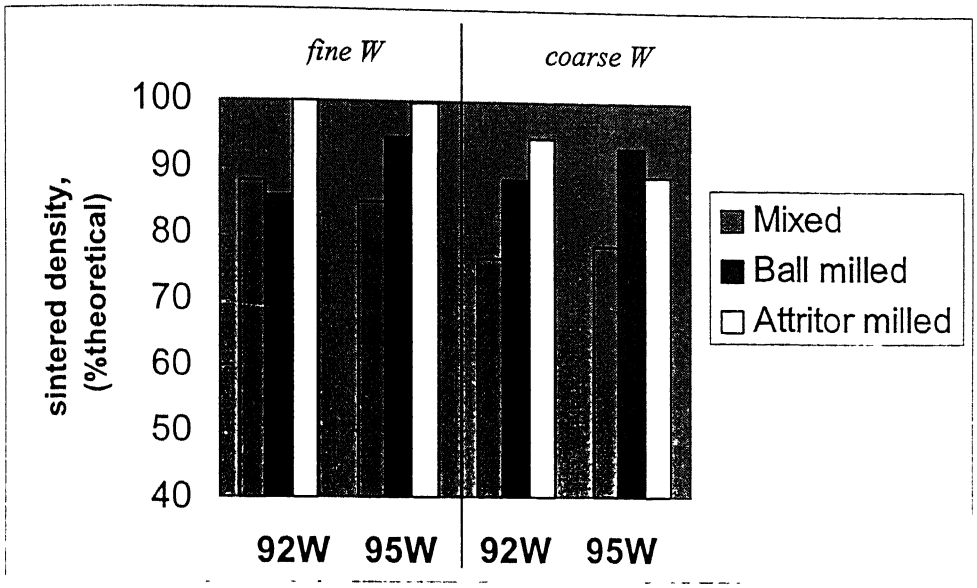

Figure 5.19: Comparison of percentage theoretical sintered density of solid-state sintered mixed, and milled powders.

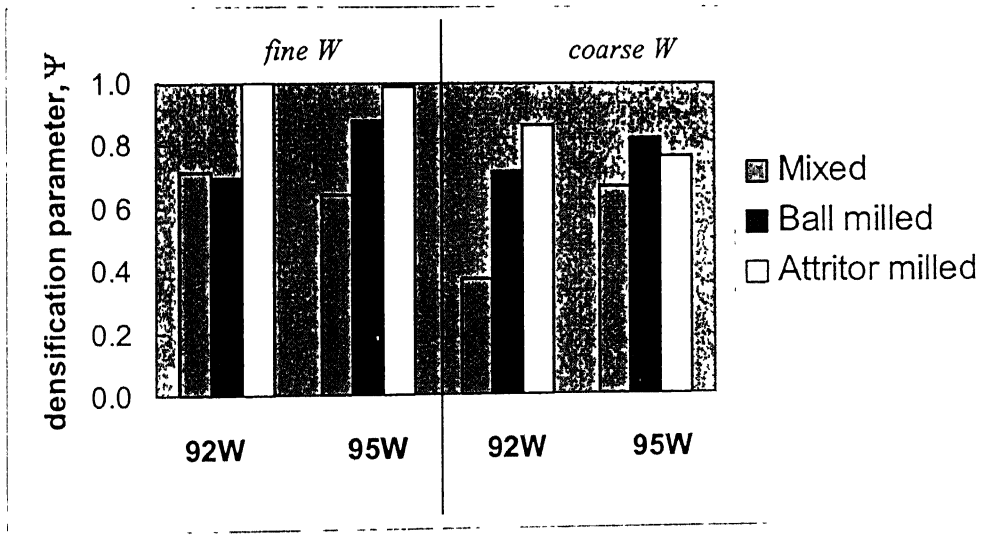

Figure 5.20: Comparison of densification parameter of solid-state sintered mixed, ball and attritor milled powders.

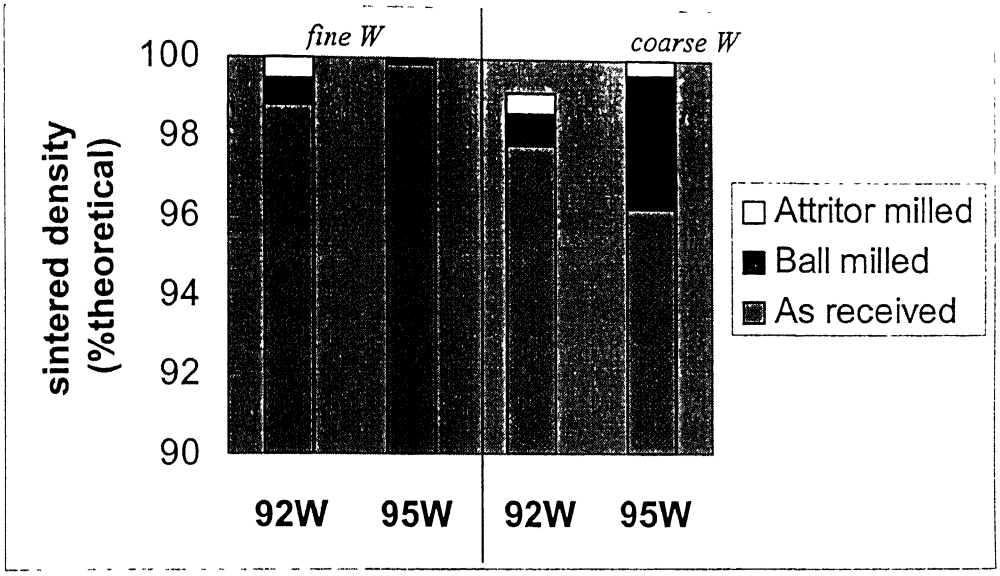

Figure 5.21: Comparison of percentage theoretical density of liquid phase sintered samples prepared by mixed, ball milled and attritor milled powders.

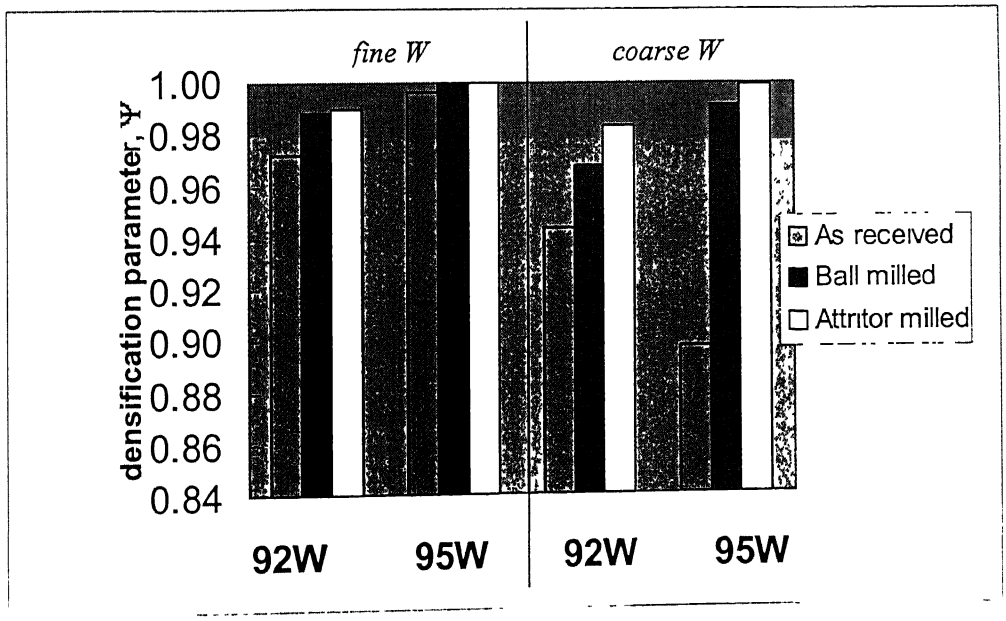

Figure 5.22: Effect of particle size and milling on densification parameters of liquid phase sintered tungsten heavy alloys.

in case of solid-state sintering but full densification was achieved in case of liquid phase sintering of compacts prepared by milled powders.

5.5 Microstructural Evolution

5.5.1 Pore Content and Average Pore Diameter

Figure 5.23 shows the percentage volume fraction of pore in solid-state sintered compacts. It was observed that volume fraction of pore decreases with milling and

reduction in average particle size. In case of 92wt% tungsten alloy with finer average particle size full densification was achieved. So no pore sites were found.

Table 5.2 summarizes the average pore size of solid-sate sintered compacts prepared by mixed, ball milled and attritor milled powders Average pore size was found higher for compacts prepared by coarser powder.

Table 5.2: Average pore size for solid-state sintered compacts

Compositions	Average Pore Size (μm)		
	Mixed	Ball Milled	Attritor Milled
92.5W (fine)-6.15Ni-1.1Fe-0.25Co	9.0	4.8	*
95.1W (fine)-3.45Ni-1.45Fe	8 0	5.6	3.8
92.5W (coarse)-6.15Ni-1.1Fe-0.25Co	10.8	4.9	5.4
95.1W (coarse)-3.45Ni-1.45Fe	14.3	4.7	5.3

** Full densification was achieved*

5.5.2 Volume Fraction of Matrix

Figure 5.24 shows the comparison of volume fractions of matrix in sintered compacts prepared by mixing, ball milling and attritor milling. For higher binder content and finer tungsten particles, higher volume fraction of matrix was observed. It was observed that milling increased the volume fraction of matrix. In case of attritor milled samples, volume fraction of matrix was highest.

5.5.3 Dihedral Angle

Figures 5.25 to 5.27 show the results of dihedral angle measurement in mixed, ball-

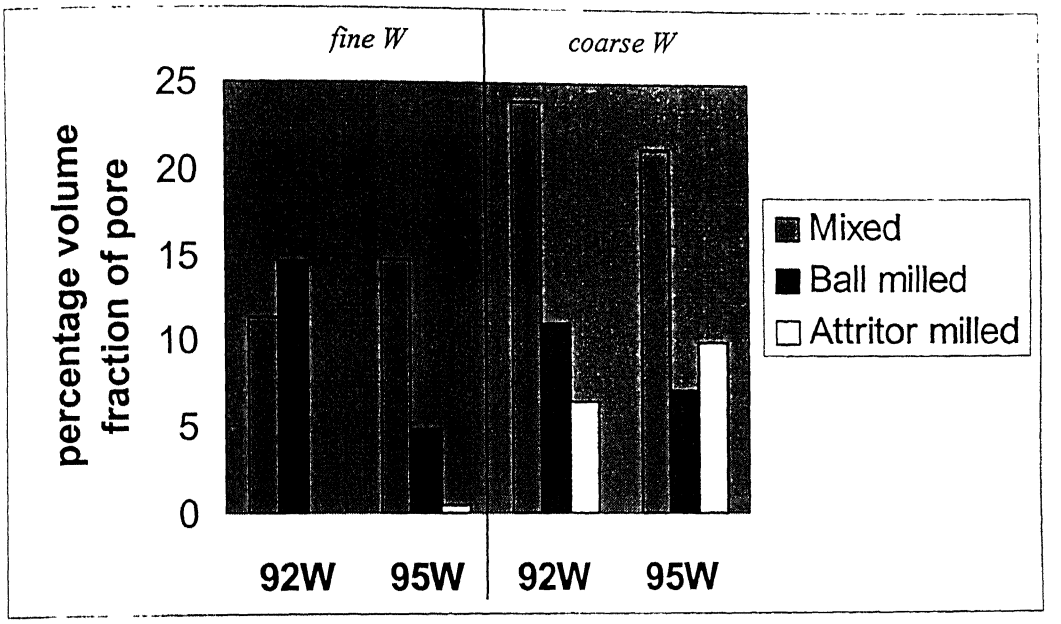

Figure 5.23: Effect of particle size and milling on pore fraction of solid-state sintered W-Ni-Fe heavy alloys.

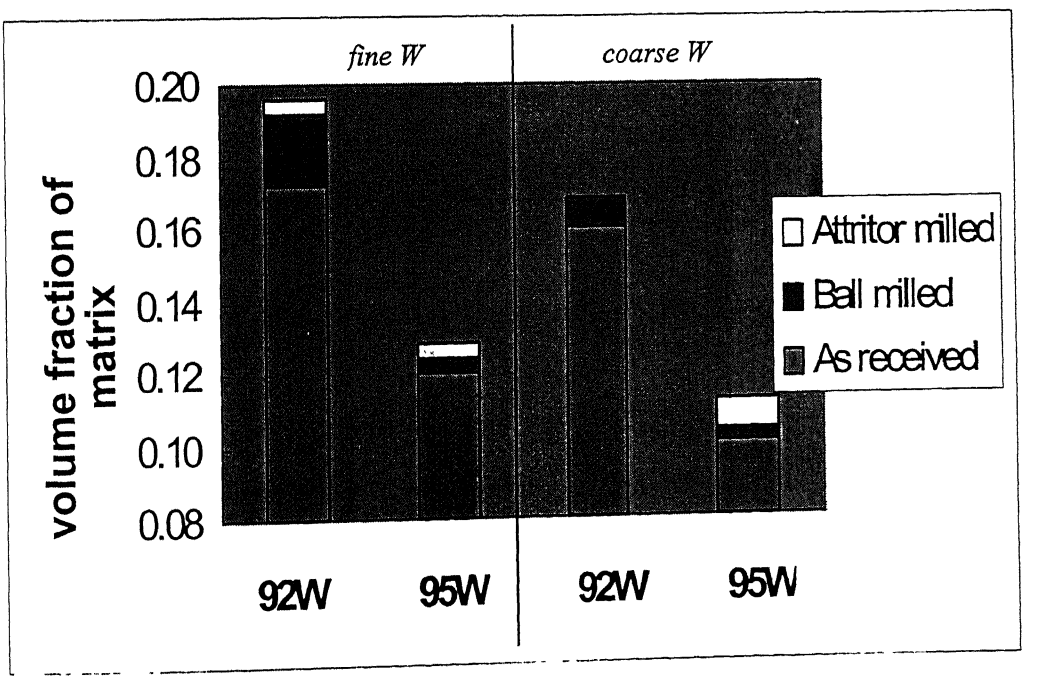

Figure 5.24: Effect of particle size, binder content and milling on volume fraction of matrix.

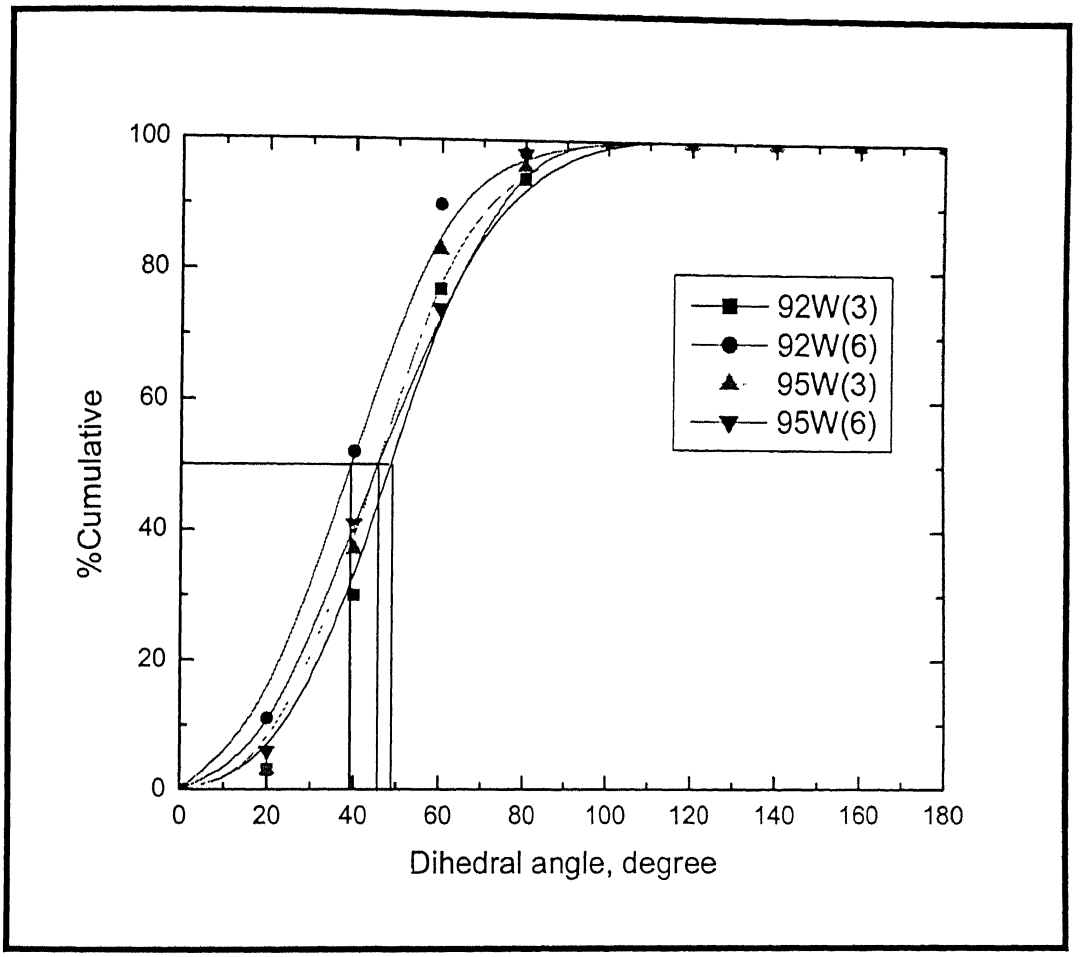

Figure 5.25: Effect of particle size and binder content on dihedral angle of liquid phase sintered samples prepared by mixed powders.

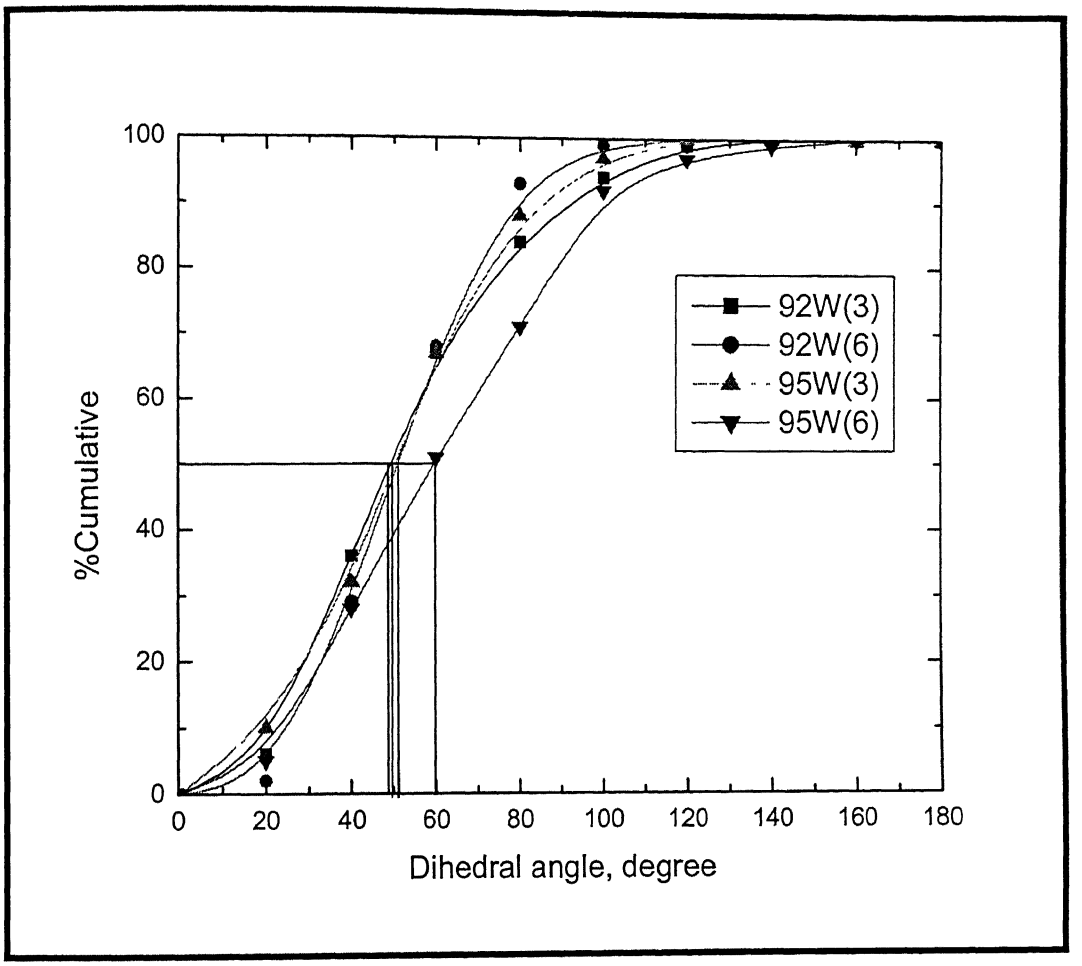

Figure 5.26: Effect of particle size and binder content on dihedral angle of liquid phase sintered samples prepared by ball milled powders.

milled and attritor milled compositions respectively. Figure 5.28 shows the variation in dihedral angle with binder content, powder size and type of milling. It was observed that milling reduced dihedral angle. Dihedral angle is lowest in case of attritor milled powder compact. It is also clear from the Figure 5.28 that dihedral angle increases with increase in tungsten content.

5.5.4 Contiguity and Connectivity

Figures 5.29 and 5.30 show the effect of binder content, powder size and milling conditions on contiguity and connectivity respectively. It is evident that both contiguity and connectivity reduces with decrease in powders size, and increase in binder content. Milling caused a significant decrease in both contiguity and connectivity.

5.5.5 Interface Area of Tungsten Matrix Per Unit Volume, (S_{WM})

Figure 5.31 shows the effect of milling, particle size and compositions on tungsten matrix surface area per unit volume. Higher S_{WM} values were observed incase of compacts prepared from finer tungsten particles and higher binder content. Milling also increases the S_{WM} values.

5.5.6 Grain Size

Figure 5.32 shows the effect of binder content, particle size, milling. and addition of alloying element i.e. Co. It was observed that milling reduced the average tungsten grain size. Finer particle size causes the smaller spheroid size. It was also observed that addition of alloying element caused lower spheroid size.

5.6 Mechanical Properties

5.6.1 Macro-Hardness

Figure 5.33 shows the variation in bulk hardness values (VHN) of solid-state sintered compacts prepared by mixed, ball and attritor milled powder, with change in particle size, binder content and type of milling. It was observed that hardness values increased with milling and reduction in particle size.

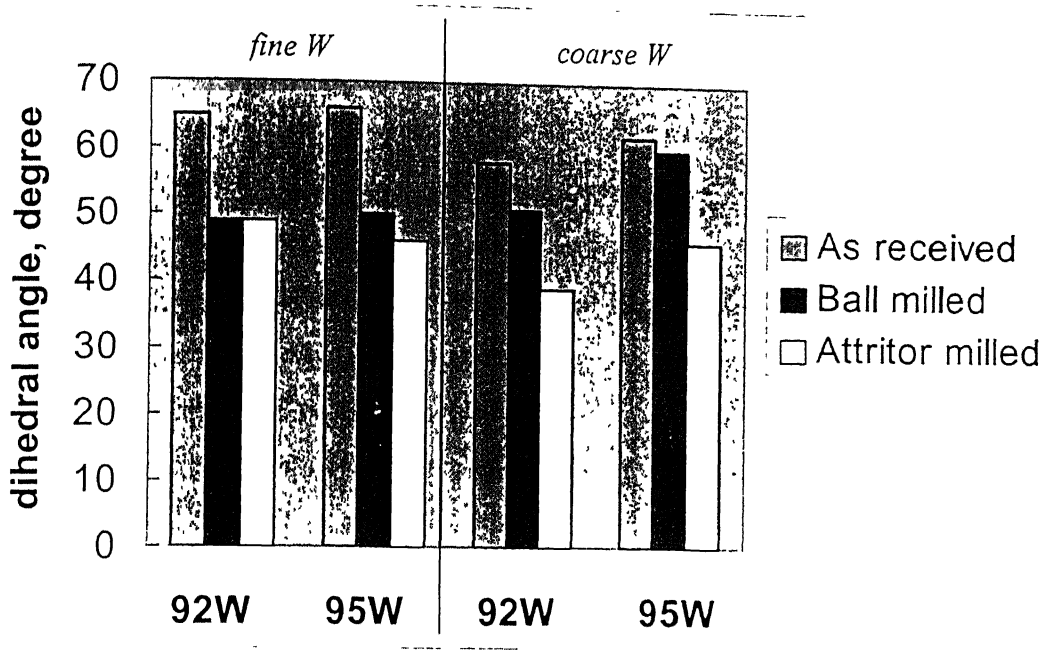

Figure 5.28: Effect of particle size, binder content and milling on dihedral angle.

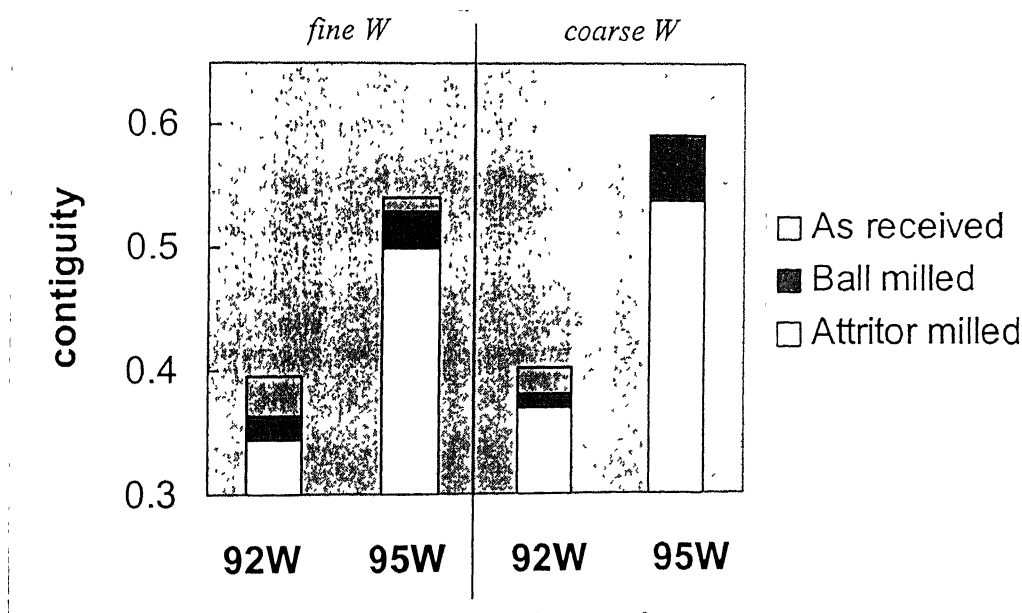

Figure 5.29: Effect of particle size, binder content and type of milling on contiguity.

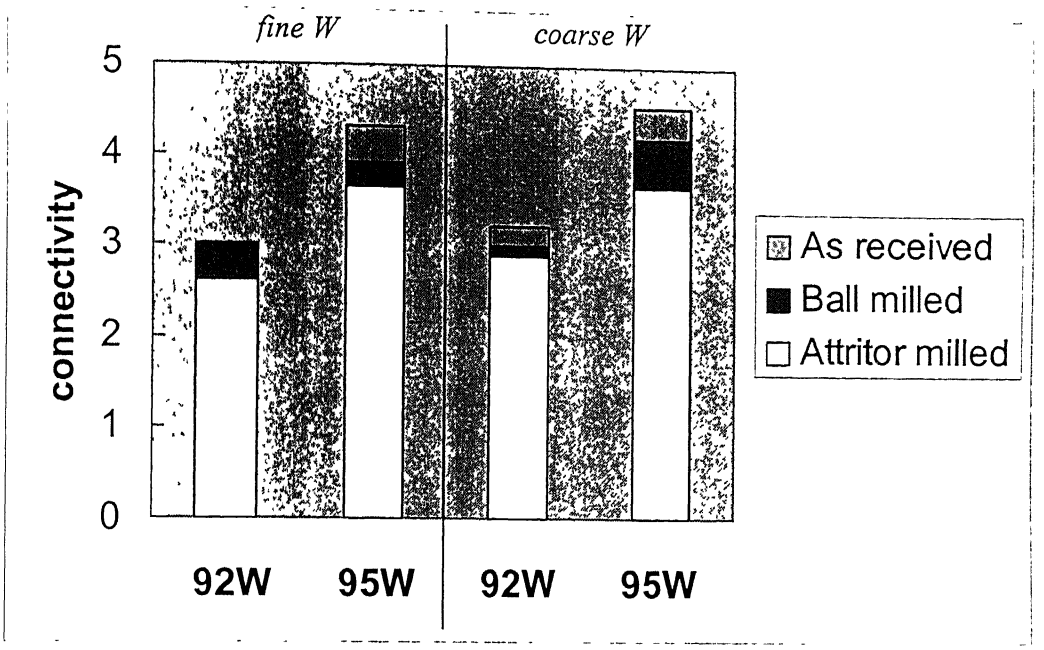

Figure 5.30: Effect of particle size, binder content and type of milling on connectivity.

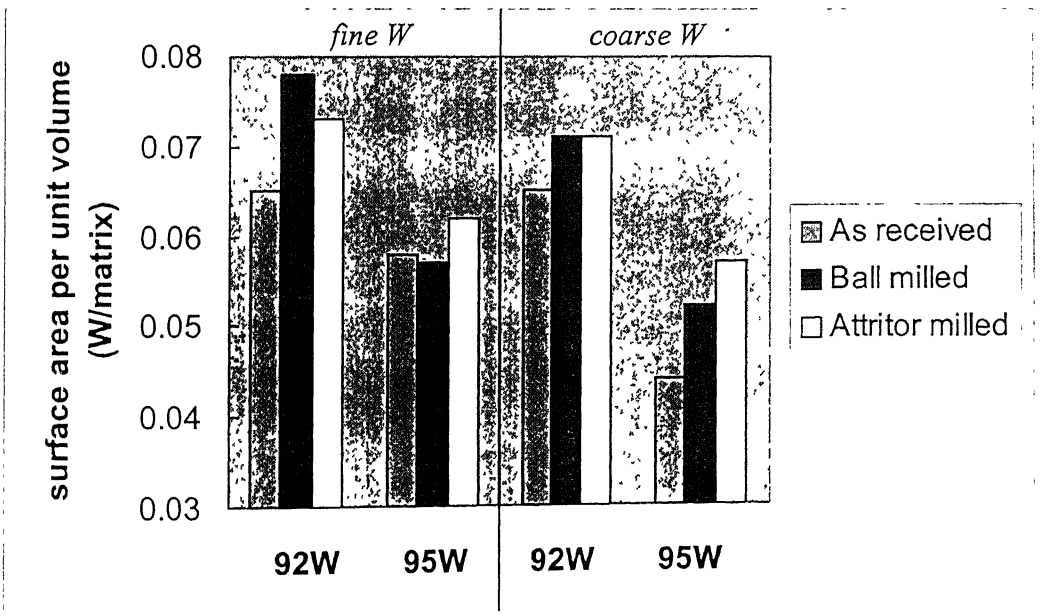

Figure 5.31: Effect of milling, particle size and composition on tungsten-matrix interface area per unit volume.

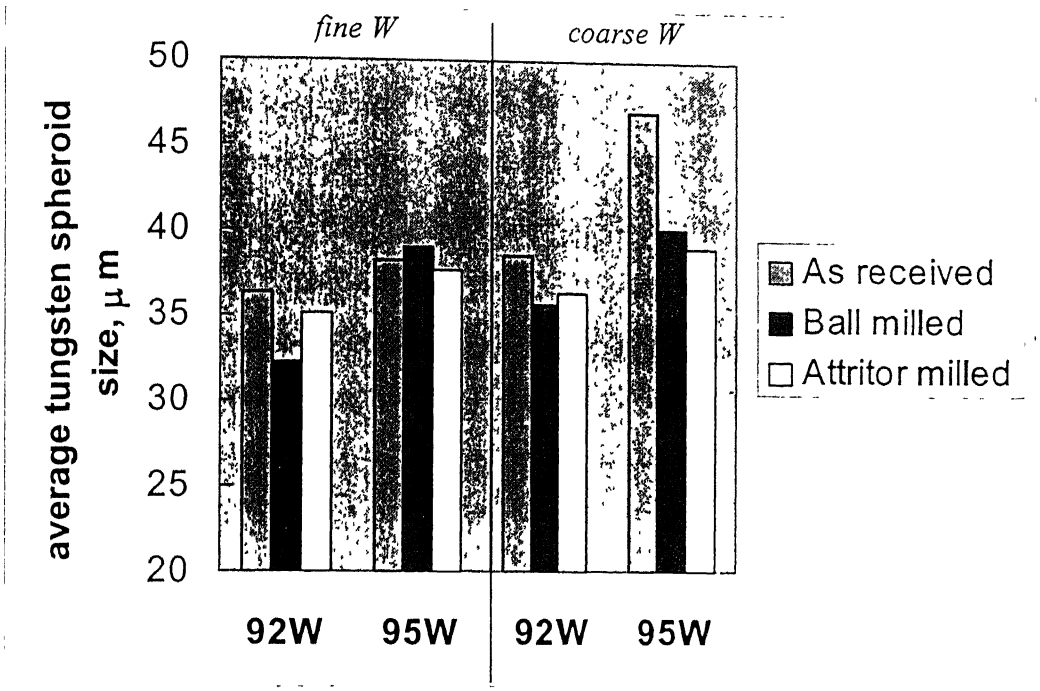

Figure 5.32: Effect of powder size, binder content and milling on the average tungsten spheroid size.

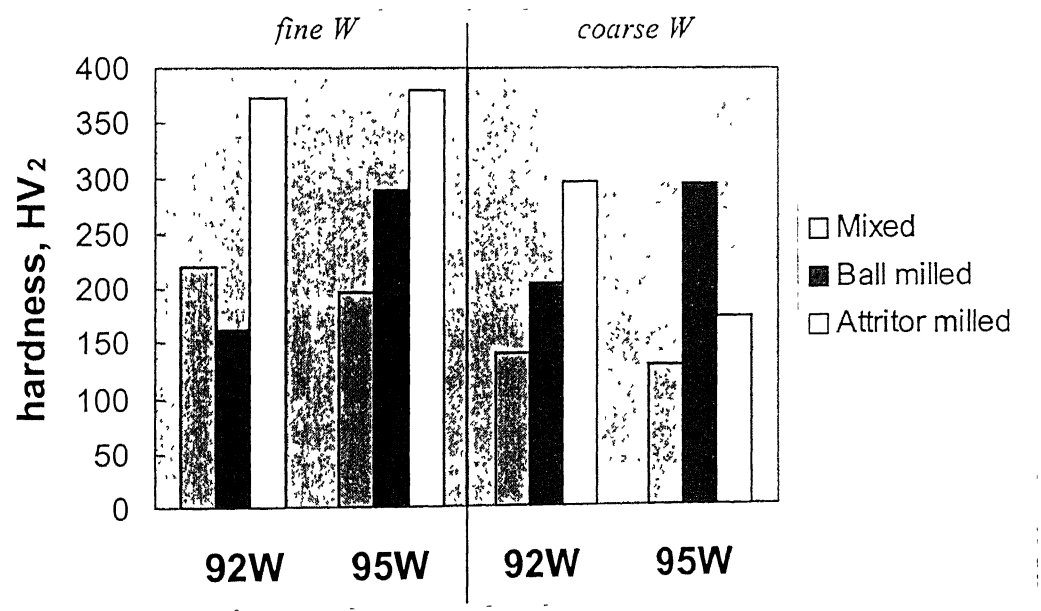

Figure 5.33: Effect of milling and particle size on hardness of solid-state sintered tungsten heavy alloys.

Figure 5.34 shows the effect of milling, particle size and fourth alloying element addition on bulk hardness values. It was observed that hardness slightly increased with decrease in average particle size and powder milling. Addition of cobalt increased the hardness.

5.6.2 Micro-Hardness

Figure 5.35 shows the effect of average particle size and milling on micro-hardness of matrix phase. It was found that micro-hardness of matrix phase increases with milling and reduction in average particle size. In case of sintered compacts prepared by attritor milling hardness of matrix was highest.

5.6.3 Strength and Ductility

It was observed that milling reduced the ductility drastically. Results of tensile test are summarized in Table 5.3.

Table 5.3: Strength and ductility of W-Ni-Fe heavy alloys

Tungsten Content	Tensile Strength, MPa	Yield Strength, MPa	% Elongastion
92W (fine), mixed	642	520	5.5
95W (fine), mixed	775	981	7.0
95W (coarse), attritor milled	850	1046	3.1

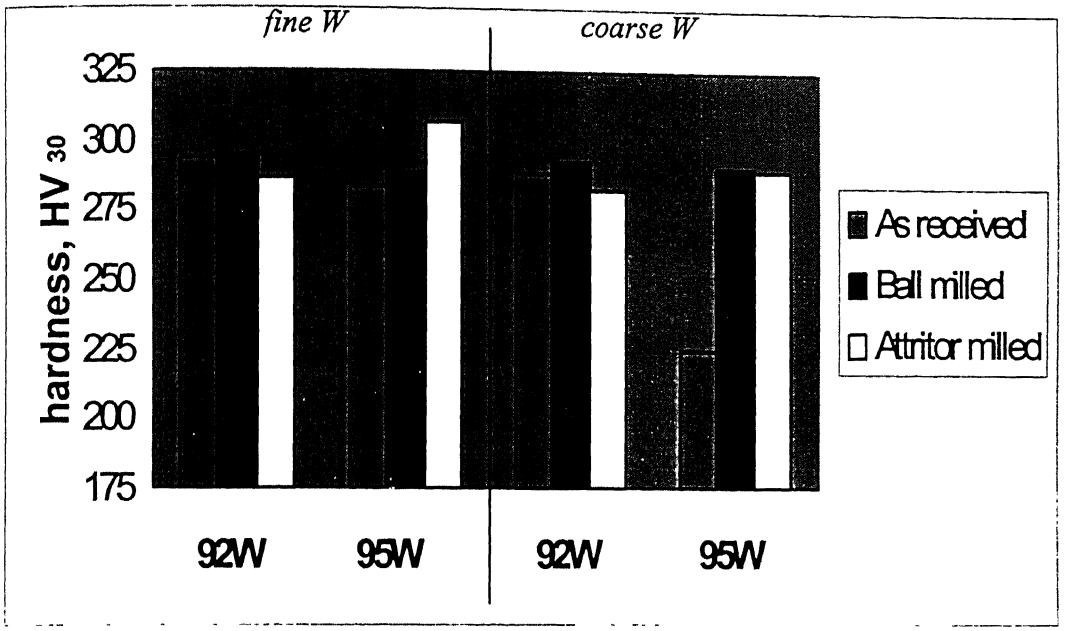

Figure 5.34: Effect of powders milling and average particle size on hardness of liquid phase sintered tungsten heavy alloys.

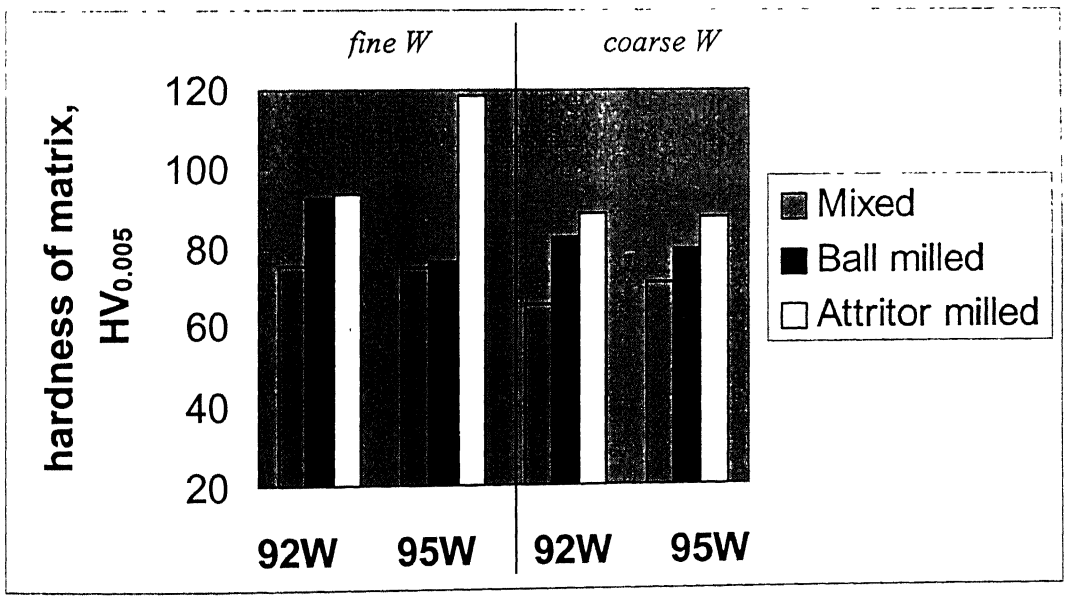

Figure 5.35: Effect of milling and particle size on micro-hardness of matrix phase.

Chapter 6
DISCUSSION

6.1 Milling

It is clear from Table 4.1 that milling reduced the average particle size. In the initial microforging stage particles are deformed in the absence of agglomeration by welding and fracture. Eventually, particles becomes so severely deformed and embrittled by cold work that they enter in secondary stage, during which the particles fracture by a fatigue failure mechanism and/or by the fragmentation of fragile flakes.

As the particle size becomes finer, coupling forces tend to become greater, and the agglomerates become stronger. In the later stage, milling forces that deagglomerate the particles reach equilibrium with coupling forces present; after this, tendency to agglomerate increases and excessive milling may cause increase in particle size. That's why excessive milling should be avoided or surface active agents or lubricants should be used to nullify the forces of welding and thereby inhibit the agglomeration. In our case milling was done for 3 h only, so these agents were not used.

In case of attritor milling average particle size is lowest because when a large number of fine particles are produced by attrition, the degree of refinement is very high. Elemental tungsten milled powders by both type of mill, are shown in Figure 6.1. Attritor milling is high energy milling process and it is clear from Figure 6.1 that in case of attritor milling the degree of deformation is higher than ball milling.

Powder size distribution becomes narrower due to milling, because particles larger than average are reduced in the size at the same rate that fragments smaller than average grow through accretion of smaller particles and wear debris produced by attrition.

6.2 Effect of Milling on Green Density

As the particle size decreases surface area increases, this causes an increase in interparticle frictional force during compaction which leads to lower green density. Tungsten powder is harder as compared to nickel and iron powder hence increase in tungsten content in mix, makes compaction more difficult.

(a) Ball milled

(b) Attritor milled

Figure 6.1: Scanning electron micrograph of milled elemental tungsten powder.

Milling causes narrower particle size distribution, due to which interstitial voids do not get fill up. Milling also causes reduction in average particle size, and work hardening of powders which reduces compressibility.

6.3 Density and Densification Parameter

In solid-state sintering densification occurs mainly due to grain boundary diffusion. As the powder size decreases, the interfacial area per unit volume increases which results in higher diffusivity, so rate of sintering increases and higher densification can be achieved.

Liquid phase sintering mechanism for W-Ni-Fe heavy alloys is through particle fragmentation, particle rearrangement and solution-reprecipitation. Melt phase penetration along the interface boundaries is ensured because of the low dihedral angle between the binders and tungsten phase. Such penetration of liquid helps in enhanced solution-reprecipitation mechanism. The capillary pressure imposed by liquid phase, which pulls the solid particles towards each other is also responsible for initial densification by rearrangement. The capillary stress in liquid phase sintering can be expressed as [39]

$$P_n = \frac{5.2\gamma_{LV} Cos\theta}{D(\Delta L / L_0)} \qquad \ldots\ldots\ldots\ldots\ldots \quad (6.1)$$

where P_n is the capillary pressure, D is the diameter of solid particles, γ_{LV} is the liquid/vapour surface energy, θ is the solid/liquid/vapour wetting angle, and $(\Delta L/L_0)$ is the linear sintering shrinkage given by the compact length change (ΔL) divided by the initial length (L_0). As the $(\Delta L/L_0)$ increases in the latter stage of sintering, capillary pressure decreases. Typical initial values for P_n are the order of a few MPa (for a γ_{LV} of 2 Jm^{-2} and particle size of 100 μm, the estimated capillary pressure goes from 10 to 1 MPa as the linear shrinkage goes from 0.01 to0.1). For the finer particles capillary pressure will be higher. Since capillary pressure is inversely proportional to particle size, reduction in particle size by 50% results in a two fold increase in the capillary pressure. Grain sliding and rearrangement occur rapidly in the very beginning of sintering, which enhance densification. During sintering dislocation density increases considerably in the

contact region of particles. Capillary force is helpful to induce dislocations in the earlier stage at the contact region [40].

Milling causes high dislocation density, improved homogeneity, finer structure (laminar structure; initially brittle and ductile particles weld up and form laminar structure which further fragmented due to work hardening) and change in shape (flaky powders; provides higher surface area per unit volume) which result in higher dislocation and surface diffusion, hence higher densification in solid state-sintering of milled powder.

Milling also causes particle refinement which results, increase in capillary pressure according to equation 6.1. As the particle size decreases contact area between particles increases and distance for diffusion decreases that results in enhanced sintering. This leads compacts prepared by ball and attritor milled powders having higher sintered density in comparison to those, which are prepared from mixed powders. In case of ball milled powder extent of milling was limited however in case of high-energy attritor mill very vigorous milling occurred which resulted in highest sintered density of attritor milled powder samples. Due to reduction in particle size inter-particle friction increases during compaction, which results in lower green density. Reduction in particle size leads to higher sinter density that's why densification parameter increases with milling and reduced particle size according to equation 4.3.

6.4 Microstructural Evolution

6.4.1 Pore Content and Average Pore Diameter

Figures 6.2 to 6.4 show the photomicrographs of solid-state sintered samples prepared by mixed, ball and attritor milled powder respectively. It is clear from Figure 6.2 to 6.4 that pores (one pore is encircled in Figure 6.2 (a)) in present are bigger in case of compacts prepared by mixed powders in comparison to those, which are prepared by milled powders. In case of coarser particle size interstitial voids will be bigger. Since in solid-state sintering void removal occurs through volume diffusion, which is very difficult, bigger pores remains in case of compacts prepared by coarser powder. As we have already discussed in previous section of same chapter that milling increases

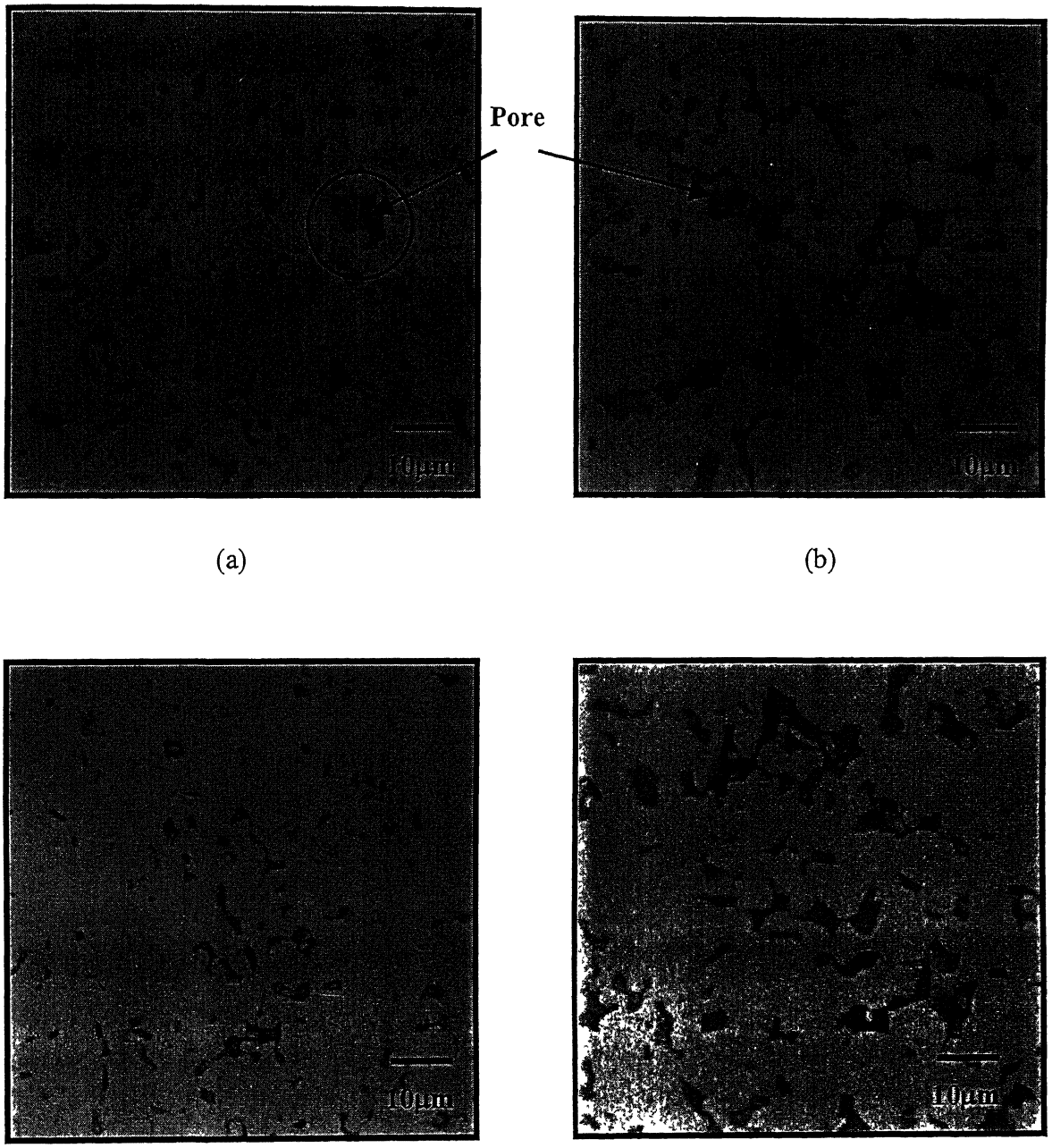

Figure 6.2: Optical micrograph solid-state sintered compacts prepared by mixed powders of (a) 92.5W (fine)-6.15Ni-1.1Fe-0.25Co, (b) 92.5W (coarse)-6.15Ni-1.1Fe-0.25Co, (c) 95.1W (fine)-3.45Ni-1.45Fe and (d) 95.1W (coarse)-3.45Ni-1.45Fe..

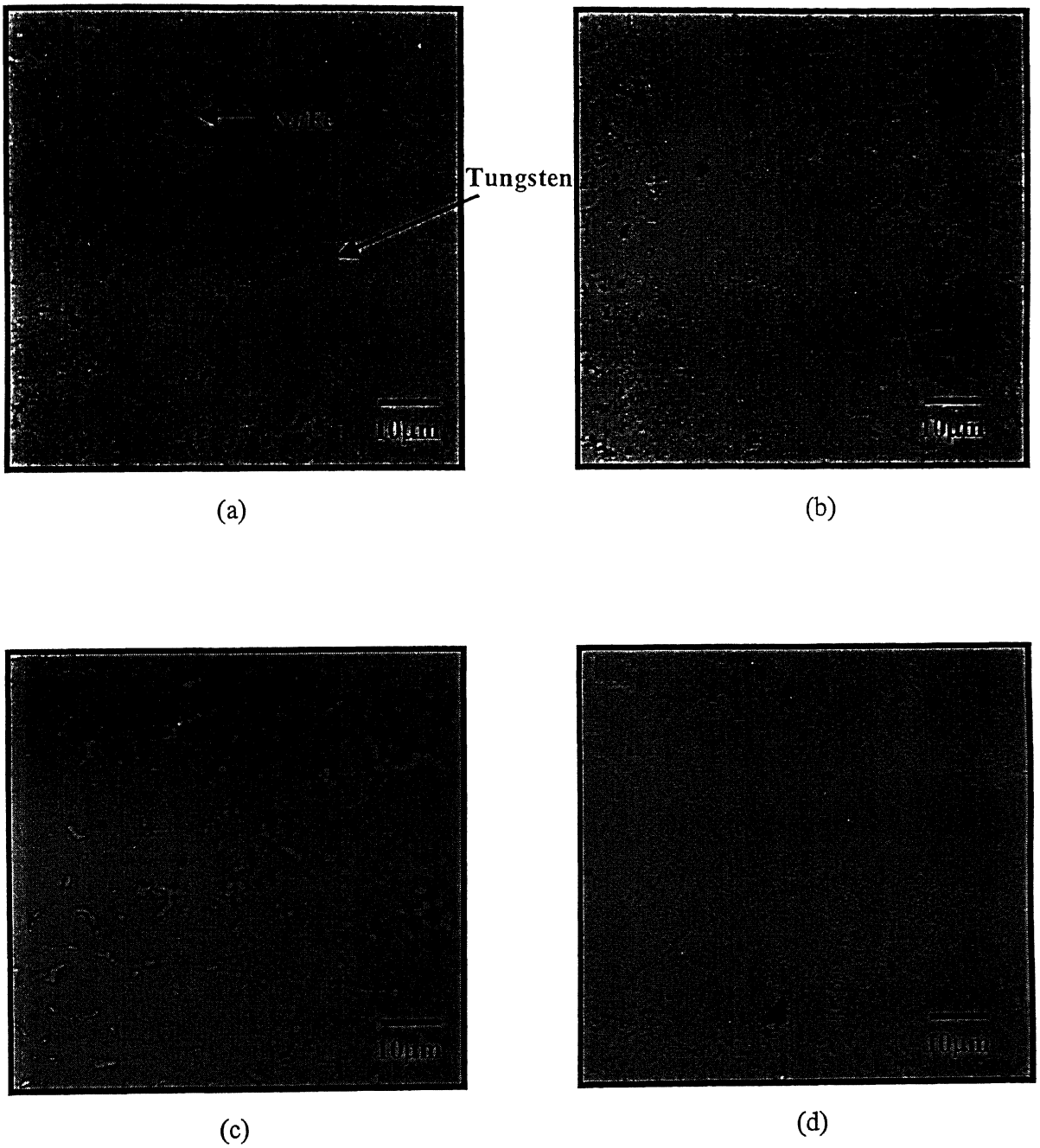

Figure 6.3: Optical micrograph solid-state sintered compacts prepared by ball milled powders of (a) 92.5W (fine)-6.15Ni-1.1Fe-0.25Co, (b) 92.5W (coarse)-6.15Ni-1.1Fe-0.25Co, (c) 95.1W (fine)-3.45Ni-1.45Fe and (d) 95.1W (coarse)-3.45Ni-1.45Fe.

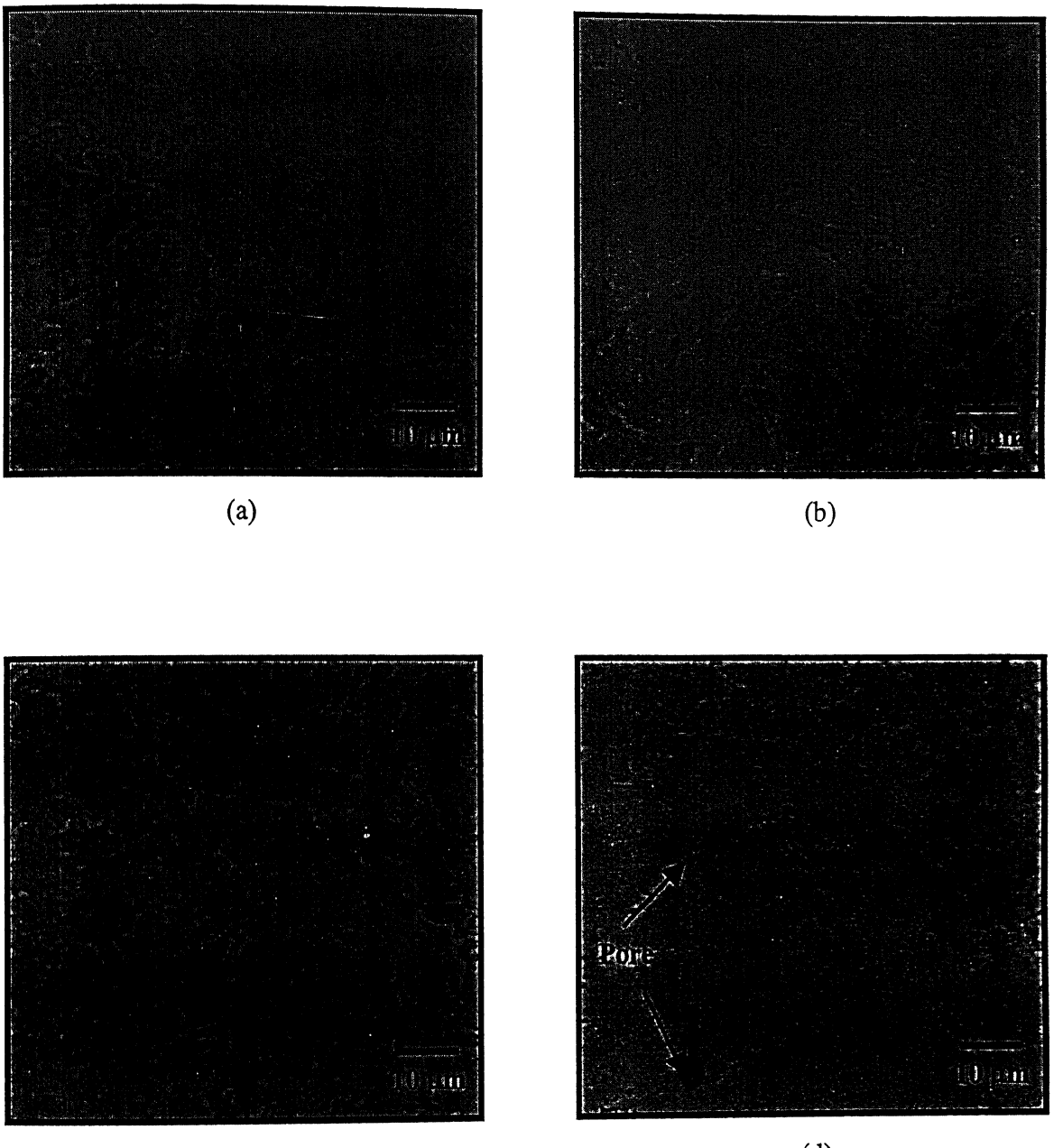

Figure 6.4: Optical micrograph solid-state sintered compacts prepared by attritor milled powders of (a) 92.5W (fine)-6.15Ni-1.1Fe-0.25Co, (b) 92.5W (coarse)-6.15Ni-1.1Fe-0.25Co, (c) 95.1W (fine)-3.45Ni-1.45Fe and (d) 95.1W (coarse)-3.45Ni-1.45Fe.

dislocation density and reduces particle size, higher densification can be achieved by milled powders, so pore fraction and size will be lower.

6.4.2 Volume Fraction of Matrix

In case of tungsten heavy alloys, matrix is mainly a solid solution of tungsten in binding elements (Ni, Fe, Co). Some intermetallic may also form depending on the interaction of binders with tungsten. Maximum solubility of tungsten in the binder metal falls in the sequence Ni (40%)-Co (35%)-Fe (33%) [41]. As the particle size decreases, surface area per unit volume increases, so better dissolution of tungsten in liquid occurs. As the extent of milling increases particle size decreases and stored energy increases which results in the higher dissolution of tungsten, so volume fraction of matrix increases. That's why highest volume fraction of matrix observed in attritor milled powder compacts.

6.4.3 Dihedral Angle

During sintering binders melt down. After exposure to the liquid, a stabilized solid liquid structure emerges as shown by the two-particle configuration in Figure 6.4. The equilibrium condition occurs when the solid grains form stable necks with a surrounding liquid. The stable neck size X is given by the grain size G and dihedral angle ϕ,

$$X = G \sin(\phi/2) \qquad \text{..... (6.2)}$$

Due to milling ductile binders cover up hard tungsten powders as shown in Figure 5.17. During sintering layer of binders melt down and penetrates between grains. That's why tungsten/tungsten contact (contiguity) reduces and smaller neck size forms. Due to milling better dissolution of tungsten occurred and composition of matrix changed, which resulted reduction in dihedral angle.

6.4.4 Contiguity and Connectivity

The tungsten spheroid distribution becomes wider with increasing binder content. For smaller particles capillary pressure will be higher according to equation 6.16 which

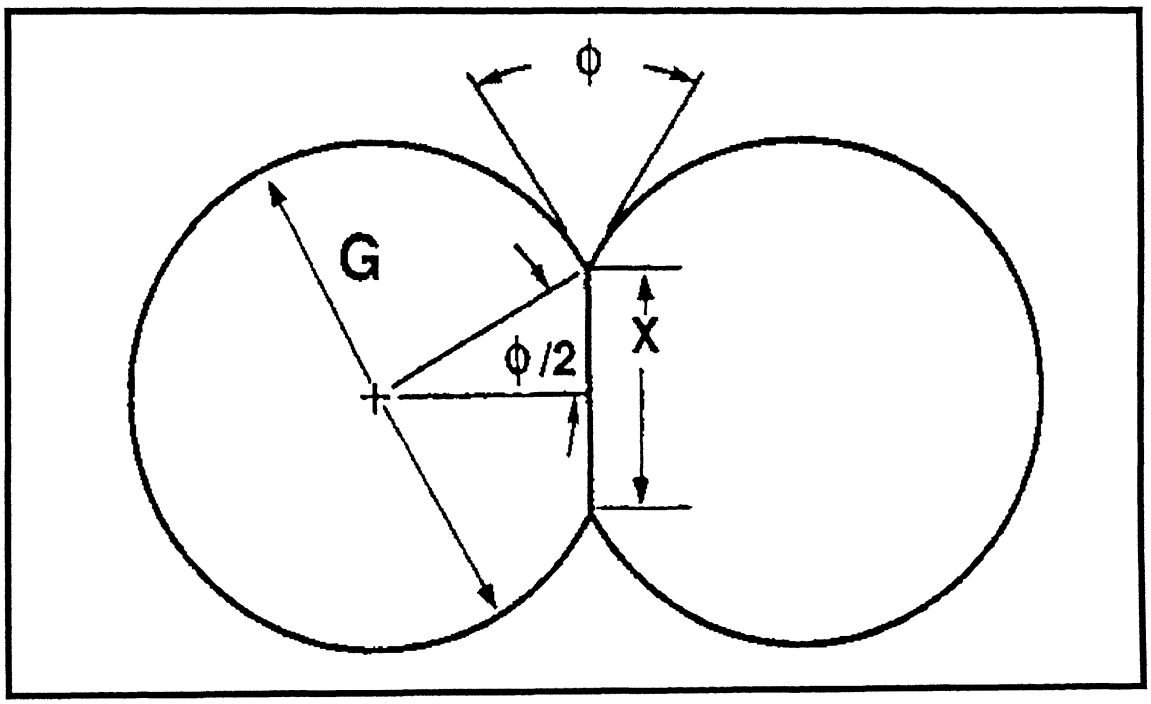

Figure 6.5: Two- particle configuration in equilibrium state [15].

results in better melt penetration across the interface. This causes a decrease in contiguity. Milling increases homogeneity that's why chances of liquid pool formation (shown in Figure 6.5) reduces. During milling, the binder phase get welded on the surface of the tungsten particles, which forms melt during sintering, so chances of tungsten/tungsten contact reduces. It can be seen in microstructures shown in Figures 6.5 and 6.6 that in case of mixed powder compacts there is too much tungsten spheroid coalescence but milling resulted better separation of tungsten spheroids.

Number of connecting grains in two-dimensional micrograph is called connectivity. Connectivity depends on dihedral angle and solid content. With the decrease in tungsten content and milling, connectivity also decreases due to a reduction in tungsten-tungsten contact.

6.4.5 Interface Area of Tungsten/Matrix Per Unit Volume, (S_{WM})

The grain matrix interface area per unit volume (S_{WM}) vary approximately as

$$S_{WM} = \pi N_V G^2 \qquad \ldots\ldots\ldots\ldots \qquad (6.3)$$

where N_V is the grain density and G is average grain size [42]. If the tungsten particle size is very small, final grain population will be high in comparison to that for coarser powder for any sintering period and temperature. Compacts with higher amount of binders will have high S_{WM} values. Milling reduces particle size, contiguity, and connectivity, which result in better separation of W/W spheroids. Due to this tungsten-matrix interfacial area increased and higher S_{WM} values were observed.

6.4.6 Grain Size

In liquid phase sintering binders melt down during sintering. Tungsten has solubility in Ni-Fe melt, so it starts solution re-precipitation in the second stage of sintering and finally grain coarsening occurs. Milling reduces powder size. So in case of milled powder compacts, initial powder size is lower than that for mixed powder compacts. That's why smaller spheroids form in the same sintering temperature and

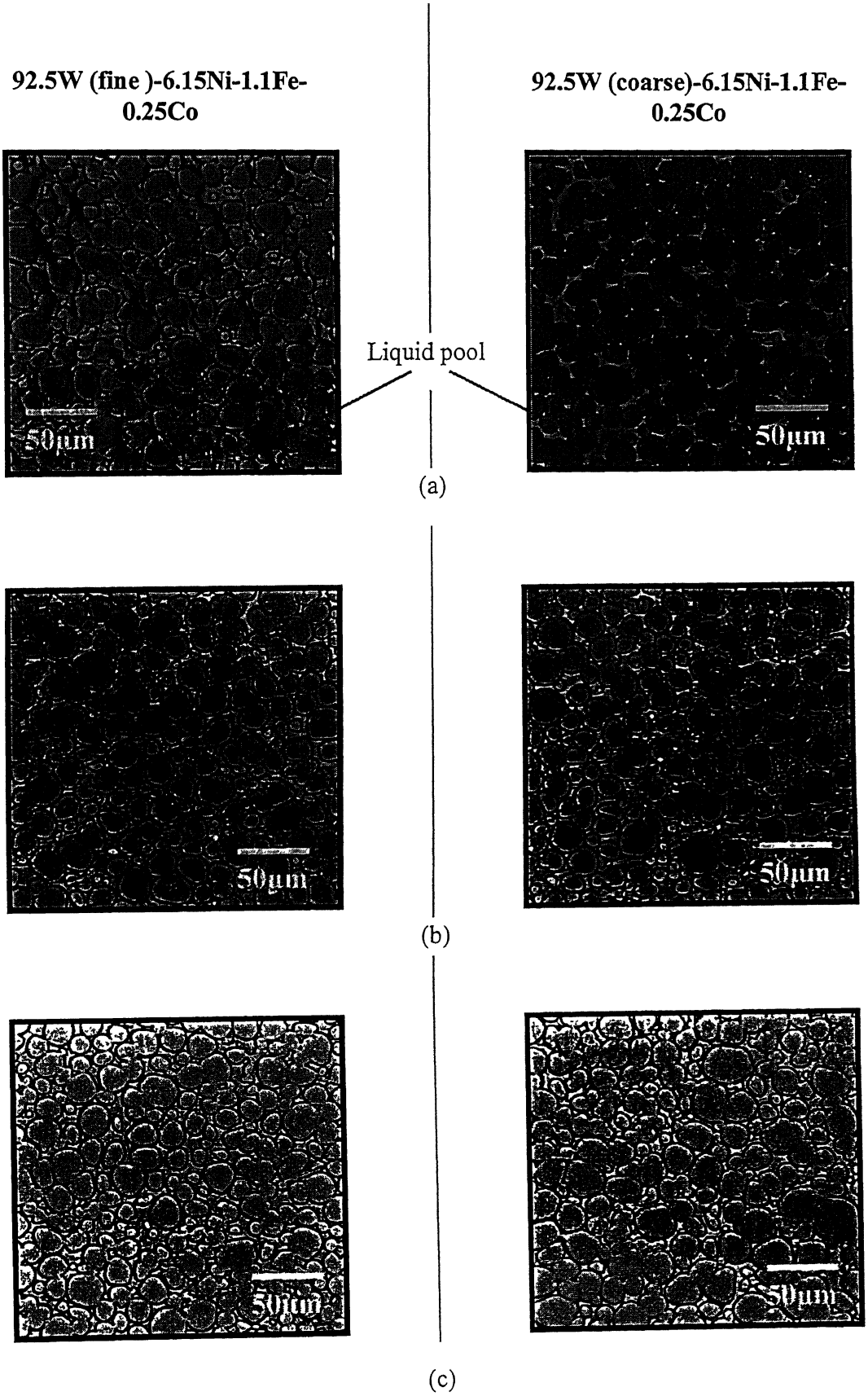

Figure 6.6: Optical micrograph of liquid phase sintered W-Ni-Fe-Co heavy alloys prepared by (a) mixed, (b) ball milled, and (c) attritor milled powder.

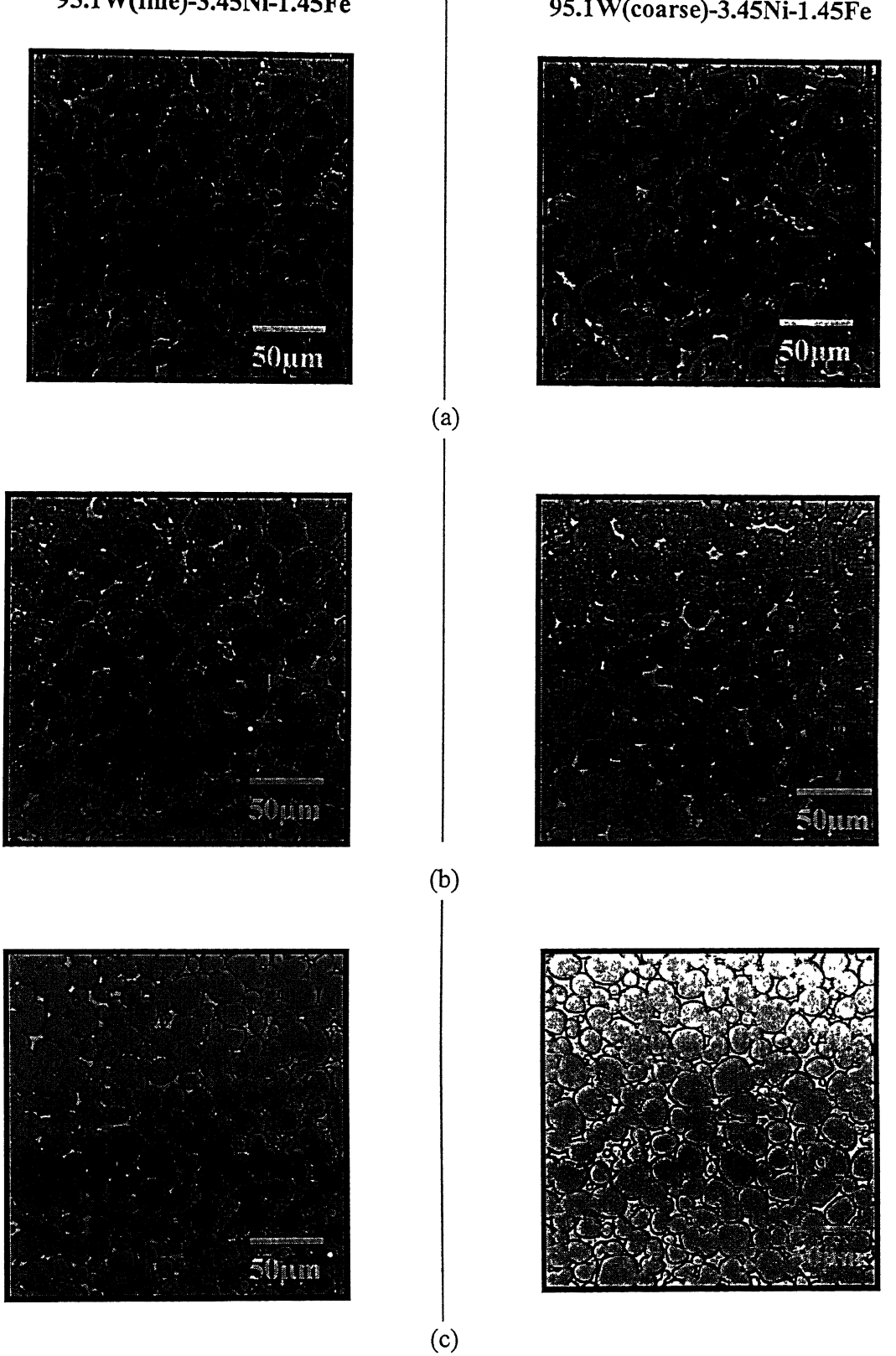

Figure 6.7: Optical micrograph of liquid phase sintered W-Ni-Fe heavy alloys prepared by (a) mixed, (b) ball milled, and (c) attritor milled powder.

time. Cobalt preferentially get dissolves in the matrix and prevent tungsten grain coarsening.

6.5 Mechanical Properties

6.5.1 Macro-Hardness

As the particle size reduces higher percentage theoretical sintered density can be achieved. Sine higher sintered density can be achieved with milled powder, volume fraction of pore will be lower in case of milled powder. Due to lower volume fraction and average size of pore in compacts prepared by milled powder hardness will be higher.

The effect of milling on hardness was not very clear, as only a slight increase in hardness values were found. With smaller powder better solutioning of tungsten in matrix and hence densification occurs. Milling increases amount of tungsten in matrix because better solutioning occurs due to proper mixing, which resulted increased bulk hardness values.

6.5.2 Micro-Hardness

Tungsten is harder phase and matrix is softer phase in tungsten heavy alloys. Matrix forms by nickel and iron having some dissolved tungsten. As the average tungsten particle size reduces better dissolution of tungsten in matrix occurs. Due to milling homogeneity increases and particle size decreases, which are also responsible for, better dissolution of tungsten in matrix. It also confirms from measurement of volume fraction of matrix in compacts prepared by milled powder that volume fraction of matrix increase due to milling, which means higher amount of tungsten gets dissolve in the matrix in comparison to compacts prepared by mixed powders. Since the amount of harder tungsten increases in matrix micro-hardness of matrix phase increases due to milling.

6.5.3 Strength and Ductilty

It was observed that samples prepared by mixed powder possesses higher ductility than those prepared by milled powders. However these primary results were totally

against the expected, since all the microstructural parameters were in favor of high ductility.

When microstructure of attritor milled samples were studied, it was found that there is carbon deposition due to cracking of organic lubricants. Milling was done in acetone media. Milled powder became sticky due to incomplete evaporation of acetone. Thais caused the agglomeration of organic lubricant (4% acrawax was used for making tensile samples). During sintering cracking of acetone and lubricant occurred which caused carbon deposition. Agglomerated lubricant left big pores, which reduces the ductility. Due to improper mixing tungsten also segregates and forms very contiguous structure. Figure 6.7 shows the microstructure of attritor milled liquid phase sintered tungsten heavy alloy having 95% W. 4% acrawax was also mixed in this sample. It is clear from Figure 6.7 that contiguity is very high and pores are there..

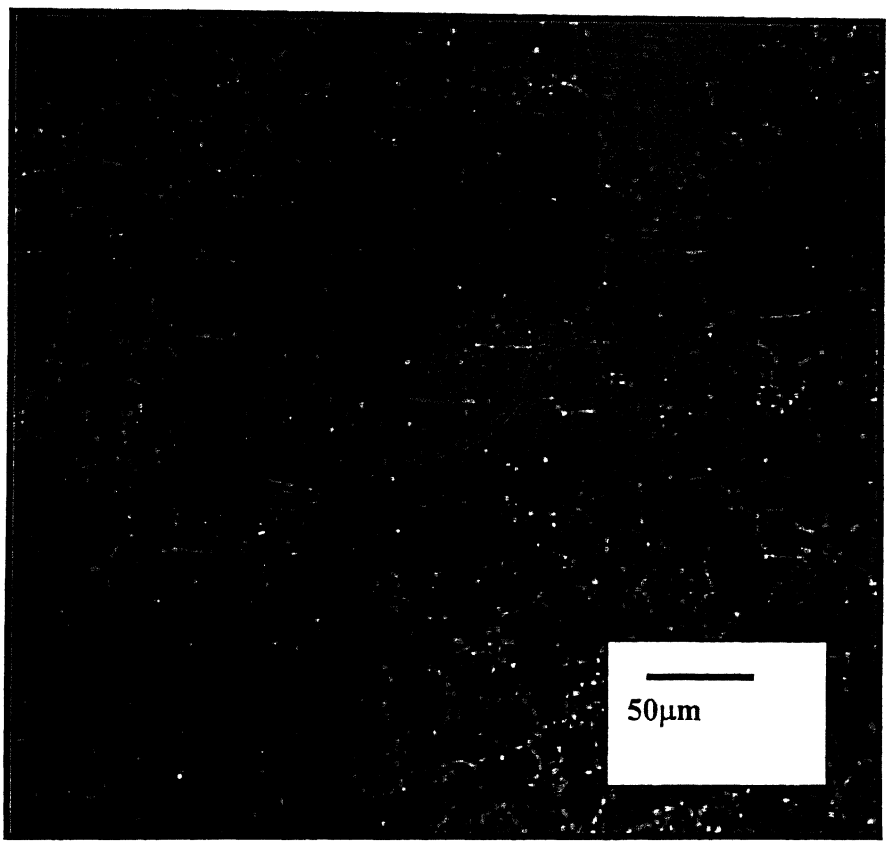

Figure6.8: Optical microstructure of solid-state sintered tungsten heavy alloy prepared by attritor milled powder, having 95%W (4%acrawac as lubricant).

SUMMARY

The present work was focused on effect of milling on sintering behavior and microstructural evolution in W-Ni-Fe heavy alloys. On the basis of chapter 5 and chapter 6 we can conclude that milling causes narrower particle size distribution and reduction in average particle size, which induces higher frictional force during compaction. This results in lower green density of compacts. Milling also changes the morphology of powders and increases homogeneity of mix. This results in higher sintered density both in solid-state and liquid phase sintering due to higher rate of sintering. It was observed that full densification could be achieved even in solid-state sintering of compacts prepared by milled powders.

Milling reduces dihedral angle, contiguity, connectivity, pore content and pore diameter, grain size and increases volume fraction of matrix, micro and macro hardness and tungsten/matrix interface area per unit volume.

Since tensile samples prepared by milled powders were possessed higher density but lower ductility it was concluded that due to improper mixing of constituent powders with lubricant (acrawax) some bigger pores were remained which caused early fracture and results in lower ductility

Due to presence of acetone in milled powders it becomes sticky and proper mixing could not occur. Carbon also deposited due to cracking of acetone and organic lubricant So it is suggested for future work that any alternative lubricant should be used in lower amount and the way of mixing should be better.

References

[1] G.S. Upadhyaya, Sintered Metallic and Ceramic Materials, John Willey & Sons, Ltd., Chichester, England, 1999.

[2] G.S. Upadhyaya. "Molybdenum and Tungsten- Their Relative Assessment," *International Journal of Refractory and Hard Metals*, Sep. 1987, vol. 6, no. 3.

[3] A. Upadhyaya, "Tungsten Heavy Alloys for Ordnance and Thermal Management *Applications," Trans. Indian Inst. Met.*, Feb , 2002, vol. 55, no. 1-2, pp. 51-69.

[4] A. Upadhaya, "Processing Strategy for Consolidating Tungsten Heavy Alloys for Ordnance Applications," *Materials Chemistry and Physics*, 2001, vol. 67, pp. 102-109.

[5] K.S. Churn and R.M. German, "Fracture Behavior of W-Ni-Fe Heavy Alloys," *Metallurgical Transactions A*, 1984, vol. 15, no. 2, pp. 331-338.

[6] G.S. Upadhyaya, "Sintered Heavy Alloys-A Review," International Journal of Refractory & Hard Metals, March 1986, vol. 5, no 2

[7] S.K. Rout, "Effect of Thermo-Mechanical Treatment on Stereological Aspects of W-Ni-Fe Heavy Alloys," M. Tech. Thesis, IIT Kanpur, 2002.

[8] T.B. Massalski, "Binary Alloy Phase Diagrams," ASM International, Materials Park, OH, USA, 1990.

[9] G.V. Raynor and V.G. Rivlin, "Phase Equilibria in Iron Ternary Alloys," Institute of Metals, London, no. 4, 1988.

[10] S. G. Caldwell, "Tungsten Heavy Alloys," ASM Hand Book, P.W. Lee and R. Lacocca (eds.), Powder Metal Technologies and Applications, Materials Park, OH, USA, 1998, v. 7, pp. 914 –921.

[11] S.G. Caldwell, "Variation of Ni to Fe Ratio in W-Ni-Fe Alloys: A current Perspective," Tungsten and Tungsten Alloys - 1992, A. Bose and R.J Dowding (eds.), Metal Powder Industries Federation, NJ, USA, 1992, PP. 89-96.

[12] S. Eroglu and T. Baykara, "Effect of Powder Mixing Technique and Tungsten Powder Size on the Properties of Tungsten Heavy Alloys," *Journal of Materials Processing Technology*, 2000, vol. 103, pp. 288-292.

[13] A.Asthana and G. S. Upadhyaya, "Effect of Different Ball Millings on Size Distribution of Tungsten Powder," *International Journal of Refractory and Hard Metals*, Sep. 1985, vol 4, no. 3.

[14] C. Suryanarayana, M. L. Ovecoglu and B. Özkal, "A Comparison of Sintering

Characteristics of Ball and Attritor Milled W-Ni-Fe Heavy Alloys," Journal of Mat. Res., Jul 1996, vol. 11, no. 7, pp. 1673-1682

[15] R.M. German, Powder Metallurgy Science, 2nd edition, Metal Powder Industries Federation, Princeton, NJ, USA, 1994.

[16] H.J. Ryu, S. H. Hong and W. H. Baek, "Microstructure and Mechanical Properties of Mechanically Alloyed and Solid-state Sintered Tungsten Heavy Alloys," *Materials Science and Engineering A*, 2000, vol.291, pp. 91-96.

[17] R.M. German, P. Lu and B. M. Marx "Liquid Phase Sintering of Tungsten Heavy Alloys," *The International Journal of Powder Metallurgy*, 2001, vol. 37, no. 6, pp.45-56.

[18] G.S. Upadhyaya and V. Srikanth, "Effect of Tungsten Particle Size and Binder Composition on Sintered Properties of Heavy Alloys," *Modern Developments in Powder Metallurgy*, 1985,vol.15-17, pp. 51-75.

[19] Y. Song, S. Ahn and D. N. Yoon, "Chemically Induced Migration of Liquid Film in W-Ni-Fe Heavy Alloys," *Acta Metallurgica*, 1985, vol. 33, no. 18, pp. 1907-1910.

[20] T. Kang and D.N. Yoon, "Coarsening of Tungsten Grain in Liquid Nickel-Tungsten Matrix," March 1978, *Meatallurgical* Transactions, vol. 9A, no. 1, pp. 433-438.

[21] D.N. Yoon and W.J. Huppmann, "Grain Growth and Densification During Liquid Phase Sintering of W-Ni," *Acta Metallurgica*, 1979, vol. 27, pp. 693-698.

[22] D.N. Yoon and W.J. Huppmann, "Chemically Driven Growth of Tungsten Grains During Sintering in Liquid Nickel," *Acta Metallurgica*, 1979, vol. 27, pp.973-977.

[23] R.M. German, Liquid Phase Sintering, Plenum Press, New York, USA, 1985.

[24] H. Park, W. Baik, S.L. Kang and D. Yoon, "The Effect of Molybdenum addition on the liquid phase sintering of W Heavy Alloys," *Metallurgical and Materials Transactions A*, Oct. 1996, vol. 27A, no. 10, pp. 3120-3125.

[25] E. Kim, M. Hong, W.H. Baek and I. Moon, "The Effect of Manganese Addition on the Microstructure of W-Ni-Fe Heavy Alloys," *Metallurgical and Materials Transactions A*, March 1999, vol. 30A, no. 3, pp 627-632.

[26] H.S. Song, J. W. Noh, W.H. Baek, S. Joong, L. Kang, and B.S. Chun, "Undulation of W/Matrix Interface by Resintering of Cyclically Heat Treated W-

Ni-Fe Heavy Alloys," *Metallurgical and Materials Transactions A*, Feb. 1997, vol. 28, no. 2, pp. 485-489.

[27] H.D. Park, W.H. Baek, S.L. Kang, and D.Y. Yoon, "The Effect of Molybdenum Addition on the Liquid Phase Sintering of W Heavy Alloys," *Metallurgical and Materials Transactions A*, Oct. 1996, vol. 27, no. 10, pp. 3120-3125.

[28] A. Bose and R.M. German, "Microstructural Refinement of W-Ni-Fe Heavy Alloys by Alloying Additions," *Metallurgical Transactions A*, Dec. 1988, vol. 19, no. 12, pp. 3103.

[29] T. Antonsson and L. Ekbom, "Initial Stage of Liquid Phase Sintering: Liquid Reaction and Particle Growth in W-Ni-Fe- (Co)," *Powder Metallurgy*, 2001, vol. 44, no. 4, pp. 325-332.

[30] S.H. Hong, S.L. Kang, D. N. Yoon, and W.H. Baek, "The Reduction of the Interfacial Segregation of Phosphorus and Its Embrittlement Effect by Lanthanum Addition in a W-Ni-Fe Heavy Alloy," *Metallurgical and Materials Transactions A*, Dec. 1991, vol 22, no.12, pp. 2969-2974.

[31] H.K. Yoon, S.H. Lee, and D.N. Yoon, "Effect of Vacuum Treatment on Mechanical Properties of W-Ni-Fe Heavy Alloy," *Journal of Materials Science*, 1983, vol. 18, no. 4, pp. 1374-1380.

[32] T. Kohno and O. Mayama, "Effect of Sintering and Post-Sintering Heat Treatment on the Mechanical Properties of the W-Ni-Fe Heavy Alloys," International Conference on Powder Metallurgy, The Institute of Metals, London, U K., 2-6 July 1990, vol. 1, pp 324-331.

[33] J.W. Noh, M.H. Hong, G. Kim, S.L. Kang, and D.Y. Yoon, "The Cause of Matrix Penetration of W/W Grain Boundaries During Heat Treatment of W-Ni-Fe Heavy Alloys," *Metallurgical and Materials Transactions A*, Dec. 1994 vol.25, no. 12, pp. 2828-2831.

[34] J. Noh, E. Kim, H. Song, W. Baek, K. Churn, and S.L. Kang, "Matrix Penetration of W/W Grain Boundaries and Its Effect on Mechanical Properties of 93W-5.6Ni-1.4Fe Heavy Alloys," *Metallurgical Transaction A*, Nov. 1993, vol. 24A, no. 11, pp.2411-2416.

[35] H.S. Song, J.W. Noh, W.H. Baek and K.S. Churn, "Ageing Treatment on the Heavy Alloy," International Conference on Powder Metallurgy, The Institute of

Metals, London, U.K., 2-6 July 1990, vol 3, pp. 231-234.

[36] M.H. Hong, S. Lee, J.W. Noh and Y.W. Kim, "The Effect of Thermo -Mechanical Treatment on the Microstructure and Failure Behavior of Sintered W heavy Alloys," International Conference and Exhibition on Powder Metallurgy and Particulate Materials, Metal Powder Industries Federation and APMI International, Toronto, Canada, May 8-11, 1994, vol. 5, pp.279-288.

[36] E. Ernst, F. Thummler, P. Beiss, R. Wahling and V. Arnhold, "Friction Measurements During Powder Compaction", *Powder Metallurgy International*, 1991, vol. 23, no. 2, pp. 77-84.

[37] K.M. Ramakrishnan and G.S. Upadhyaya, "Effect of Composition and Sintering on Densification and Microstrucutre of Tungsten Heavy Alloys Containing Copper and Nickel," *Journal of Materials Science Letter*, 1990, vol. 9, 456-459.

[38] J. Liu, A.L. Cardamone and R.M. German, "Estimation of Capillary Pressure in Liquid Phase Sintering," *Powder Metallurgy*, 2001, vol. 44, no. 4, pp. 317-324.

[39] W. Schatt and E. Friedrich, "Dislocation Activated Sintering Process," *Powder Metallurgy*, 1985, vol. 28, no. 3, pp.140-144.

[40] G.S. Upadhyaya, "Electronic Mechanism of Sintering: Some Case Studies on Real System," *Bulletin of Material Science*, 1994, vol.17, no. 6, pp. 921-934.

[41] R.M. German, Sintering Theory and Practice, John Wiley& Sons, Inc., New York, USA.

Appendix I

Cylindrical compacts prepared by mixed powders, sintered at 1400°C, 1h, H_2 (compaction pressure-200MPa)

Parameters measured		Alloys			
		92.5W (fine)	92.5W (coarse)	95.1W(fine)	95.1W (coarse)
Weight, (g)	Green	10.2530	10.0605	7.8000	13.0840
	Sintered	10.2280	10.0275	7.7980	13.0480
Height, (mm)	Green	7.70	7.16	5.74	8.84
	Sintered	6.80	6.84	5.14	8.32
Diameter, (mm)	Green	12.74	12.74	12.74	12.74
	Sintered	11.08	11.76	11.18	11.84
Density, (g/cm^3)	Green	10.44	11.022	10.6	11.61
	Sintered	15.5995	13.4968	15.4542	14.2438
%Theoretical density	Green	59.00	62.29	58.31	63.86
	Sintered	76.2	88.1	84.9	78.32
Weight loss, %		0.24	0.33	0.13	0.27
Densification parameter		0.71	0.37	0.64	0.66

Cylindrical compacts prepared by ball milled powders, sintered at 1400°C, 1h, H_2 (compaction pressure-200MPa)

Parameters measured		Alloys			
		92.5W (fine)	92.5W (coarse)	95.1W(fine)	95.1W (coarse)
Weight, (g)	Green	6.8682	6.2442	5.4933	4.4298
	Sintered	6.8300	6.2216	5.4378	4.3624
Height, (mm)	Green	4.80	4.56	4.28	3.4
	Sintered	4.26	3.00	3.50	2.76
Diameter, (mm)	Green	12.8	12.8	12.8	12.8
	Sintered	11.6	11.4	10.7	10.9
Density, (g/cm^3)	Green	14.24	13.62	12.77	12.96
	Sintered	15.18	15.64	17.22	16.94
%Theoretical density	Green	80.49	77.00	70.24	71.30
	Sintered	85.81	88.4	94.7	93.1
Weight loss, %		0.56	0.36	1.01	1.52
Densification parameter		0.696	0.714	0.878	0.823

Cylindrical compacts prepared by attritor milled powders, sintered at 1400°C, 1h, H_2, (compaction pressure-200MPa)

Parameters measured		Alloys			
		92.5W (fine)	92.5W (coarse)	95.1W(fine)	95.1W (coarse)
Weight, (g)	Green	6.8682	6.2442	5.4933	4.4298
	Sintered	6.8300	6 2216	5.4378	4.3624
Height, (mm)	Green	4.80	4.56	4.28	3.4
	Sintered	4.26	3.00	3.50	2.76
Diameter, (mm)	Green	12.8	12.8	12.8	12.8
	Sintered	11.6	11.4	10.7	10.9
Density, (g/cm^3)	Green	14.24	13.62	12.77	12.96
	Sintered	15.18	15.64	17.22	16.94
%Theoretical density	Green	80.49	77.00	70.24	71.30
	Sintered	85.81	88.4	94.7	93.1
Weight loss, %		0.56	0.36	1.01	1.52
Densification parameter		0.696	0.714	0.878	0.823

Appendix II

Cylindrical compacts prepared by mixed powders, sintered at 1500°C, 1h, H_2 (compaction pressure-200MPa)

Parameters measured		Alloys			
		92.5W (fine)	92.5W (coarse)	95.1W(fine)	95.1W (coarse)
Weight, (g)	Green	9.1169	7.7869	9.2205	8.0026
	Sintered	9.0930	7.7580	9.1960	7.9325
Height, (mm)	Green	6.84	5.52	6.88	5.48
	Sintered	5.70	4.76	5.74	4.80
Diameter, (mm)	Green	12.74	12.74	12.74	12.74
	Sintered	10.78	10.94	10.60	10.98
Density, (g/cm^3)	Green	10.4558	11.0661	10.5133	11.4557
	Sintered	17.4869	17.3169	18.1545	17.4969
%Theoretical density	Green	59.1	62.5	57.8	63.0
	Sintered	98.83	97.79	97.72	93.91
Weight loss, %		0.21	0.57	0.26	0.62
Densification parameter		0.972	0.943	0.996	0.89

Cylindrical compacts prepared by ball milled powders, sintered at 1500°C, 1h, H_2 (compaction pressure-200MPa)

Parameters measured		Alloys			
		92.5W (fine)	92.5W (coarse)	95.1W(fine)	95.1W (coarse)
Weight, (g)	Green	5.4700	7.2660	5.7865	6.1540
	Sintered	5.3245	7.405	5.6385	5.9620
Height, (mm)	Green	4.36	5.54	4.40	4.52
	Sintered	3.52	4.42	3.54	3.66
Diameter, (mm)	Green	12.8	12.8	12.8	12.8
	Sintered	10.46	10.78	10.54	10.7
Density, (g/cm^3)	Green	9.7496	10.1923	10.2201	10.5806
	Sintered	17.60	17.45	18.25	18.12
%Theoretical density	Green	55.10	57.60	56.20	58.18
	Sintered	99.48	98.63	100.0	99.62
Weight loss, %		2.65	3.10	2.50	3.10
Densification parameter		0.988	0.968	1.0	0.991

Cylindrical compacts prepared by attritor milled powders, sintered at 1500°C, 1h, H_2, (compaction pressure-200MPa)

Parameters measured		Alloys			
		92.5W (fine)	92.5W (coarse)	95.1W(fine)	95.1W (coarse)
Weight, (g)	Green	7.59	4.70	3.05	5.61
	Sintered	7.50	4.66	3.00	5.54
Height, (mm)	Green	6.84	3.96	2.82	4.96
	Sintered	5.08	2.80	1.84	3.4
Diameter, (mm)	Green	12.8	12.8	12.8	12.8
	Sintered	10.3	10.76	10.64	10.70
Density, (g/cm^3)	Green	8.6249	8.8568	8.4030	8.7854
	Sintered	17.7258	17.5426	18.3600	18.1828
%Theoretical density	Green	48.75	50.06	46.20	48.32
	Sintered	100.0	99.14	100.0	99.99
Weight loss, %		1.20	0.50	1.52	1.19
Densification parameter		0.990	0.983	1.000	0.999

Appendix III

Macro-hardness of sintered compacts prepared by mixed powders, sintered at 1400°C, 1h, H_2

(compaction pressure-200MPa)

Alloy	No. of Observ.	D_1	D_2	Hardness HV_{30}	Average Hardness HV_{30}	Standard Deviation σ_n
92.5W (fine)	1	410.4	413.9	218	220.7	2.31
	2	409.2	408.7	222		
	3	407.2	409.2	222		
92.5W(coarse)	1	518.9	514.6	139	139	0.0
	2	514.3	517.2	139		
	3	514.0	518.7	139		
95.1W (fine)	1	438.5	432.4	196	196.6	1.15
	2	432.9	436.2	196		
	3	434.5	431.8	198		
95.1W (coarse)	1	532.1	530.3	131	129.0	4.35
	2	548.0	546.3	124		
	3	530.4	530.7	132		

Macro-hardness of sintered cylindrical compacts prepared by ball milled powders, sintered at 1400°C, 1h, H_2

(compaction pressure-200MPa)

Alloy	No. of Observ.	D_1	D_2	Hardness HV_2	Average Hardness HV_2	Standard Deviation σ_n
92.5W (fine)	1	155.1	152.2	157	161.8	3.21
	2	150.9	150.5	163		
	3	152.3	150.6	162		
92.5W (coarse)	1	132.1	132.1	212	203.0	13.07
	2	132.1	134.5	209		
	3	139.1	141.9	188		
95.1W (fine)	1	113.2	114.4	286	288.3	6.80
	2	114.4	114.4	283		
	3	112.5	115.5	296		
95.1W (coarse)	1	112.5	113.8	290	294.0	8.71
	2	107.9	118.9	288		
	3	109.7	111.3	304		

Macro-hardness of cylindrical compacts prepared by attritor milled powders, sintered at 1400°C, 1h, H_2, (compaction pressure-200MPa)

Alloy	No. of Observ.	D_1	D_2	Hardness HV_2	Average Hardness HV_2	Standard Deviation σ_n
92.5W (fine)	1	10.1	97.9	371	371.6	4.04
	2	100.4	100.4	368		
	3	98.9	99.8	376		
92.5W (coarse)	1	112.8	111.0	296	295.3	8.38
	2	114.6	115.8	297		
	3	110.9	107.5	311		
95 1W (fine)	1	97.8	101.0	375	379.0	6.08
	2	99.7	99.0	376		
	3	97.3	98.6	386		
95.1W (coarse)	1	155.8	151.1	157	172	13.45
	2	144.2	140.5	183		
	3	146.1	144.5	176		

Appendix IV

Macro-hardness of cylindrical compacts prepared by mixed powders, sintered at 1500°C, 1h, H_2

(compaction pressure-200MPa)

Alloy	No. of Observ.	D_1	D_2	Hardness HV_{30}	Average Hardness HV_{30}	Standard Deviation σ_n
92.5W (fine)	1	349.6	351 1	302	300.6	1.52
	2	353.5	351.4	299		
	3	350.5	351.2	301		
92.5W (coarse)	1	357.0	359.4	289	293.3	4.50
	2	354.1	351.4	298		
	3	357.6	353.5	293		
95.1W (fine)	1	347.8	353.3	302	302.6	4.04
	2	345.9	349.1	307		
	3	353.3	351.5	299		
95.1W (coarse)	1	358.7	354.8	291	283.6	9.45
	2	360.8	357.9	287		
	3	369.5	367.1	273		

Macro-hardness of cylindrical compacts prepared by ball milled powders, sintered at 1500°C, 1h, H_2

(compaction pressure-200MPa)

Alloy	No. of Observ.	D_1	D_2	Hardness HV_{30}	Average Hardness HV_{30}	Standard Deviation σ_n
92.5W (fine)	1	368.6	359.6	280	287	6.55
	2	354.6	356.4	293		
	3	356.4	361.8	288		
92.5W (coarse)	1	361.5	356.0	281	281	4.04
	2	365.1	365.8	278		
	3	357.0	362.8	286		
95.1W (fine)	1	359.9	362.9	284	286	2.64
	2	352.2	363.3	289		
	3	362.5	358.6	285		
95.1W (coarse)	1	359.8	355.6	290	290	2.0
	2	357.2	360.8	288		
	3	358.2	354.7	292		

Macro-hardness of cylindrical compacts prepared by attritor milled powders, sintered at 1500°C, 1h, H_2, (compaction pressure-200MPa)

Alloy	No. of Observ.	D_1	D_2	Hardness HV_{30}	Average Hardness HV_{30}	Standard Deviation σ_n
92.5W (fine)	1	352.2	358.0	294	294.3	4.51
	2	355.5	348.7	299		
	3	351.4	363.6	290		
92.5W (coarse)	1	351.5	351.6	300	298.3	1.52
	2	351.8	354.2	298		
	3	350.6	356.2	297		
95.1W (fine)	1	370.1	359.9	278	281	4.58
	2	368.7	360.3	279		
	3	358.5	362.1	286		
95.1W (coarse)	1	345.5	352.9	304	297.6	5.68
	2	359.6	352.1	293		
	3	354.2	353.6	296		

Appendix V

Micro hardness of compacts prepared by mixed powder, sintered at 1500°C, 1h, H_2

Alloy	No of Obser	Tungsten				Matrix			
		Diagonal length, (μm)	Hard-ness $HV_{0\,05}$	Mean Hard-ness	STDEV σ_n	Diago -nal length , (μm)	Hardness, $HV_{0\,005}$	Mean Hard-ness	STDEV σ_n
92.5W (fine)	1	15.5	386	410.2	23.25	10.4	85.7	75.2	7.92
	2	15.5	386			11.0	76.6		
	3	14.6	435			11.8	66.0		
	4	15.0	415			10.8	79.0		
	5	14.7	429			11.6	68.9		
92.5W (coarse)	1	15.0	412	412.2	6.94	12.0	64.4	65.0	8.78
	2	14.9	418			10.7	81.0		
	3	15.2	401			11.7	67.7		
	4	15.0	412			13.4	51.6		
	5	14.9	418			12.4	60.3		
95.1W (fine)	1	15.2	401	412.8	15.54	11.1	75.2	74.6	9.38
	2	15.3	396			11.2	73.9		
	3	14.8	420			10.6	82.0		
	4	14.6	435			12.5	59.3		
	5	15.0	412			10.6	82.5		
95.1W (coarse)	1	16.3	350	382.2	26.65	11.0	77.0	71.2	4.33
	2	15.1	407			11.4	71.3		
	3	15.6	381			11.5	70.1		
	4	15.1	407			11.3	72.6		
	5	16.1	358			12.0	65.0		

Micro hardness of compacts prepared by ball milled powder, sintered at 1500°C, 1h, H_2

Alloy	No. of Observ.	Tungsten				Matrix			
		Diagonal length, (μm)	Hard-ness, $HV_{0\,05}$	Mean Hard-ness	STDEV σ_n	Diagonal length, (μm)	Hard-ness, $HV_{0\,005}$	Mean Hard-ness	STDEV σ_n
92.5W (fine)	1	15.2	401	414.4	8.44	9.5	103	92.2	9.01
	2	15.0	412			10.0	92		
	3	14.8	423			9.8	94		
	4	14.9	418			9.8	94		
	5	14.9	418			10.8	78		
92.5W (coarse)	1	17.0	319	372.8	32.82	11.6	68.9	82.1	9.86
	2	15.1	407			11.1	75.2		
	3	15.5	386			10.1	90.9		
	4	15.6	381			10.4	85.7		
	5	15.8	371			10.1	90.9		
95.1W (fine)	1	15.1	407	401.0	18.97	10.6	82.5	76.2	7.33
	2	15.6	381			11.4	71.3		
	3	15.6	381			10.8	79.0		
	4	14.8	423			11.8	66.0		
	5	15.0	412			10.6	82.5		
95.1W (coarse)	1	15.8	371	383.2	13.66	11.4	71.3	79.4	13.74
	2	15.3	396			9.8	95.0		
	3	15.3	396			11.1	75.0		
	4	15.9	367			10.0	92.0		
	5	15.5	386			12.0	64.0		

Micro hardness of compacts prepared by attritor milled powder, sintered at 1500°C, 1h, H_2

Alloy	No. of Observ.	Tungsten				Matrix			
		Diagonal length, (μm)	Hard-ness, $HV_{0.05}$	Mean Hard-ness	STDEV σ_n	Diagonal length, (μm)	Hard-ness, $HV_{0\,005}$	Mean Hard-ness	STDEV σ_n
92.5W (fine)	1	15.1	407	419.2	17.72	10.6	82.5	93.2	8.24
	2	15.0	412			9.5	96.0		
	3	15.2	401			9.4	105 0		
	4	14.5	441			10.1	90.9		
	5	14.6	435			10.1	90.9		
92.5W (coarse)	1	14.5	441	402.0	23.55	10.0	92.0	88.2	13.79
	2	15.2	401			10.7	81.0		
	3	15.5	386			9.2	110.0		
	4	15.6	381			10.5	84.0		
	5	15.2	401			11.1	74.0		
95.1W (fine)	1	14.4	447	462	21.83	8.8	120.0	118.4	5.94
	2	14.6	435			8.7	122.0		
	3	13.9	480			9.0	115.0		
	4	14.2	460			8.6	125.0		
	5	13.8	487			9.2	110.0		
95.1W (coarse)	1	14.0	473	499	45.40	9.8	96.0	87.2	17.45
	2	14.5	441			9.1	112.0		
	3	13.0	549			11.8	66.0		
	4	13.7	494			10.5	84.0		
	5	13.1	540			10.8	79.0		